universität wien

# MASTERARBEIT / MASTER'S THESIS

Titel der Masterarbeit / Title of the Master's Thesis

## „Detecting permafrost degradation using combined stable isotopes ($^{2}H$ and $^{18}O$) and anthropogenic $^{129}I$ isotope chemistry in rock glacier meltwaters"


verfasst von / submitted by

Jakob Müller, BSc


angestrebter akademischer Grad / in partial fulfilment of the requirements for the degree of

Master of Science (MSc)

Wien, 2023 / Vienna 2023

| | |
|---|---|
| Studienkennzahl lt. Studienblatt / degree programme code as it appears on the student record sheet: | A 066 815 |
| Studienrichtung lt. Studienblatt / degree programme as it appears on the student record sheet: | Masterstudium Erdwissenschaften |
| Betreut von / Supervisor: | Dipl.-Geogr. Dr. Sabine Kraushaar |

-

## Acknowledgements

This thesis would not have been possible without the support and help of certain people. First, I would like to sincerely thank Dipl. Geogr. Dr. Sabine Kraushaar for giving me the opportunity for this master's thesis as a contribution to the project GeoHype, and for providing me with guidance and encouragement throughout the whole process. I also want to thank Jun.-Prof. Dr. Jan Blöthe, Till Groh, and Stefan Haselberger for their valuable support during long days in the field during the sampling campaigns.

Many thanks also go to the department for Isotope Physics in the Faculty of Physics of the University of Vienna and especially to Dipl.-Phys. Dr. Johannes Lachner for the great help with Iodine-sample-preparation and acceleration mass spectrometry measurements at VERA. Moreover, thanks go to AgroIsoLab GmbH for analysing the stable isotope samples. I would also like to thank David Keil for his company and fruitful cooperation in the laboratory, where experiments sometimes need more effort than expected.

I would also like to express my gratitude and thanks towards my colleagues and friends Tobias Hofer, David Keil, Andreas Schönfelder, and Eva Stadlbauer for their support throughout the project – be it through encouraging words, providing their opinions and advice, sharing their expertise, proof-reading, or simply by keeping me company during the many hours spent writing this thesis. In this regard I want to especially thank Eva Stadlbauer, who supported me with her company, patience, and motivation throughout the writing process.

Above all, a heartful thanks goes to my family and friends for your continual emotional and moral support. I would not have come this far without you. Thank you.

# Table of contents

Geologic translations from German literature and maps are based on Wörterbuch der Geologie (Schweizer, 2012)

# List of figures

# List of tables

# List of abbreviations

| | |
|---|---|
| a | year [anno] |
| AMS | acceleration mass spectrometry |
| APIM | Alpine Permafrost Index Map |
| Atoms/l | atoms per litre |
| AMWL | Austrian meteoric water line |
| ANIP | Austrian Network of Isotopes in Precipitation and Surface Waters |
| ANOVA | analysis of variance |
| $A_R$ | isotopic mass |
| BP | before present |
| d-excess | deuterium excess |
| e.g. | for example [exempli gratia] |
| EC | electric conductivity |
| EMMA | end member mixing analysis |
| ERT | electronical resistivity tomography |
| fig. | figure |
| ga | giga-annum |
| GBq/a | gigabecquerel per anno |
| GMWL | global meteoric water line |
| GNIP | global network of isotopes in precipitation |
| i.a. | inter alia |
| IUPAC | International Union of Pure and Applied Chemistry |
| ka | kilo-annum |
| LMWL | local mean water line |
| m.a.s.l. | meter above sea level (Adriatic Sea) |
| m/a | metres per year |
| mm/a | millimetres per year |
| mg/a | milligram per anno |
| mg/kg | milligram per kilogram |
| MWL | mean water line |
| NFRP | nuclear fuel reprocessing plants |
| PCA | Principal Component Analysis |
| SI | International System of Units *or* stable isotopes |
| TBp | terabecquerel |
| VERA | Vienna Environmental Research Accelerator |
| VSMOW | Vienna Standard Mean Ocean Water |
| µS/cm | microsiemens per centimetre |

# List of chemical formulas

| | |
|---|---|
| $^{1}H$ | Hydrogen-1 |
| $^{2}H$ = D | Hydrogen-2 = Deuterium |
| $^{3}H$ | Tritium |
| $^{16}O$ | Oxygen-16 |
| $^{17}O$ | Oxygen-17 |
| $^{18}O$ | Oxygen-18 |
| $^{127}I$ | Iodine-127 |
| $^{129}I$ | Iodine-129 |
| $Ca_2^+$ | Calcium cation |
| $Cl^-$ | Chloride |
| $HNO_3$ | Nitric acid |
| $I^-$ | Iodide |
| $IO_3^-$ | Iodate |
| $KNO_3$ | Potassium nitrate |
| $Mg_2^+$ | Magnesium cation |
| $Na^+$ | Sodium cation |
| $NH_3$ | Ammonia |
| $NO_3$- | Nitrate |
| SiO | Silicon dioxide |
| $SO_4^{2-}$ | Sulfate |

# 1 Introduction and theoretical background

One of the big challenges awaiting humankind in near future is the climate crisis. Climate change is expected to lead to weather extremes, the extinction of up to a third of all animal and plant species by 2050 (Thomas et al., 2004), droughts (Spinoni et al., 2018) and floods (Tabari, 2020), and rising sea levels (Cazenave & Cozannet, 2014), to name just a few effects of a changing climate in the following decades. Already in the last 20 years, the number of flood-related disasters has increased over 130 % in comparison to the 20 years before (UNEP, 2022). Water stress on a global level is directly linked to the climate crisis. The dramatic shrinkage of freshwater reservoirs is caused through rising sea levels, droughts, draining of rivers and lakes, and thawing of the cryosphere. In Europe, 30 % of the population is affected by water stress (EEA, 2021) – this number is expected to increase in the following years.

In the Alps, the effects of global warming are visible – even more than on world average (Bosco et al., 2009; Gobiet et al., 2014). As a consequence of rising temperatures weather extremes become more frequent, ice thawing and soil erosion are accelerated, alpine risks in general are increasing (Bosco et al., 2009; Gobiet et al., 2014; Theurillat & Guisan, 2001). Recent examples are the landslide at Piz Cengalo in 2017 (Mergili et al., 2020) and the Marmolada glacier avalanche in the Dolomites in July 2022, where eleven mountaineers died, as a result of dramatic ice shrinking of 30 % over the past ten years (Olivieri & Bettanini, 2022; Santin et al., 2019). By 2100, almost all alpine glaciers below 4,000 m.a.s.l. will be disappeared (Shannon et al., 2019). This prediction is alarming, considering the hydrological importance of glaciers and mountains in their role of natural ‘water towers’ “to sustain environmental and human water demands downstream” (Immerzeel et al., 2020).

Their loss will lead to substantial and lasting changes in the alpine water balance. It is thus of immense importance to put research effort into remaining water source after the disappearance of glacier ice. One of them is ice stored below the earth’s surface in form of permafrost. It is an important freshwater reservoir due to its isolating cover of debris or soil, which makes it less sensitive to climate variation than glaciers and so makes it respond slower to climate changes than glaciers (Arenson et al., 2022; Potter, 1972). Ice stored in permafrost is considered to melt 10 – 100 times slower than surface glacier

ice (Brighenti et al., 2019). A prominent, because detectable with the naked eye, form of permafrost are rock glaciers. They also play a high major role in the water system of mountainous regions, especially in regions with arid climate (Arenson et al., 2022; Blöthe et al., 2016). Between the 29° and the 32° South in the Andes, today they are even of higher importance than ice glaciers (Azócar & Brenning, 2010). Although intact rock glaciers in Austria only store a 12$^{th}$ of ice glaciers ice volume (T. Wagner, Kainz, Helfricht, et al., 2021), they still contain a water volume equivalent of 83.7 ± 16.7 Gt or 68–102 trillion litres (Jones, Harrison, Anderson, et al., 2019).

Research on the cryosphere in general and on permafrost and rock glaciers as a major form of it in particular is called for (Jones, Harrison, Anderson, et al., 2019; Krainer & Ribis, 2009; T. Wagner, Kainz, Helfricht, et al., 2021; Yang et al., 2019). This thesis follows up on those calls and contributes to answering questions with the help of hydrochemistry, stable water isotopes (SI) and the anthropogenic radionuclide iodine-129 ($^{129}$I). With the help of those tracers the origin of spring waters, and following, the thawing permafrost can be investigated.

## 1.1 Alpine water balance

Mountains are a natural ‘water towers’ (Immerzeel et al., 2020; Viviroli et al., 2007) and thus play an important role in downstream hydrology. Typical estimations of mountain-block recharge, the part of lowland aquifer recharge originating from adjoining mountains, reach from 5 – 50 % (Markovich, Manning, et al., 2019). This confirms that reservoirs in mountain contribute considerable amounts to lowland groundwater (Markovich, Manning, et al., 2019). The size of aquifers and dynamic groundwater storage is highly dependent on the geologic background. Little weathered bed rocks build coarser deposits, which are not capable of storing big amounts of water (Cochand et al., 2019). Thus, a substantial part of water is only stored as ice in glaciers and permafrost. Globally, 68-102 trillion litres of water are stored inside rock glaciers (Jones, Harrison, Anderson, et al., 2019). In Austria alone, rock glaciers store 1.04 to 1.91 km³ (depending on the calculation method) and ice glaciers store 12.42 km³ of ice, which corresponds to an equivalent of 2.22 to 4.08 times the yearly drinking water consumption in Austria for rock glaciers and 26.58 times for ice glaciers, respectively (T. Wagner, Kainz, Helfricht, et al., 2021). 85 % of Austrian rock glacier ice is located

in the federal state of Tyrol (T. Wagner, Kainz, Helfricht, et al., 2021). However, exact ice volume calculations are difficult, Krainer and Ribis (2012) calculated the ice volume stored in Tyrolean rock glaciers about five times lower with 0.19 – 0.27 km³.

Glaciers and permafrost are considered as very vulnerable to “changes in air temperature, precipitation patterns, sublimation, and evapotranspiration” (Arenson et al., 2022) in long terms. With global warming, the alpine water balance is about to change drastically. Markovich et al. (2019) point out that further research on the origin and quantification of groundwater in mountainous regions is needed, especially with regard to understanding the effect of current climate processes and predicting a future one. Especially rock glaciers will play a significant hydrological role in the coming decades (Jones, Harrison, Anderson, et al., 2019). Their debris cover, which functions as protection against temperature fluctuations, also makes them much more difficult to investigate, resulting in uncertainties regarding their extents and thus, ice volumes of orders of magnitudes higher than those for glaciers (Arenson et al., 2022). Much is unknown about dynamics, ice volume, discharge behaviour, water quality (Jones, Harrison, Anderson, et al., 2019), but also on pathways of permafrost melt waters and its contributions to streamflow (Arenson et al., 2022). This thesis tries to contribute to closing some of those research gaps.

## 1.2 Permafrost

Permafrost is defined as ground with a temperature of 0°C or below for a duration of at least two following years (Krugger & Stern, 2009; Muller, 1943). It can be divided into two layers. The upper layer starting below the earth’s surface is called the active layer. It is characterized by seasonal freezing and thawing processes. Beneath this active layer, there is the passive layer. It is permanently frozen all over the year (Woo, 2012). Permafrost is considered a significant part of the cryosphere (Biskaborn et al., 2019).

The global distribution of permafrost is limited by latitude, altitude, and climate. In the northern hemisphere, 22 % of the exposed land surface was covered by permafrost in the 1990s (J. Brown et al., 1997; Gruber, 2012). Its distribution in the southern hemisphere is limited to the not ice-covered parts of Antarctica and some areas in South America. Permafrost in the Alps is described as isolated permafrost, it has no direct connection to the arctic permafrost areas (Van Huissteden, 2020). In contrast to areas

with continuous permafrost, where groundwater recharge is impeded by a consistent ice layer, groundwater generation is possible in areas with discontinuous permafrost (Woo, 2012). In the Alps, permafrost dissemination is by altitude and exposition (Pokrovsky, 2014). It covers much bigger areas than glaciers in the Alps (Boeckli et al., 2012).

Information for a permafrost inventory can be derived from borehole temperature, ground surface temperature, rockfall scar, trench or construction site, surface movement, geophysical prospecting, other indirect evidence, and rock glacier mapping (Cremonese et al., 2011). Revealing an exact distribution of permafrost in the Alps is a major subject of current research projects. It is difficult to map permafrost because of the effort needed to prove it directly (Gruber, 2012). Therefore, indirect evidence is of importance. Projects like the Alpine Permafrost Index Map (APIM) (see Fig. 1) aim to calculate the distribution and show the likelihood of permafrost existence in the Alps with statistical models based on observations (*Alpine Permafrost Index Map (APIM)*, 2018; Boeckli et al., 2012).

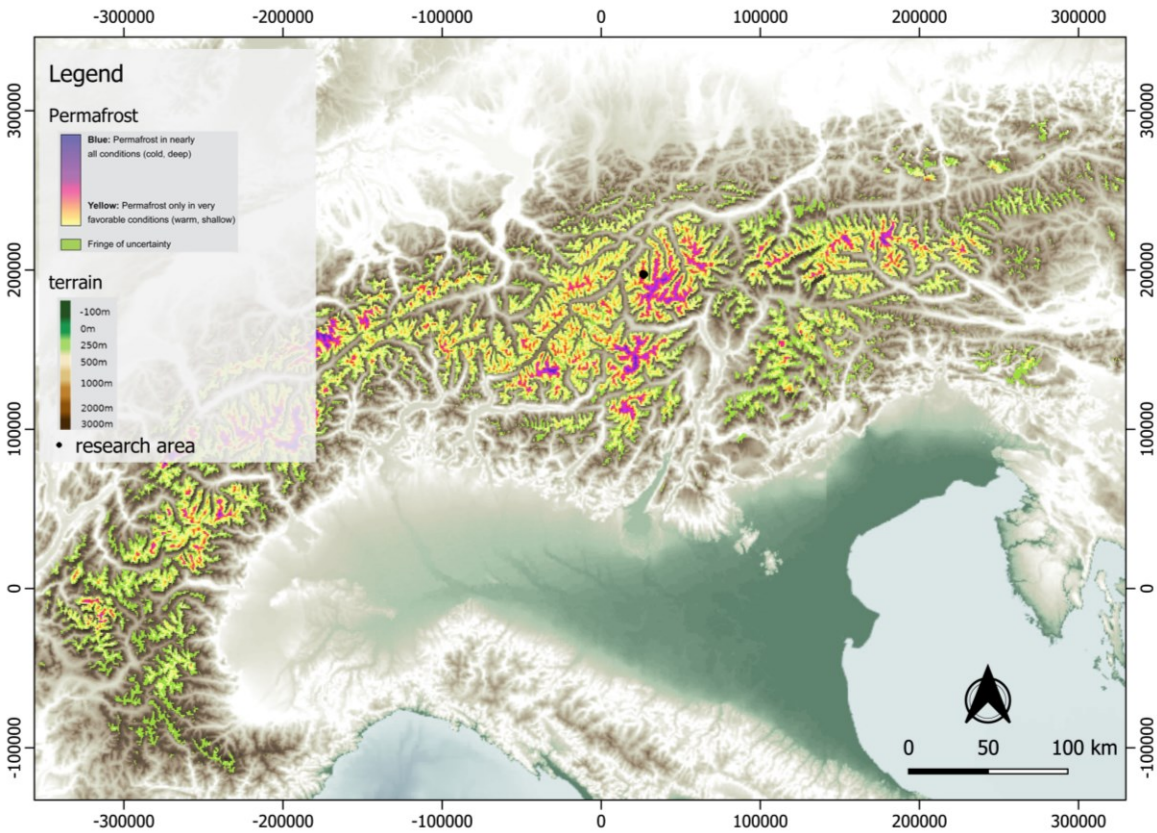


*Fig. 1: Expected permafrost distribution in the Alps following global scale calculations (APIM); an underlaying topographic map and hill shades provide topographic information. Data retrieved*

*from Alpine Permafrost Index Map (APIM), (2018). Coordinate Reference System: EPSG:31254 - MGI / Austria GK West*

Within the current climate change ground temperatures are rising significantly. In the period of 2007 to 2016, permafrost warmed by 0.29 °C ± 0.12 °C. In mountain regions, permafrost temperatures increased by 0.19 °C ± 0.05 °C (Biskaborn et al., 2019). This temperature increase provokes massive decrease in permafrost volumes. Several case studies show this permafrost degradation in high alpine environment. For instance Scandroglio et al. (2021) calculated a tremendously shrinking ice volume from 6,790 m³ ± 640 m³ in 2006 to 3,880 m³ ± 1,000 m³ in 2019 in the Steintaelli Ridge at 3,100 m.a.s.l. (Swiss Alps) with the help of an electrical resistivity tomography (ERT) time series. On a global scale, a thawing of 40 % of all permafrost is estimated, should climate warming stabilizes at 2°C according to the Paris Agreement (Van Huissteden, 2020, p. 490). With each additional degree of warming, 4 million km$^2$ of permafrost area are to thaw (Chadburn et al., 2017). The speed of permafrost loss is unprecedented and, depending on calculation methods, at least 2.4 times faster than it was during the end of the last glacial (Van Huissteden, 2020, p.492).

### *1.2.1 Rock glacier*

Rock glaciers are periglacial forms of permafrost consisting of rocks and ice being covered by debris (Krainer & Mostler, 2002). The term rock glacier is used for creeping perennially frozen ice rich debris on mountain slopes, as well as for debris covered glaciers in permafrost free areas (Haeberli et al., 2006). Since Wahrhaftig & Cox (1959) and others published ground breaking studies about rock glaciers, this most prominent expression of permafrost became a popular object for researchers all around the globe. Rock glaciers are either formed by a transition from glacial to periglacial or by periglacial processes (Anderson et al., 2018; Jones, Harrison, & Anderson, 2019; Jones, Harrison, Anderson, et al., 2019; Whalley & Martin, 1992). Their debris cover is why their ice body is considered as being much more resilient to increasing temperatures than glacier ice (Potter, 1972; T. Wagner, Kainz, Helfricht, et al., 2021).

Fig. 2 illustrates the zones of an active rock glacier. The highest area of a rock glacier is the rooting zone, where snow, ice, and debris material are accumulating. Towards

the valley, the rock glacier body reveals a characteristic tongue form with lava stream shaped lobes (A. Kääb, 2013; Andreas Kääb & Weber, 2004) in either single lobes or more complex multiple coalescent lobes (Frauenfelder & Kääb, 2000). Ridges and furrow-formed surface structures correspond to spatial and temporal variations within the rock glacier material (Haeberli et al., 2006). At the front there is the toe with a steep scarp. In this thesis, the terminology is used as from Krainer & Ribis (2012) and other authors in alpine rock glacier studies: An 'active rock glacier' is still in movement, an 'inactive rock glacier' looks active but is not moving, a 'fossil rock glacier' or 'relict rock glacier' is at complete stillstand and lacks of an ice-core (Ikeda & Matsuoka, 2002; A. Kääb, 2013; Kerschner, 1978).

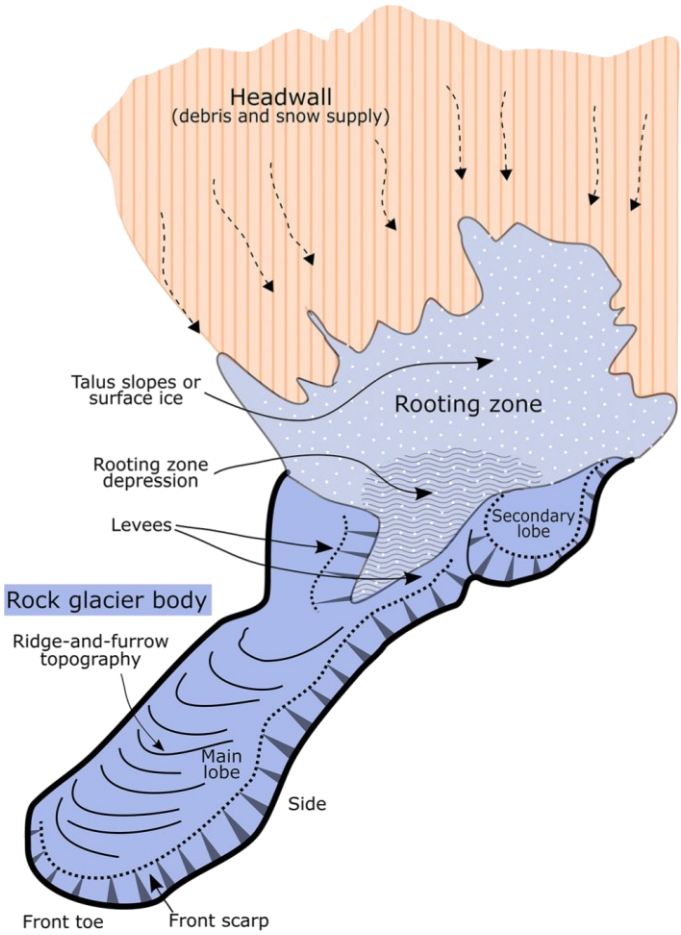


*Fig. 2: Schematic illustration of a rock glacier indicating the zone of debris and snow supply (headwall), the rooting zone of the rock glacier and the rock glacier body. Main components and terminology named after Brardinoni et al. (2019)*

Due to their inner architecture and their debris cover, rock glaciers are thought to be of major importance for future water safety (Pruessner et al., 2021). Alpine rock glaciers formed several thousand years ago in the early Holocene after the Würm glaciation. They often need thousands of years to form which makes dating a challenging task, but some were found to be at least 8.4 ka of age (Schmidt, 2009). The flow velocity of active rock glaciers is lower than the velocity of ice glaciers, it does not exceed flowing rates of cm/a to dm/a (Potter, 1972). Water is a main factor for inter-annual time scale creeping (Cicoira et al., 2019).

Rock glaciers make out the most common feature of Alpine permafrost (Boeckli et al., 2012; Krainer & Ribis, 2012). In the Tyrolean Alps, there are 3,145 documented rock glaciers of which 16.4 % are active, 29.1 % inactive, and 54.5 % fossil. Altogether, they cover 167.2 km², what makes rock glaciers more common in the Alps than ice glaciers (Krainer & Ribis, 2012).

### *1.2.2 Internal structure and hydrology*

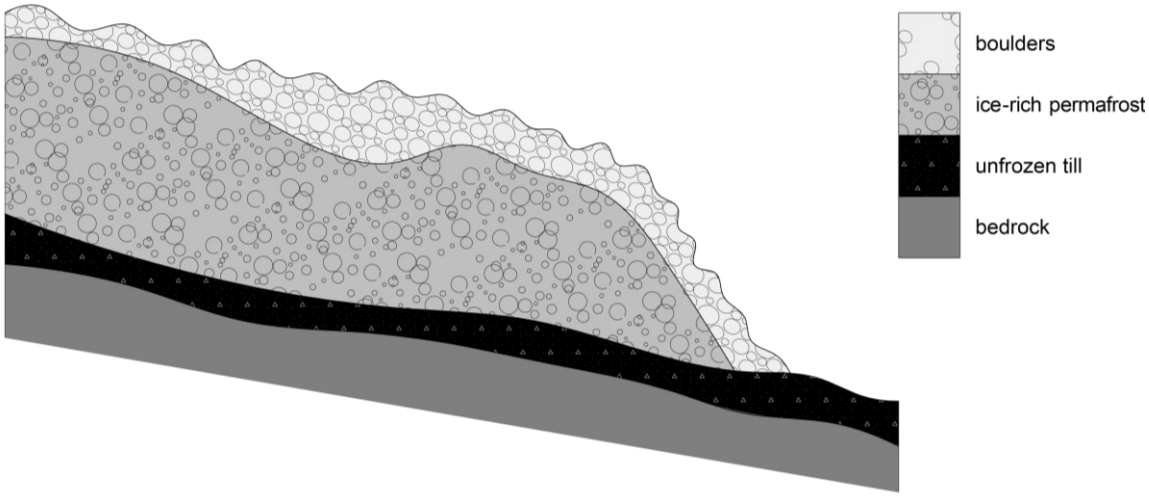


*Fig. 3: Schematic internal structure of a rock glacier based on ground penetrating radar (GPR), seismic refraction and gravimetry; after H. Hausmann et al. (2007)*

The internal structure of rock glaciers determines their hydrologic behaviour (Cicoira et al., 2019). Above the underlying bedrock, there is a layer of unfrozen, fine-grained till (see Fig. 3). This layer has a thickness of decimetres to some meters and is seen as potentially water-conductive. It is followed by an ice-rich permafrost which marks the thickest layer with some tens of meters and makes up the majority of a rock glaciers volume. Rock glaciers have a blocky surface of some meters of thickness, which is highly conductive to water. This blocky cover is the reason why rock glaciers are thought to be more resilient to climate variations than ice glaciers (Anderson et al., 2018; Jones, Harrison, Anderson, et al., 2019; Potter, 1972; Pruessner et al., 2021).

Their discharge is highly variable throughout a year and also during a day (Krainer et al., 2007). Rock glaciers are not capable of storing water for a long time, precipitation and snowmelt waters are quickly released. Following, electrical conductivity (EC) is very low after rain events. EC is high in dry periods with low discharge, mainly driven by

groundwater influence. Discharge temperatures of active rock glaciers are constantly below 1°C. Discharge patterns are similar to glaciers, but the yearly mean specific discharge is lower (Krainer & Mostler, 2002). $\delta^{18}O$ values (discussed further in 3.3.1) of rock glacier springs are much more constant than rain over the year with a slight increase of values from May to October (Krainer et al., 2007).

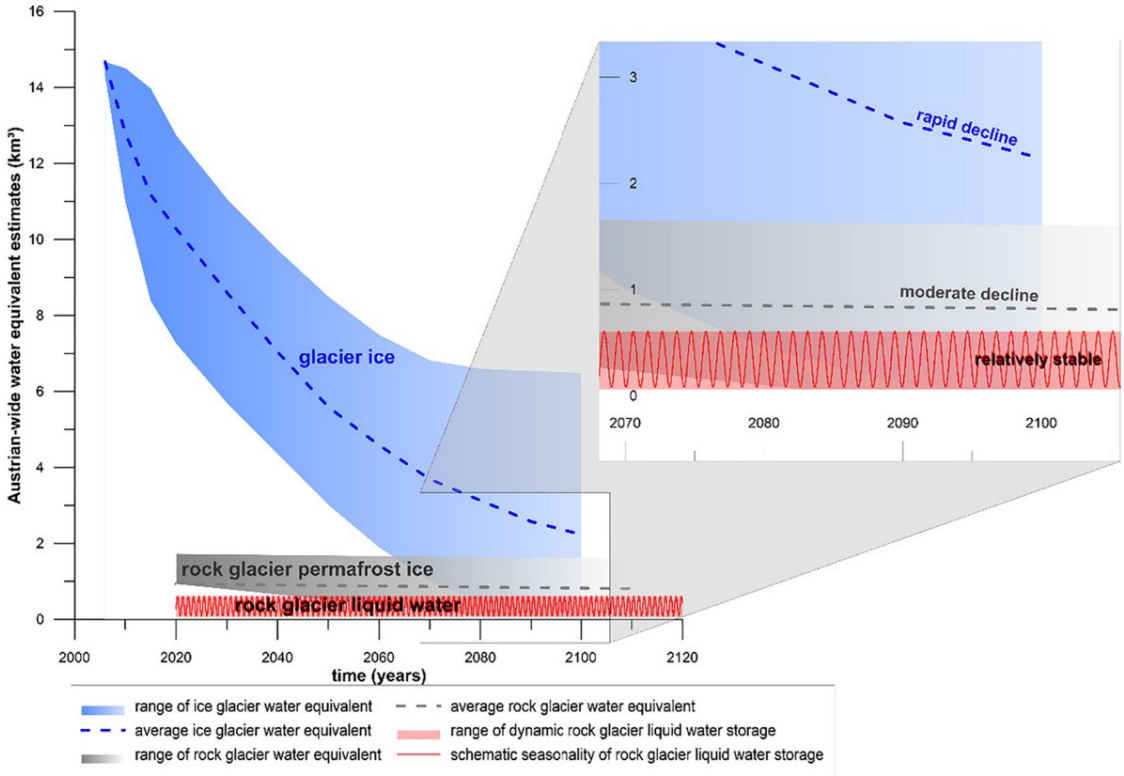


*Fig. 4: Comparison of volumes of water stored in glacier ice, rock glaciers' permafrost ice, and rock glacier liquid water in Austria. Source: T. Wagner, Kainz, Helfricht, et al. (2021).*

In Austria, estimates of water volumes stored in mountainous regions were done recently by T. Wagner et al. (2021). They comprised available data for Austria and estimated rock glacier water storage as 8.3 % of total Austrian ice volume. Although its percentage seems low in comparison to ice glaciers, its ice is much more resilient and will be of significant importance towards the end of the century, when ice glaciers volume is decreased by at least 85 % (see Fig. 4, Wagner 2021). Water captured in the unfrozen base layer of rock glaciers is of minor importance (volume ratio 1:20), but can increase with increasing pore volume, when permafrost ice melts (T. Wagner, Kainz, Helfricht, et al., 2021). Latest research underlines the importance of rock glacier for the water balance of high altitudes, especially after winters with little snow, a quarter of

streamflow can be addressed as rock glacier internal ice melt (Munroe & Handwerger, 2022).

### *1.2.3 Methods of investigation and state of the art*

While there is no doubt of the increasing importance of rock glaciers as water reservoirs, there is great need for research on them. As Jones et al. (2019) point out that there is no global map of rock glaciers. The creation of rock glacier inventories has been subject of research in the last decades, and still is today. Different approaches are used for different purposes and for mutual verification to differentiate active from inactive and relict rock glaciers (Scotti et al., 2013). The variation of mapping techniques, area and volume estimations of rock glaciers are leading to multiplying errors in the calculation of their water storage (Brardinoni et al., 2019).

Conventional ways to gather direct information about rock glaciers include core drilling and borehole measurements. In the Lazaun in the southern Ötztal Alps, deeper parts of the rock glacier passive layer were dated through an analysis of core drillings with an age of 8,960 a BP, shallower parts were datet with 2,240 a BP (Krainer et al., 2015). In remote places, it can be demanding to supply the heavy equipment needed for direct exploration (Krainer et al., 2015). Information involving ice content, ice distribution within the ground, and other features is not retrievable with these invasive techniques. Easier to apply in alpine environments are Electrical Resistivity Tomography (ERT) and seismic refraction tomography (SRT). The equipment can be carried by a human, and it can produce a two-dimensional picture of the internal structure like ice and rock distribution out of electrical resistivity and seismic refraction data. If used in perpendicular directions building a raster, a petrophysical four-phase model (4PM) can be used to calculate volumes of ground ice (Halla et al., 2021; Hauck et al., 2011). Similar information can be gained by using ground-penetrating radar (GPR). Monnier & Kinnard (2015) calculated an average ice content of two thirds for rock glaciers in the Dry Andes by measuring refracted radar waves. Using ERT, SRT, as well as GPR to calculate ice contents are good methods to calculate ice volumes (Halla et al., 2021; Monnier & Kinnard, 2015), but it still needs effort to carry equipment into remote places. They also cannot give information about the age of ice.

With satellite-based, airplane-based, or drone-based systems, surface information of the ground can be produced in good accuracy. With the help of those non-invasive remote sensing systems movements rates of the ground can be calculated (Brardinoni et al., 2019; Groh & Blöthe, 2019; Morche et al., 2014). Computer modelling is a promising way to calculate runoff even from difficult sources like permafrost slopes in fine structured valleys in mountainous regions like high alpine valleys. The Glacier Evolution and Runoff Model (GERM) has been expanded with an extension for permafrost. Another physics-based model named SNOWPACK was established lately (Pruessner et al., 2021). These highly parameterized calculation approaches are still in development and not perfectly applicable to real world implementation, though. Other statistical methods use physical parameters from field investigations. A high number of easy collectable field values (including EC, Temp, altitude, inclination and others) suggests a way to combine their evidence. In the year 1901 Pearson defined the principle of reducing multidimensional rooms to a smaller number of displayable theoretical dimensions. In a Principal Component Analysis (PCA) reduced dimensions then can be plotted in a bi- or tri-dimensional space to show correlations in the data. A loading matrix represents the contribution of original variables on the calculated principal components (Camargo, 2022). The method has been applied on various fields of aquifer research, including investigations on permafrost and rock glaciers. A statistical technique based on hydrochemistry called hydrograph separation is a method to understand the origin and flow paths of headwaters. It has been used in studies for natural water systems in various climates zones (Klaus & McDonnell, 2013) as well as rock glacier outflow to untangle the origin and seasonal variation of spring waters (Williams et al., 2006). Hydrograph separation can be done with various chemical parameters based on end-member mixing analysis (EMMA) to trace back spring water to its origin. EMMA was established in the early 1990s by Hooper & Christophersen (1992; 1990) and has been applied to various issues of in this field, as also in the analysis of high elevation watersheds (L. E. Brown et al., 2006; Dwivedi et al., 2019; Engel et al., 2016; Gui et al., 2019; Jódar et al., 2017; Markovich, Dahlke, et al., 2019; Penna et al., 2014). A direct way for this endmember mixing could be to utilize the age of the water:

A relatively new way to investigate permafrost waters is the application of the mostly anthropogenic emitted radionuclide $^{129}I$. It was formerly used rarely for this purpose but

reveals a great potential to distinguish between waters formed before and after the beginning of the nuclear age (Herod et al., 2016; Kamleitner et al., 2019) and therefor, information about permafrost passive layer (Buraglio et al., 2001; Fabryka-Martin et al., 1985; Hou et al., 2009; Osterc & Stibilj, 2011; L. Y. Zhang & Hou, 2013). In a small catchment in the Yukon Territory, Canada, which is dominated by discontinuous permafrost and has a big relief a major contribution of pre-event waters was found (Boucher & Carey, 2010). To conclude, what these findings show is that conventional water parameters as described above can be combined with the radionuclides emitted by human activity since the atomic age set in. This can be done by relatively easy water sampling methods as field work.

## 1.3 Goals and limitations

Considering the thawing speed of ice in mountainious regions, there is a strong need for further research on permafrost and rock glaciers (Jin et al., 2022; Jones, Harrison, Anderson, et al., 2019; Klaus & McDonnell, 2013). Especially the hydrologic behaviour of this ground ice needs to be known better (Jin et al., 2022). Few is known about discharge behaviour, dynamics, water quality and ice volume (Jones, Harrison, Andernson, et al., 2019), but also the pathways permafrost melt waters take and their contribution to streamflow are hardly known (Arenson et al., 2022). According to Jones et al. (2019) and Jin et al. (2022), especially hydrochemical studies are important, besids research in the fields of geocryology and hydrogeology. Learning more about degrading permafrost will enable a general improvenment of water resources management (Jin et al., 2022).

This call for research shows the relevance of this thesis at hand. In its course, the question of appropriate methods for investigating permafrost thaw will be adressed. More precisely, whether the combination of $^{129}I$ and stable isotopes ($^{2}H$ and $^{18}O$) is an applicable method to detect and quantify permafrost degradation in an inner alpine valley.

$^{129}I$ is used as an environmental tracer in different fields (see chapter 3.4.5). Lately, it has also been used successfully to explore the age of high alpine spring waters (Kamleitner et al., 2019). Thus, the assumption this research is based on is the following: The basic concept of $^{129}I$ as a tracer for permafrost degradation already

showed its applicability in comparable environments. In combination with other well-known water tracers, this concept can be applied to a small high alpine catchment, dominated by rock glaciers as permafrost form. With additional information about runoff volumes, the rate of permafrost passive layer melt can be calculated.

Based on this, three research questions are addressed. First, it is of interest if water samples coming from different sources differ significantly from each other in their isotopic signature. This marks the basis for further analysis. In detail, research question 1 is formulated as follows:

***Research question 1**: Is there a significant difference in the geochemical signature of glacier ice, rain waters, and spring waters in a small alpine catchment?*

*1.1. …in the footprint of the stable isotopes $^{18}O$, $^{2}H$, and the anthropogenic isotope iodine-129 ($^{129}I$)?*

*1.2. …in other parameters (temperature, EC, deuterium excess)?*

Answering these questions will entail the approvement of the method. Based on that, a better understanding about the alpine water balance can be achieved by facilitating the method for permafrost and rock glaciers research. In a next step, a detailed look on the situation in a high alpine valley follows:

***Research question 2**: In a small mountain catchment:*

*2.1. Can a seasonal trend be found in $^{129}I$-concentration?*

*2.2. Where are the springs located that are interpreted as permafrost fed?*

A campaign design with subsequent sampling throughout a summer season gives the opportunity to investigate time dependent trends of $^{129}I$-concentrations. Increasing passive layer melt water (old water) fractions towards the end of a summer season could result in decreasing $^{129}I$-concentration. A view on spring-locations with higher and lower $^{129}I$-concentrations can entail an insight into geographical patters. If such patterns became visible, findings of this study can be transferred to similar environments. Further permafrost research would benefit from that knowledge. Even if there is no

specific pattern recognizable, this finding would still ease further research. For the location of the Kaiserbergtal Valley some detailed specific drainage-characteristics such as spring-location will become known exactly. As a subsequential question to a positively answered research question 1 follows.

***Research question 3**: How much of springs' runoff is fed by permafrost passive layer?*

*3.1. Which percentage of springs' runoff is fed by passive layer?*

*3.2. At which rate does the passive layer melt?*

There are already studies on permafrost and rock glacier discharge. The result of this questions will give an insight to mountain block discharge behaviour and add a puzzle piece towards a better understanding of permafrost melt to get a better picture of future water resources. Especially in the Andes, where rock glaciers already constitute the most important water source (Jones, Harrison, Anderson, et al., 2019), the findings of this research will be of relevance. At the same time, it will enable future research on the development of the Kaiserbergtal rock glacier and its runoff.

The aim of this study is to contribute to closing some of the existing research gaps and follow upon calls of earth scientists for further research in the field of hydrogeology and hydrochemistry of permafrost and rock glaciers. One important goal of this thesis is to investigate this new field of application for $^{129}I$, which has been used little for the time being. Gathering information on relative age of waters with the help of $^{129}I$ poses a great potential towards other aging methods. There is a potential for overcoming the problem of future's limited usability of tritium ($H_3$) as a tracer due to its short half-life of 12.3 a. Keeping the climate crisis in mind, it will be of more and more importance to understand permafrost hydrology better as it marks a water resource of growing attention.

While this thesis will contribute to closing the research gap in the understanding of the contribution of permafrost melt waters to streamflow in a small case study, it cannot be expected that the following research gives a detailed picture of the discharge regime in the investigated valley. Due to limited resources the sample size and sampling period are not sufficient for that, and answers can only be taken as evidence of the applicability of the method in a high alpine environment like the Kaiserbergtal Valley (see chapter

2). From looking at the results, it is not possible to make conclusions on permafrost in general. For this purpose, the sample size is too small. But it can give hints on trends and enhance investigations on how much of this ice is melting from permafrost in the Austrian Alps. Questions of a broader usage must be subject of future research. Moreover, the knowledge of exact permafrost volumes is crucial for answering the question of how long permafrost will be present in Alps if climate forecasts are accurate. The amount of stored water cannot be calculated with the here presented method. This method can only provide a thawing rate of permafrost passive layer but no absolute passive layer volumes.

## 1.4 Organisation of the study

This thesis is structured into five main chapters. In the first chapter, the fundamental structure and aims of the study as well as background information on the subject matter are given. A special focus of the study lies on rock glaciers as the main expression of permafrost in the researched valley, as well as stable isotopes and $^{129}I$ as the key tracers for their investigation. The second chapter introduces the study area, the Kaiserbergtal Valley, where field work for the study was done. Briefly, some key aspects like location, geology, climate, geomorphology, and hydrology are discussed. In the third chapter, an overview of the chosen methods follows, before in chapter 4, the results are presented. Finally, chapter 5 discusses the results and chapter 6 sums things up including thoughts about the impact of this study for future research.

The study design aims to answer the demonstrated questions (see chapter 1.3) with the background of the state of the art in the fields of permafrost research (see chapter 1.2) and isotopic hydrogeochemistry (see chapters 3.3 and 3.4). To gain data for answering the research questions, investigations in an appropriate location are crucial. The field work was done in the summer months of the year 2018 in Kaiserbergtal Valley (see chapter 2) from July to September in a monthly interval. Water samples were analysed regarding their isotopic ratios of $^{2}H/^{1}H$ and $^{18}O/^{16}O$ by a specialized laboratory (AgroIsoLab GmbH, Germany). As a second major analysis tool, the content of the anthropogenic iodine isotope $^{129}I$ is quantified. This information will be based on carefully taken samples which were analysed with a specialised sample preparation technique at the Vienna Environmental Research Accelerator (VERA) at the faculty of

physics in Vienna (see chapter 3.4.6). A combination of those $^{129}I$ analysis, $^{2}H/^{1}H$ and $^{18}O/^{16}O$ ratios and other well-established techniques led to answers for the research questions set in chapter 1.3.

# 2 Study area

For environmental studies, the selection of the right location is a delicate task, because it must meet specific requirements. For the study of high alpine permafrost, a list of obvious and some at first glance not too obvious requirements must be met. As an area for hydrological systems, a catchment with good defined watersheds is of importance to have an accurate picture of precipitation drainage in the area and to exclude the possibility infiltrating waters from unexpected areas. An underlaying aquifer could interact with seeping atmospheric waters or freshly thawed ice. The area must be situated in high altitude with permafrost occurrence, which starts in altitudes varying from 2,000 m.a.s.l. in north facing slopes to over 3,000 m.a.s.l. in south facing slopes in Austria (Schrott et al., 2012). In this study, rock glaciers are in the focus. An alpine valley with many rock glaciers can meet those requirements very well and can be chosen by analysing pre-existing high resolution orthophotos, airborne laser scan data and literature.

The Alps are well investigated and underlaying studies provide a good understanding of the area in geological time scales (see chapter 2.2), as well as its precent condition reaching from permafrost distribution to meteorological information (see chapters 2.4 to 2.7). To support the methodological approach of isotope analysis and distinguish between recent precipitation and old ice-sourced waters, all those endmembers must be present. The most challenging of those requirements might be accessible guaranteed old ice. A reliable source for old ice is ice from the lower centre like the glacier snout. The statistical validity can benefit from a big number of samples, therefore a valley with many small springs is optimal. The workability in the field benefits from a moderately sized investigation area because alpine environments are often not accessible for motorized vehicles and sometimes even hard to access by foot. Finally, an easily accessible area is a significant simplification. An appropriate research area had to be found.

## 2.1 Location

All required characteristics discussed above are met in the upper Kaiserbergtal Valley. The Kaiserbergtal Valley is an almost 14 km² sized valley located in the federal state of

Tyrol, more precisely in the Kaunertal Valley in the district of Landeck (see Fig. 5). As a side valley of the Kaunertal Valley in the Ötztal Alps with a west-east orientation, it is situated between the Oberinntal Valley/Radurschltal Valley and the Kaunertal Valley. Its course is slightly curved, the upper part is west-east orientated, and the lower part is south-west north-east orientated. The catchment size of the investigated upper Kaiserbergtal Valley is 6.63 km². The elevation of the research area ranges from 2,450 m.a.s.l., just before the discharge of the hydrological separated Kaiserbergferner enters the stream, to the highest peaks with 3,200 m.a.s.l.

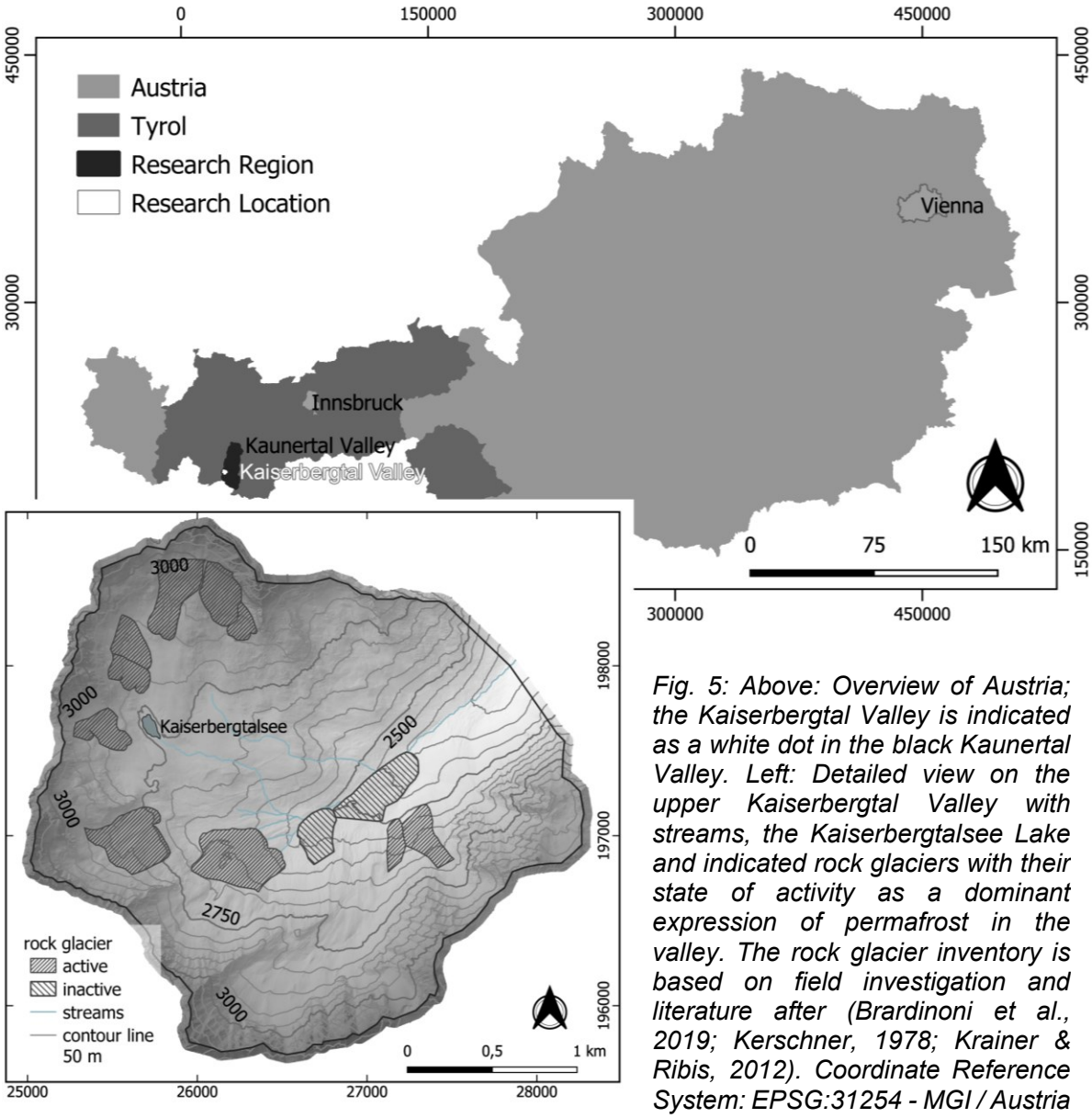


*Fig. 5: Above: Overview of Austria; the Kaiserbergtal Valley is indicated as a white dot in the black Kaunertal Valley. Left: Detailed view on the upper Kaiserbergtal Valley with streams, the Kaiserbergtalsee Lake and indicated rock glaciers with their state of activity as a dominant expression of permafrost in the valley. The rock glacier inventory is based on field investigation and literature after (Brardinoni et al., 2019; Kerschner, 1978; Krainer & Ribis, 2012). Coordinate Reference System: EPSG:31254 - MGI / Austria GK West*

First scientific work in the Kaiserbergtal Valley was done by Kerschner (1978) and continued by Karl Krainer and others in the 1990s. The Kaiserbergtal Valley gained more and more attention as a research area and is now a well explored study site for various earth scientific fields (Brardinoni et al., 2019; Groh & Blöthe, 2019; Hausmann et al., 2012; Krainer & He, 2006; Krainer & Mostler, 2002). Brardinoni et al. (2019) made the most recent rock glacier inventory with nine rock glaciers in the upper part of the valley in different states of activity. The basis mapping of their inventory was done by field work and geomorphological mapping of Karl Krainer. Thanks to his and other substantial work, much is already known about rock glaciers in the valley (Hausmann et al., 2012; Kerschner, 1978; Krainer, 2011, 2015a; Krainer & He, 2006; Krainer & Ribis, 2009, 2012). An important characteristic of the selected research area is the residual glacier within the research area. It is very likely that there is no hydrological connection of the south-eastern part with the glacier and the rest of the valley, due to a hypothetical watershed, indicated by topology and moraines of past glaciations (see chapters 2.3 and 2.4). Following, the assumption can be made that all old waters in the northern part are originated from permafrost.

## 2.2 Geology

Geology depicts the appearance of the world. From the beginning of the universe to recent times everything is in motion and continuously reshaping. Today, the alpine range is still undergoing orogenesis. Recent uplifting rates in the region of the Tyrolian Alps are considered around 1 mm/a (Sternai et al., 2019).

The research area is situated in the Ötztal nappes, which are part of the Eastern Alps. The Ötztal nappes are, together with the Silvretta nappes, the crystalline basal complex of the Upper Austroalpine nappes (Pfiffner, 2014, p. 245). Stratigraphically they are situated in between the Northern Calcareous Alps above and the deeper laying Penninic units (Pfiffner, 2014, p. 296). Kaindl et al. (1999) divide the evolution of the Ötztal nappes in three major metamorphic events. The high-temperature metamorphosis in the Caledonian (0.45 ga) is dominated by migmatites. The high-pressure regional metamorphosis in the Variscian (0.32 ga) “characterizing the mild pressure dominated part of the amphibolite facies” (Tollmann, 1985), is dominated by eclogites and amphibolites. Purtscheller & Sassi (1975) constitute metamorphosis near

the alumosilicates triple point for the Ötztal Crystalline with mainly andalusite occurring in Kaunertal Valley, also shown in the map 'Geologische Übersichtskarte der Republik Österreich' of the geological federal institute auf Austria (GBA) (Schuster et al., 2015). The third metamorphic event is the geographically diverse Eo-Alpine metamorphism (ca. 0.1 ga) (Kaindl et al., 1999). This Alpine metamorphism reached greenschist-facies conditions in Kaunertal Valley. Only towards the south-east, aluminosilicates show higher metamorphic grades (Hoinkes et al., 1999, 1997; Tropper & Hoinkes, 1996).

Following the GeoFast Map number 172 by Krenmayr (2016) and a historical map by Hammer (1923), a majority of the bedrock is consisting of orthogneiss in shapes of augen gneiss and flaser gneiss, the latter is characterized by a distinctive greater foliation. Following Krenmayr (2016) in the south-western part of the research area muscovite garnet and muscovite garnet gneiss are prevailing. Moreover, Strauhal et al. (2017) describe the area around the Gepatsch Reservoir in the Kaunertal Valley as para gneiss dominated with some ortho gneiss and minor volumes of amphibolite. This literature-based information could be verified in the field.

## 2.3 Past glaciations

Within late glacial times in the Alps, at the end of the Würm Stade (respectively Weichsel Stade in northern Europe), the big glaciers started shrinking. This process continues until today. Glaciers did not shrink continuously but in repetitive phases of rapid shrinking, stagnation, and episodes of regrowth of mostly smaller extent (Schmidt, 2009). As remnants of these cycles, stade moraines can be found in the field. Most areas of Kaiserbergtal Valley are thought to have experienced glaciation in the Daun Stade, and also in the following Egesen Stade with slightly smaller extents (Kerschner, 1978). The Egesen Stade during the younger Dryas (Patzelt et al., 1976) was the latest series of glacial extensions in the Tyrolian Alps reaching maximum extension 12.3 to 12.4 ka BP (Kerschner & Ivy-Ochs, 2008). Following Kerschner (1978), the research area in the upper valley was definitely covered by the Kaiserbergferner glacier these times (solid medium and thin lines in Fig. 6). 10.5 ka BP, the big glaciers of the Alps were smaller than today (Nicolussi et al., 2001). The picture of oscillated shrinking and regrowth continued. In modern times, the latest glacial advances happened in the 1820s and the 1850s (dashed lines in Fig. 6) building a remarkable moraine, which can

be found over wide areas of the Austrian Alps known as the '1850s moraine' (Holzhauser, 1982).

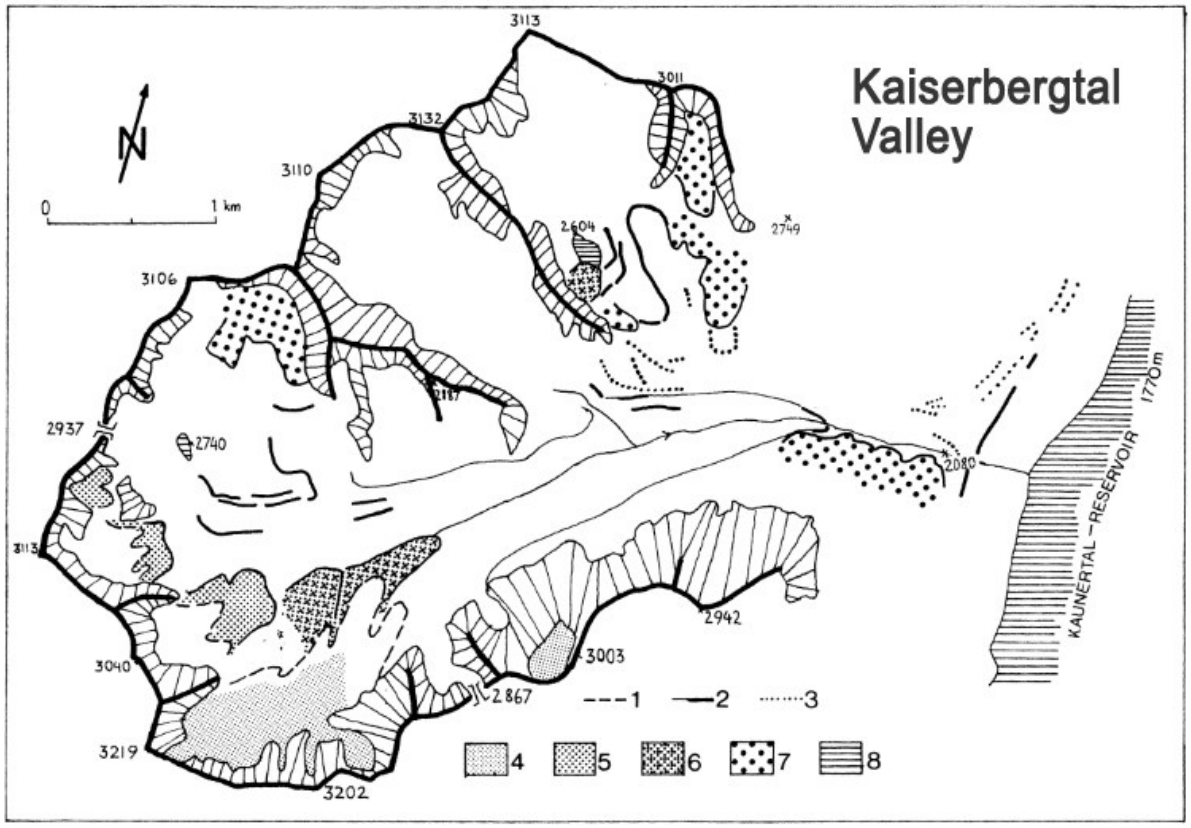


*Fig. 6: "Kaiserbergtal. Western Ötztal Mountains, glacial and periglacial deposits. (1) Mid-19th century extent of glaciers; (2) Egesen Stade moraines (medium line) and hypothetical extent of Egesen Stade maximum (thin line; (sic!) (4) extent of glaciers in 1940; (5) active rock glacier; (6) inactive rock glacier; (7) fossil rock glacier; (8) lake; elevations in m.a.s.l." (Kerschner, 1978); fig. after Kerschner (1978b)*

## 2.4 Geomorphology

Geomorphological processes gave the valley its present appearance. They determine its shape, but also influence the water regime for both, groundwater and surface water, to a great extent. In the last 50 years, several rock slides occurred in the Kaunertal Valley. This shows how prone the gneisses of the Ötztal Crystalline nappe are to rock slope activity (L. Vehling et al., 2017). In the upper Kaunertal Valley, the glacier eroded valleys and remaining big moraines and cirques dominate the landscape. Rock slopes feed into talus slopes and rock glaciers, which is another sign of large-scale rock slope activity. No high vertical rock walls can be found, while the rock slopes in the valley are steep with an average inclination around 50° (L. Vehling et al., 2017).

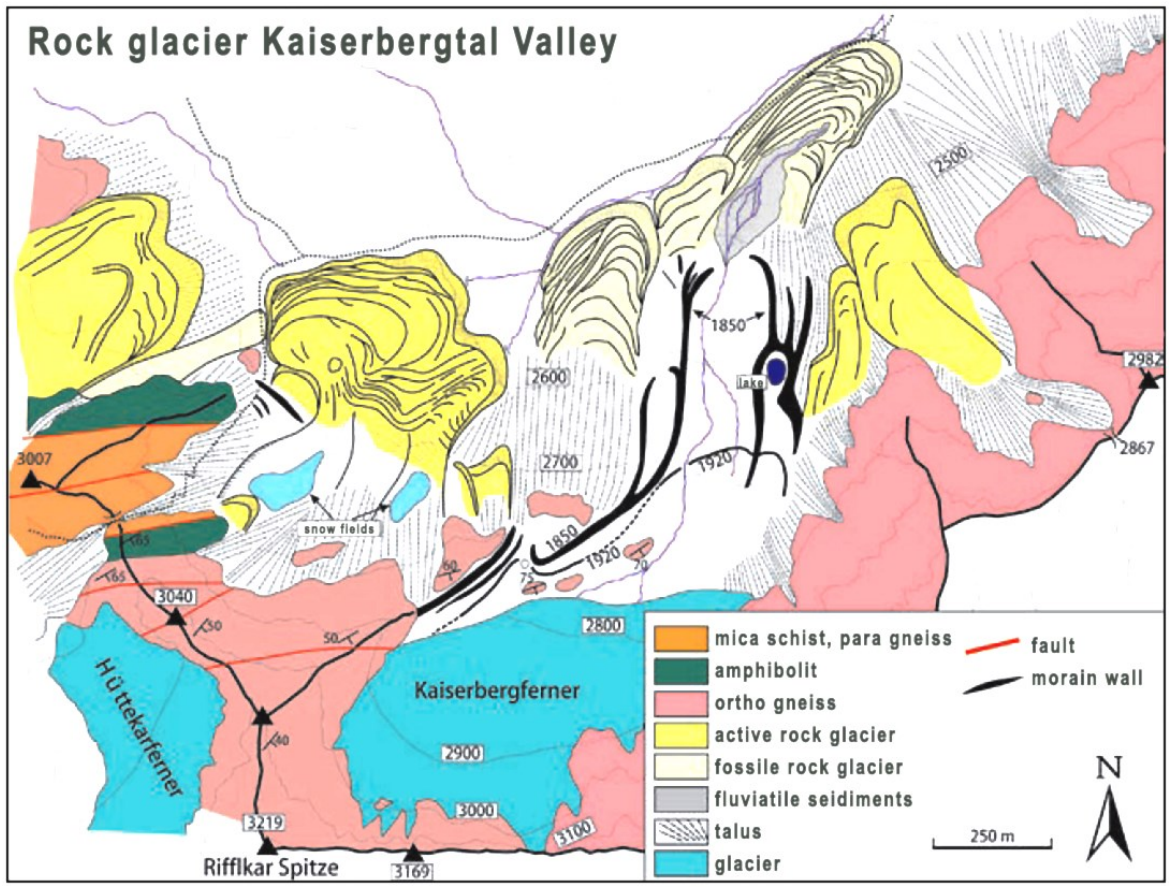


*Fig. 7: Detailed geomorphological map of the southern Kaiserbergtal Valley from the early 2000s with lithology and geomorphologic details showing rock glacier occurrence; translated after Krainer (2015).*

In the Kaiserbergtal Valley, the following stone types can be found: mica schist, para gneiss, amphibolite, and ortho gneiss. The mountain range in the upper valley consists primarily of ortho gneiss. In the west however, there are some mica schist, para gneiss and amphibolite. Glaciers and rock glaciers shape the landscape of the valley. The Kaiserbergferner glacier has nearly disappeared until today: It reached below 2,600 m.a.s.l. in 1850, today its end is located at an altitude of 2,900 m.a.s.l. and there is only a small glacier left. Moraine walls show its former extent. Following the moraine of the former Kaiserbergferner Glacier walls downhill, a cirque filled with water can be found. Further down, fluviatile sediments on the former rooting zone of a fossil rock glaciers show the recent melt water discharge regime. Above this fossil rock glacier, a little uphill, there are various active rock glaciers on the north and west facing slopes. Their present movement becomes visible by looking at their characteristic rock glacier tongues with high inclinations. They are moving through big fields of talus that, based

on the valley's geology seen in Fig. 7, primarily consist of ortho gneiss and in some extent of para gneiss.

## 2.5 Modern permafrost and rock glacier inventory

The present state of permafrost in the Kaiserbergtal Valley is a result of its geological history and the climate state. The formation of the Alps and the uplift of the continental crust led to the west-east orientation of the valley. Climate variations in the Holocene led to geomorphological processes including major glaciations and their relics resulting in the current appearance of the valley and consequently, to the present permafrost distribution. As the following map (see Fig. 8) shows, permafrost is very likely to occur

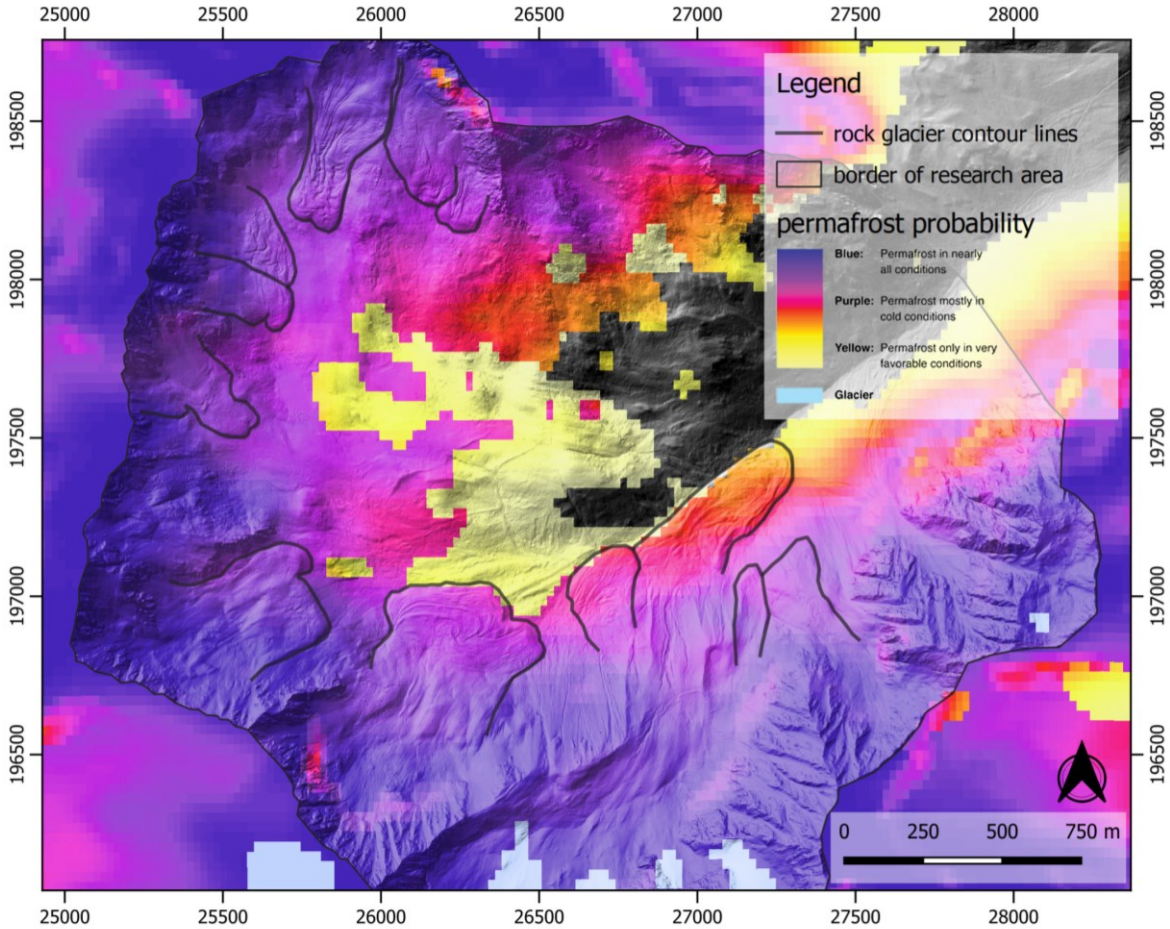


*Fig. 8: High resolution local scale map of the Kaiserbergtal Valley indicating high probability of permafrost occurrence in violet to lower probabilities in yellow. All active rock glaciers are situated in areas marked coloured in the spectrum of violet to pink. Data retrieved from Alpine Permafrost Index Map (APIM), (2018). Coordinate Reference System: EPSG:31254 - MGI / Austria GK West*

in all aspects and conditions of the underground in the higher parts of the research area. Towards lower elevations, permafrost probability decreases, indicated by pink and orange colours. The geographical centre of the area, including the exposed glacier-grinded ridge in the east of the Kaiserbergtalsee Lake, has a low probability of permafrost occurrence following the Alpine Permafrost Index Map (2018).

As already stated, rock glaciers make up the main form of permafrost in the Kaiserbergtal Valley. The here used rock glacier inventory (see Fig. 5 and Fig. 8) is based on former research done in the area. The most recent rock glacier inventory was done by Brardinoni et al. (2019). The best researched main rock glacier by Krainer (i.e. 2015) in the centre of the research area marks the lowest point of obvious permafrost occurrence in the valley. The smaller rock glacier in the east of it and the orographically following lowest rock glacier are described as inactive by Kerschner (1978) and as relict by Krainer (2015). The main rock glacier, first described by Kerschner (1978), is an impressive landmark and can be used as a point of orientation. It is located at 26 200 m, 196 800 m (easting, northing in MGI / Austria GK West) and was already investigated with a variety of methods by Brardinoni et al. (2019), Groh & Blöthe (2019), and Krainer & Mostler (2002), to name just a few. Brardinoni et al. (2019) constitute the orographically rightmost lobe of this rock glacier as highly active with velocities greater than 2 m/a, and the left and central part as less active to inactive. In general, active rock glaciers in the Kaunertal Valley catchment show average moving rates of several decimetres per year, the most active rock glaciers are exposed towards northeast and northwest (Groh & Blöthe, 2019). Helmut Hausmann et al. (2012) calculated an ice content of 45 to 60 % in the central part of the main rock glacier. So, there is a solid data basis for further research.

## 2.6 Climate

The climate in the Alps is defined by the orographic situation. The west-east orientation of the main alpine ridge causes a weather divide and leads to complex conditions, also due to a small-scaled, diverse relief (Gressel, 1973). Nevertheless, weather conditions in the Alps are better known than hardly anywhere else on earth. First records of meteorological data in the Alps began around 1800 on precipitation, followed by hours of sunshine, snow depths, and others in the following decades. In general, amounts of

precipitation are increasing with the altitude and most precipitation is falling in the highest levels. Regions like Valais in Swiss and Tyrol in Austria are enclosed by high mountains and, therefore, dryer than other regions in the Alps. The east-west orientation of alpine valleys makes precipitation fall on the northern and southern mountain ridges. Those factors make the Inntal Valley in the Tyrol one of the driest regions with a continental character and precipitation as low as 700 mm in some locations. It is characterized by the majority of precipitation falling in summer and a drier winter period (Barry, 2008, p. 386-397).

The Kaunertal Valley experiences monthly mean temperatures between -4.6 °C in January and +14.0 °C in July (see Fig. 9). Between 1953 and 2017, the mean temperatures in the research area increased, according to Fleischer (2021). At the meteorological station of Nauders at an altitude of 1,330 m.a.s.l., an increase of 1.29 °C could be observed, while at the station Obergurgl-Vent (1,938 m.a.s.l.), temperatures rose by 1.92 °C. The higher increase of temperature in accordance with the higher altitude can be explained through the general trend that alpine temperatures increase faster than temperatures on the global average (Beniston, 2006, as cited in Fleischer et al., 2021). The highest increases in temperature happen during spring (2.73 °C) and summer (2.64°C), whereas they are lower during winter (1.6 °C) and autumn (0.69 °C) (Fleischer et al., 2021).

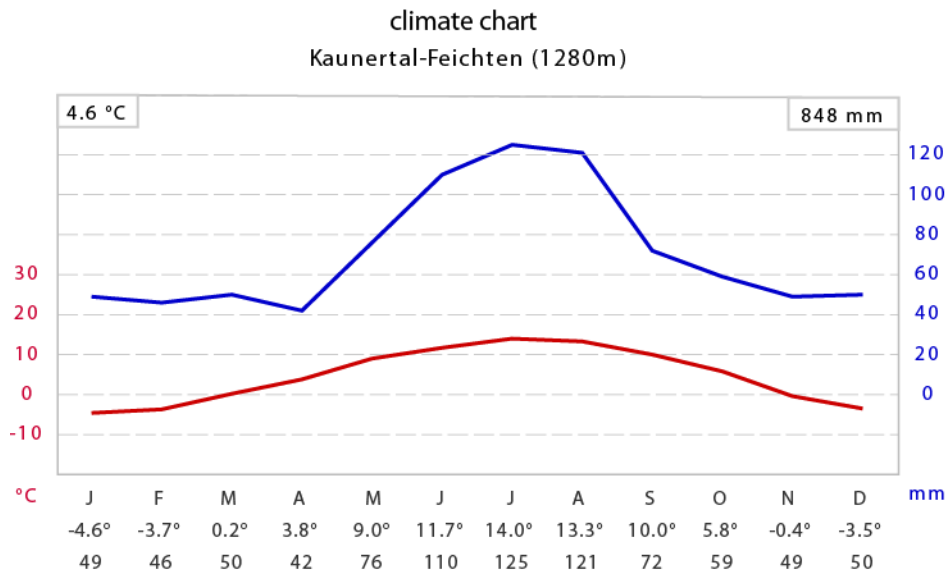


*Fig. 9: Climate chart of the nearest climate station in Feichten, located 13 kilometres out of the valley in the town of Feichten. The red line shows monthly mean temperatures in the period of 1980 to 2000, the blue line shows accumulated monthly precipitation in the same period; after Hydrographischer Dienst Tirol (2013).*

### *2.6.1 Wind*

The large-scale weather pattern in Europe is generally dominated by weather coming from the Atlantic moving eastwards across Central Europe (Gressel, 1973). According to the Wind Atlas of Austria, the Kaunertal experiences average wind speeds of 1 m/sec measured 100 m above the surface. These wind averages count to the lowest in Austria and are 2.5 to 5 m/s slower than the average winds in the surrounding mountain ridges Kaunergrat in the east and Glockturmkamm in the west. The upper Kaiserbergtal Valley, situated eastern of the Glockturmkamm Ridge, experiences annual mean wind speeds between 2 and 5 m/s in an elevation of 100 m above the surface. The valley floor experience much lower wind velocities (2 – 4 m/s) than exposed locations near the ridges (4 – 6 m/s). All values of the Austrian Wind Atlas are given with an uncertainty of 0.8 m/s based on cross validation (AuWiPot – Windatlas und Windpotentialstudie Österreich, 2011). An important weather phenomenon in the Alpine region is the luv-lee effect which influences precipitation. At mountain slopes facing the wind (luv), rain and humidity get blocked and thus accumulate, leading to more precipitation. The slopes not facing the wind (lee), on the other hand, get less precipitation. The higher the mountain ranges surrounding a valley are, the higher is the blocking effect for precipitation. Valleys and mountainsides in the lee experience föhn, “a warm, dry, downslope wind descending […] as a result of synoptic-scale, cross-barrier flow over the mountain range” (Defant, 1951) (Gressel, 1973; Haid et al., 2022).

### *2.6.2 Precipitation*

The general pattern of precipitation in the region is already discussed in the introduction to climate. Data with high resolution was collected at the Gepatsch reservoir dam 4 km northwest of the research area as a nearest point. Data was provided by the Tirolean Hydropower AG (TIWAG) and retrieved from the hydrological service of Tyrol (HD-Tirol) in 2021. Following Fig. 10, the winter before the sampling campaign most precipitation fell in January, followed by a drier period until mid of May. For the summer months, regularly falling precipitation in moderate amounts was registered with the exception of a dry period between 24$^{th}$ July and 13$^{th}$ August.

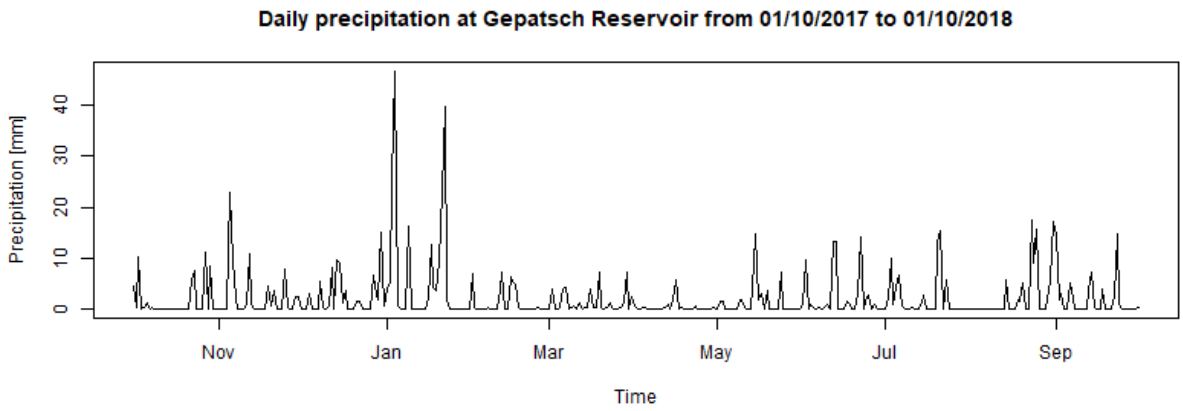


*Fig. 10: Accumulated daily precipitation for the year of the study and the winter period before (01-10-2017 to 01-10-2018); data retrieved from HD-Tirol (2021)*

A rain sampler inside the Kaiserbergtal Valley, on the half way to the research area, was sampled monthly with accumulated rain of 95 mm, 207 mm, and 74 mm for July to September, respectively (data derived by (HD-Tirol, 2021)). As those two stations show a very different picture within only 4 km geographical distance, precipitation seems to be distributed locally. Moreover, precipitation shows great monthly variability (Lucas Vehling, 2016).

Overall, the Kaunertal Valley with its side valleys is rather dry compared to both the Northern and Southern Alps. As already mentioned above in the introduction to this chapter, the reason for this local dryness is the situation as an inner Alpine valley surrounded by high mountains and luv-lee-effects. Additional precipitation might be provided by fog (Veit, 2002).

## 2.7 Hydrology

Surface water in the Kaiserbergtal Valley drains through the Kaiserbergbach Creek. It originates from the Kaiserbergtalsee lake and ends in the Gepatsch reservoir after 5.58 km. The Fagge River then leads to the Inn River. Based on the geological background (see chapter 2.2) it is unlikely that water drains into the valley from unexpected areas outside the obvious orographic catchment. Several perennial and episodic spring are located on the flanks of the valley. Most of them arise from rock glaciers or beneath talus fans. In the following, the drainage regime in the valley will be described for the snow-free part of the year.

In the upper valley, at an altitude of 2,750 m.a.s.l., there is a lake called Kaiserbergtalsee with approximately 8,100 m² (see Fig. 5 in chapter 2.1). It is surrounded by talus slopes in the north and west, which appear to be the major source of inflow. A second perennial source of water is originating from a rock glacier in the north. The lake is draining through the Kaiserbergtalbach Creek, which flows partly on surface, partly in subsurface, especially in the upper valley. The majority of discharge enters the surface again at the Egesen Stade moraine wall at 2,650 m.a.s.l., before merging with drainage from the western part of the valley.

Krainer & Mostler (2002) did case studies on active rock glacier hydrology in the Tyrolian Alps, and particularly in the Kaiserbergtal Valley. Rock glacier hydrology in the research area is dominated by local weather, the thermal properties of the debris layer and the pathway of meltwater through the rock glacier (Krainer & Mostler, 2002). They also monitored discharge rates of the main rock glacier in the centre of the research area marking a landmark. A baseflow of about 100 l/s in summers with peaks of 600 l/s caused by snowmelt in two weeks of hot weather was recognized. Rutzinger et al. (2014) measured a baseflow of 150 l/s in winter and discharge up to 600 l/s in the summer season. Moreover, they measured typical rock glacier discharge temperatures of 1 °C in winter and up to 4 °C in summer rain periods. Measurements of Kraushaar & Blöthe (2022) at a gauging station just beneath the rock glacier confirmed the summer baseflow and annual continuity. In a comparable catchment, named Innere Ölgrube, precipitation is usually drained within one to two days (T. Wagner, Kainz, Krainer, et al., 2021). Similar values are presumed for the research area.

A nameless creek originates from rock glaciers in the north-east of the lake. In the upper part of its course, fluvial sediments indicate a seasonal inflow to the lake. Most of the year it drains slowly subparallel to the major creek through a wetland-like environment, entering it at an altitude of 2,460 m.a.s.l. next to a fossil rock glacier.

Like described in chapter 2.3, there are only remnants left of the Kaiserbergferner Glacier located in the south-west of the valley, between the summits of Riffkarspitze and Kaisergratspitze. The runoff of these glacier relicts is likely separated by moraine walls from the Kaiserbergbach Creek in the upper part of the valley and only enters the main stream mostly subterraneous through a relict rock glacier on the eastern end of the research area. A small pond formed by a terminal moraine is situated on the

orographically right slope on a terminal basin. No signs of surface discharge could be found.

# 3 Methods

A broad range of activities had to be done to receive the findings, beginning with the planning of field work, acquisition of data, laboratory work to statistical analysis and embedding the results in the state of the art. The following describes the used approaches of the workflow and some essential theory on the methods.

## 3.1 Acquisition of data

A sampling procedure was established at the first sampling point and replicated at every following point in order to guarantee a continuous treatment and thus obtain comparable samples of high quality. Sampling points were first visited in a five-day field campaign in late July 2018 starting with the lowest locations at first, followed by more remote parts of the valley in the following days. Every spring was measured in the exact same way with the same sequence of tasks to guarantee an accurate and reproduceable sampling for comparable data. Every sampling point was named with an ID in the format of KB followed by 2 digits of continuous numbers and the sample type (SI – stable isotope; I – $^{129}$I), and pictures were taken. The inclination of the surrounding terrain was documented.

*Fig. 11: Water sampling from ice of the leftover of the Kaiserbergtal Glacier*

As a first step at each sampling point, a handheld GPS device was placed next to the spring while the sampling was done so it had sufficient time to calibrate and provide an exact location. Time and date were noted. A short, written description of the sample location and the ground material was done. The handheld digital conductivity meter GMH 3430 of GREISSINGER electronic GmbH was used to gather EC in µS/cm and temperature in °C within the sampling routine. For accurate and comparable results, the measuring probe was put approximately 5 cm under the water level for at least two minutes. The values were taken once the values remained stable for at least 5 seconds to guarantee accuracy. For glacier, rain and snow samples, EC was measured in a PET bottle.

Within the sampling routine, the most important task was taking water samples of stable isotopes and $^{129}I$. Stable isotope samples were taken with special sampling vials. For springs, the vials were rinsed two times with spring water before taking the final sample. Then the samples were collected, whereby care was taken to prevent sediment and organic material to enter the vial. Furthermore, it was made sure that no air was kept in the sampling vial (see Fig. 12). Glacier samples were taken from freshly molten water dropping from beneath the glacier snout (see Fig. 11). Snow samples were taken in 0.5 litre PET bottles and decanted in the small sampling vials after melting. Surface water samples were collected by submerging the vials. Rain samples were taken from the rain sampler and on a rainy day a sample could be collected from a little pond freshly formed on a stone.


*Fig. 12: Stable Isotope sampling vial next to spring KB06*

For the analysation of $^{129}I$, a sampling volume of 500 ml is a requirement (S. Szidat et al., 2000). $^{129}I$ samples were taken in commercial 0.5 litre mineral water bottles, made of Polyethylene Terephthalate (PET). The emptied bottles were rinsed for 1 minute with 1 M HCl * H2O (MilliQ) and three times with pure MilliQ water prior to field work. In the field they were rinsed two times with spring water and then filled with spring water (Geboy & Engle, 2011). Special attention was given to fill the bottles without air bubbles to prevent fractionation processes between water and air. Then, the PET bottles were instantly wrapped with two layers of aluminium foil (see Fig. 13) to prevent the samples from photoreactions with UV-rays. Samples of glacier, snow, surface water and rain were taken similarly to stable isotope samples.


*Fig. 13: Freshly wrapped 500 ml water sample for $^{129}I$-measurement in the field*


*Fig. 14: Rain Sampler in the Kaiserbergtal Valley*

The rain sampler had to match specific requirements for gathering high quality samples for hydrochemical analysis. Most important is an evaporation free sampling mechanism which was ensured by the Palmex Rain Sampler RS1 (Gröning et al., 2012). It was installed below the main rock glacier in flat terrain in a central position of the valley (see Fig. 14).

Rain and glacier ice samples were taken as endmembers in the analysis and are of immense importance for putting spring samples in relation to each other and finding their origin (see chapter 3.6). Duplicates were made as so-called total analytical duplicates, taken simultaneously in the routine, treated in the same way until they were analysed as individual samples (Geboy & Engle, 2011, p 12).

In the following months, the research area was visited two more times over the summer period in 2018 in a monthly interval for repeated water sampling. The first field campaign took place in late July and was followed by campaigns in late August and late September 2018.

## 3.2 Discharge measurement

The knowledge of spring discharge volumes is crucial to estimate the distribution of sub-catchments to the discharge of the valley. In this study it is also important as a factor for calculating the permafrost melting volumes. Discharge in alpine environments can be measured with the help of tracers.

A tracer is a substance that gives information about a natural system which cannot be gained directly (Kralik, 2018). Environmental tracers are components of the water cycle which can be either dissolved, suspended, or floating (Leibundgut et al., 2009). In hydrology, environmental tracers are used to find out how runoff is generated, to address the origin of waters, describe flow pathways and transit times. Due to their property of flowing inside the water system, they are of main importance for questions in the field of soil- and groundwater research, where the use of other observation methods is limited (Leibundgut & Seibert, 2011). There are basically two groups of tracers: Natural tracers are in the water cycle by nature, science uses their existence and behaviour to gain information about a system. Artificial tracers are put into the system additionally in planned experiments (Leibundgut & Seibert, 2011).

As most mountain streams have small cross sections, irregular riverbeds and a quite turbulent flow, the velocity-area method is not practicable. Therefore, techniques with chemical tracer injection are preferable. There are three types of tracer methods in use: first, the dilution method with constant injection where a solution with known concentration is injected continuously. Second, the integration method with instantaneous injection of a dissolved tracer material all at once. Third, for the hydraulic integration method, instantaneous injected tracer like in the integration method is sampled by continuously flowing into a sampling container, resulting in a batch with average concentration (Ralf et al., 1990). The most applicable method in high alpine environment is the integration method, the hydraulic integration with an instantaneous injection of tracer and the measurement of electronical conductivity (Ralf et al., 1990).

The principle is the complete mixing of the tracer with the river water, followed by measuring the tracer concentration further downstream. With a salt tracer, the amount of water in a stream can be estimated. This method can estimate the real flow with a precision up to 5 % (Day & Day, 1977; Johnstone, 1988; Leibundgut et al., 2009, p. 187; Moore, 2003).

Salt is injected in solid form as a fine-grained powder (Hudson & Fraser, 2008) with a certain mass (M). The required distance between input and measurement of the tracer is called the mixing length and depends on some factors: the higher the runoff, the higher is also the mixing length; meanders shorten the mixing length; the higher the roughness, the lower the mixing length (Leibundgut et al., 2009, p. 188). As a practical approximation, a distance equal to 25 times the river width is assumed to be enough for a homogeneous mixing of tracer and water (Hudson & Fraser, 2008). As the spring-runoff is estimated small, the roughness of the river bed is high, and mainly, the terrain does not allow to follow the rule of Hudson & Fraser, the mixing length was chosen smaller than the 25 times the width. The salt concentration of the natural background (c0) and the elevated concentration of the tracer (t1) is measured indirectly with an EC-meter (Ralf et al., 1990). The electrical conductivity can be taken as a proxy value for the salt concentration (Leibundgut et al., 2009, p. 107). Integrated over time from first arrival of tracer (t0) to the moment of disappearance (t1), the discharge can be calculated (Ralf et al., 1990).

$$Q = \frac{M}{\int_{t0}^{t1}(C_1 - C_0) * dt} \qquad \text{(Eq. 1)}$$

The calculation of water flows based on salt is done with tracer breakthrough curves (TBC). This equation must be adapted by a calibration factor (CF) derived by a calibration curve to correct local water conditions:

$$Q = \frac{M}{\int_{t0}^{t1}((c_1 - c_0) * CF) * dt} \qquad \text{(Eq. 2)}$$

For the estimated small spring discharge volumes in this alpine catchment, the mass balance method was chosen (Hudson & Fraser, 2008). It is based on the tracer mass and was first primarily described by Elder et al. (1990).

Electrolytes dissociate in water. The resulting solution makes water electrically conducting. Electrical conductivity (EC) is a physio-chemical parameter that gives the measure of mobile ions (Leibundgut & Seibert, 2011). EC can be determined by the resistance between two electrodes and is measured in µS/mc. Due to a higher ion mobility with increasing temperature, EC is temperature dependent and needs to be adjusted with a correction factor to normal temperature of 25°C. Typical values for rain water are between 5 – 30 µS/cm, ground water ranges be 30 to 2,000 µS/cm, whereas fresh alpine ground water usually shows values below 200 µS/cm (Cano-Paoli et al., 2019; Hölting & Coldewey, 2013, pp. 161-164).

EC is crucial for tracer-based discharge measuring with NaCl (Hölting & Coldewey, 2013), and can be used well for multivariate statistics like PCA (Andrianova et al., 2019; Buba Seli et al., 2019). The two parameters temperature and EC were measured with a single device from GREISSINGER electronic GmbH, model number GMH 3430. For discharge measurements, a weighted amount of salt (NaCl) is dissolved in water and injected into a stream. EC is measured after a distinct distance until it reaches the natural background value again. With these measurements the streams discharge can be calculated (Bolognesi et al., 2006). Sampling sites were chosen for specific reasons, they should represent the catchment as best as possible. Since it is not easy to measure discharge in alpine catchments due to the rocky surface and hardly accessible flow in between and underneath boulders, locations with feasible conditions are rare and unperfect conditions must be accepted (Bolognesi et al., 2006). For comparability reasons, measurements of different springs should be done under constant weather conditions. It must be considered that discharge fluctuates within different times of a day, as well as that previous rain influences discharge in the following hours and days (Krainer & Mostler, 2002).

## 3.3 Stable isotopes

The most commonly used tracers for environmental purposes are $^{18}O$ and $^{2}H$ in water samples (Klaus & McDonnell, 2013). Characterizing waters by those stable isotopes has a long history, based on the pioneer studies of Dansgaard (1953, 1954, 1959, 1960). The method was first applied in the 1960s (Dansgaard, 1964; Hubert et al., 1969). In the following decade, the method was refined with intensive work on $^{18}O$ by Mook et al. (1974), Fritz et al. (1976), and Sklash et al. (1976) and on $^{2}H$ by Klaus & McDonnell (2013), Herrmann et al. (1978), and Herrmann & Stichler (1980). Today it is a standard method with reference values for potential environments and a wide range of application, and it has been commonly used for more than half a century. In the late 1950s, the global network of isotopes in precipitation (GNIP) was founded in the USA to provide global monitoring data for isotopes (Aggarwal et al., 2005, p. 42). Nowadays the GNIP is situated in Vienna and provides easy access to a huge database regarding isotope measurements all around the globe (IAEA, 2022).

The utilisation of stable isotopes in science is based on the composition of water molecules. A water molecule consists of two hydrogen atoms (H) and one oxygen atom (O). At a closer look on those elements (see table 1), there are slight differences which are caused by the kinds of hydrogen and oxygen isotopes forming a water molecule what, in consequence, leads to a slightly different physical behaviour (Buttle, 1994).

*Table 1: The most common hydrogen and oxygen isotopes; retrieved from Holden et al. (2018)*

| **Stable isotope** | **Abundance [%]** | **Isotopic mass [$A_R$]** |
|---|---|---|
| **$^{1}H$** | 99.972 – 99.999 | 1.007 |
| **$^{2}H$ – Deuterium** | 0.001 – 0.028 | 2.014 |
| **$^{3}H$** | trace | 3.016 |
| **$^{16}O$** | 99.738 – 99.776 | 15.995 |
| **$^{17}O$** | 0.037 – 0.040 | 16.999 |
| **$^{18}O$** | 0.187 – 0.222 | 17.999 |

In nature all combinations of hydrogen and oxygen isotopes occur in water molecules with different frequencies. Due to their differences in isotopic mass ($A_R$), they react slower or faster in fractionation processes.

To understand processes in nature in general and the water cycle in particular, the ratios of specific isotopes proved to be most suitable. The ratios of $^{2}H/H$ and $^{18}O/^{16}O$ are the most common used (Leibundgut et al., 2009). For specific applications, specific isotope compositions of water are of major importance, as for studies on ice, $^{1}H_2{}^{16}O$, $^{1}H_2{}^{18}O$, and $^{1}H^{2}H^{16}O$ are the key isotopic compositions (Souchez & Lorrain, 2012). In any case, the analysis of waters is a delicate task because every precipitation event has a specific isotopic fingerprint which influences a hydrological catchment, and even within a rainfall event, the isotopic composition varies over time (Tappa et al., 2016).

### *3.3.1 δ-notation*

To compare the isotopic contents of samples, the δ-notation has proven as a practicable tool. As shown in Eq. 3, samples get always calibrated against a standard material to ensure a comparability of all results. For this purpose, an earths average water would be perfect, but there is ‘no average water’ (Craig, 1961) in the world. Therefore, a hypothetical standard water had to be established for $^{2}H/^{1}H$ (Hagemann et al., 1970) and $^{18}O/^{16}O$ (Baertschi, 1976). After some interim standards, today’s standard material for water analysis is the Vienna Standard Mean Ocean Water (VSMOW) (Aggarwal et al., 2005, pp. 39-41; Hoefs, 2015).

By using the following equation (Eq. 3), a reasonable value for comparison with measurements from other sites can be produced. Isotope ratios are usually given in this so called δ-notation with the unit of permille or ‰ (Slater et al., 2001). Although it is not based on the International System of Units (SI), the mainstream in the field of geochemistry uses it to measure and compare natural variations of abundance (Slater et al., 2001). The general notation follows the International Union of Pure and Applied Chemistry (IUPAC) (Hoefs, 2015):

$$\delta\ in = \frac{R_{Sample} - R_{Standard}}{R_{Standard}} \times 1000\ permille \qquad \text{(Eq. 3)}$$

Slater et al. (2001) adapted and specified the formula for water analysis:

$$\delta^{18}O_{VSMOW} = \left(\frac{R_S - R_{VSMOW}}{R_{VSMOW}}\right) \times 1000 = \left(\frac{R_S}{R_{VSMOW}} - 1\right) \times 1 \qquad \text{(Eq. 4)}$$

After sample acquisition (see chapter 3.1), sample vials were kept cool for the transport and were stored in a fridge at 6 °C. Duplicates are important to monitor the accuracy of procedure beginning at sample acquisition until the analysis of measurements. The measurements were carried out by Agroisolab GmbH, a specialist on environmental isotope analytics (Förstel, 2006). For organizational reasons, the samples from the first two campaigns were sent and analysed in one batch with a timespan of two and one month, respectively, between sampling and analysing. The samples from the third campaign were sent immediately after their acquisition and got analysed within one month after sampling. 2H/1H isotope ratios were measured with an Isoprime continuous flow mass spectrometer in combination with a liquid autosampler by Blisotec and an automatic Elemental Analyser from Eurovector (Hofem, 2018). $^{18}O/^{16}O$ isotope ratios were measured with an Isoprime continuous flow mass spectrometer in combination with a Multiflow equilibrium system by Anachem (Hofem, 2018).

### *3.3.2 Global meteoric water line (GMWL) and Austrian meteoric water line (AMWL)*

The most common way to display stable isotope data is a $\delta^2H$ - $\delta^{18}O$ diagram (Dansgaard, 1964). In such a diagram, measured data can be plotted against literature values and meteoric water lines to compare them and see variations. Other studies referring to SI normally use $\delta^{18}O$-values representatively for both (Hoffmann et al., 2005; Kamleitner et al., 2019; Thompson & Davis, 2005). The GMWL gives an adequate fit line of the relation between $\delta^2H$ and $\delta^{18}O$ in natural meteoric waters that have not experienced surface evaporation all over the planet (Clark & Fritz, 1997). It

shows the isotopic enrichment that meteoric waters undergo on the path through the atmosphere (Craig, 1961). The correlation ((Eq. 5) was first described by Craig (1961). Refined GMWLs were e.g. calculated by Rozanski et al. (1993). However, the older version of Craig (1961) is still very accurate and due to its simplicity more commonly used in science (Kralik et al., 2015).

$$\delta^2 H = 8 \times \delta^{18} O + 10 \qquad \text{(Eq. 5)}$$

A local mean water line (LMWL) can be derived from locally collected water samples. In contrast to the GMWL, it is derived from site-specific isotope ratios on a local scale (Putman et al., 2019). Its deviation from the GMWL reveals information about the origin of the water and its atmospheric alteration within transport (Tappa et al., 2016). The LMWL gives information about precipitation's origin and aggregate state, secondary evaporation and moisture recycling (Gat, 2000). As an example, a flatter slope and a lower intercept of a LMWL in comparison with the GMWL can be assigned to kinetic fractionation in secondary evaporation (Gat, 2000). The comparison of different LMWLs can provide information about the origin of groundwaters (J. Liu et al., 2010). The LMWL for Austria, the so called AMWL (Eq. 6) by Hager & Foelsche (2015) and a LMWL from Längenfeld in the Ötztal Valley (Eq. 7) by Hager & Foelsche (2015), as the nearest to the research area, using weighted annual values, are:

$$\delta^2 H = 7.5 \times \delta^{18} O + 3.2 \qquad \text{(Eq. 6)}$$

$$\delta^2 H = 8.5 \times \delta^{18} O + 12.6 \qquad \text{(Eq. 7)}$$

Hager & Foelsche (2015) calculated the AMWL from monthly mean precipitation values of 14 stations spread over Austria provided by the Austrian Network of Isotopes in Precipitation and Surface Waters (ANIP). They mark the slightly lower intercept and slope in comparison with the GMWL as mainly driven by secondary evaporation. Consequently, the higher slope and intercept of Längenfeld (Eq. 7) is less influenced by secondary evaporation. There is a newer version of the AMWL published by Kralik et al. (2017) including all isotopic measurements done in Austria including rivers, lakes,

groundwater. Here, the older AMWL based on only ANIP precipitation data from Hager & Foelsches is used due to its more frequent usage in literature.

### *3.3.3 Fractionation Processes*

Differences in molecular weight are present in almost all chemical compounds due to different isotopic compositions. The isotope composition of water undergoes an evolution from evaporation from surface waters to precipitation. The reasons for this process are diverse and are “resulting from a number of physical and meteorological parameters such as latitude, altitude, distance from the coast, amount of precipitation, and surface air temperature” (Aggarwal et al., 2005, p. 46). These differences in isotopic composition follow specific rules. The process called ‘fractionation’ is defined as the “change in isotope ratio due to mass selectivity of a chemical reaction or physical process” (G. J. Bowen et al., 2019). Isotope exchange reactions and kinetic processes are the main sources for the partitioning of isotopes in matter. Information in this chapter refers to Hoefs (2018) pp. 5 - 20, unless marked otherwise.

#### Isotope exchange

The term *isotope exchange* describes a special case of chemical equilibrium with changing isotope distribution in a substance without a net reaction being involved. It is dependent on temperature and the weight and allowed energy levels of the involved isotopes. Translation, rotation, and vibration of a molecule sum up to its total energy. There is also a theoretical dependence on pressure which is below detection limit, tough (Clayton & Steiner, 1975). Newer studies only describe measurable effects at very high pressures (Driesner, 1997).

The resulting fractionation factor is defined as the ratio of numbers of isotopes in a chemical compound divided by the number of isotopes in another compound.

#### Evaporation-Condensation processes

Significant isotope fractionations can be produced by evaporation and condensation, because of differences in vapor pressures of isotopic compounds. Lighter molecules consisting of lighter isotopes are more likely to enrich in the vapor phase. For example,

$H^1H^2O$ has a slightly lower vapor pressure than $H_20$, so the concentration of 2H in the liquid phase is lower than in ice (Ingraham & Criss, 1993, 1998). This can be observed also in clouds where the vapor is continuously depleted of heavy isotopes with increasing condensation, because heavy isotopes are more likely to condensate in rain drops and precipitate, and clouds get a lighter isotopic signature (Hoefs, 2015, p. 271).

### Kinetic effects

Kinetic effects are the second major source of isotope fractionation. They "are associated with incomplete and unidirectional processes like evaporation, dissociation reactions, biologically mediated reactions, and diffusion" (Hoefs, 2018, p. 10). In any reaction, an enrichment of lighter isotopes in reaction products can be observed. Most isotope fractionation effects are mass dependent, and it was long thought to be the only vital reason for fractionation. This is most likely true for the water cycle, mass-independent effects for oxygen are only reported for meteorites (Clayton et al., 1974) and sulphates (Bao et al., 2000, 2001). Furthermore, diffusion is of great relevance for fractionation. Light isotopes are quite more mobile than heavier ones which can lead to fractionation. This is easily imaginable in gases but occurs also in solution and solids. Since light isotopes react faster to evaporation processes (Merlivat & Jouzel, 1979), the remaining water is enriched in heavier isotopes with a specific relation to the GMWL. This relation seems easily explainable by fractionation processes, but is rather complex due to near surface interactions and re-fractionation, which is mainly dependent on the humidity and leads to only small enrichment of heavy isotopes in the reservoir (Craig & Gordon, 1965).

### The influence of season, geographical location, and temperature

The fractionation is mainly driven by the temperature at the location of precipitation. At higher temperatures (lower altitude and summertime), the $^{18}O$-fraction is higher, which leads to a heavier $\delta^{18}O$ signature. At lower temperatures, for example in high altitudes and wintertime, the fraction of $^{18}O$ is lower, which corresponds to a lighter $\delta^{18}O$-signature (Kralik et al., 2015). The isotopic composition of rain is highly dependent on the season and the location. Kazimierz Rozanski et al. (1992) did detailed investigations on those patterns. With a focus on Europe, $\delta^{18}O$ values are most negative in December and January and the least negative in July with exemplary values of -14 and -7 per mile

respectively in Vienna, following a slightly left skewed sinus curve within the course of a year.

### Snow, rain, and the altitude effect

Liquid precipitation undergoes an isotopic evolution also while falling from the cloud to earth's surface. In contrast to rain, hail and snow preserve the isotopic composition of the cloud much better while fluttering to the ground because of lacking evaporation (Gat, 1996). This is why hailstone was used to research isotopic compositions in clouds (Jouzel et al., 1975). Rain in the summer period primarily underlies kinetic fractionation, whereas winter rain and snowfall mainly experience equilibrium fractionation (Tian et al., 2018). Summer precipitation in the eastern Alps is characterized by the least negative SI values (Masiol et al., 2021). Deuterium excess (see chapter 3.3.4) is elevated by colder conditions and even more in frozen precipitation (Gat, 1996).

The fact that raindrops are experiencing evaporation while precipitating leads to a slight enrichment of heavy isotopes in warm temperature, in cold temperatures the contrary process (condensation) leads to a lighter footprint (Kern et al., 2020). Clark & Fritz (1997) call this phenomenon the altitude effect and give values reaching from - 0.15 ‰ to - 0.5 ‰ per 100 m altitude difference. Hager & Foelsche (2015) calculate an altitude effect for Austria with - 0.19 ‰ per 100 m altitude difference which is in good accordance with values for Italy and Switzerland, both neighbouring countries of Austria situated in the Alps, which were calculated with about - 0.2 ‰ per 100 m altitude difference (Giustini et al., 2016; Hoefs, 2015). Close to the research area, Giustini et al. (2016) mapped $\delta^{18}O$-values for Italy and calculated values of below -12 ‰ for high mountainous regions in northern Italy experiencing an altitude effect of -0.23 ‰ per 100 m. Fresh snow is lacking this evaporation, yet there are older studies that found an even larger altitude effect with about 3 ‰ per 100 m altitude difference (Moser & Stichler, 1970), what is negated nowadays (Clark & Fritz, 1997). Finally, there is small indication of an altitude effect on stable isotopes in alpine snowfall due to overlaying processes like higher seasonal variability and melting and refreezing (Dietermann & Weiler, 2013). Previews studies in the upper Kaunertal Valley have shown that an altitude effect is hardly detectable and therefore negligible for permafrost investigations in this region (Czarnowsky, 2016; Kamleitner, 2017).

Rainfall events seem to have a small variability in their isotopic composition in alpine catchments (Fischer et al., 2017). At a closer look on a single event, there is a remarkable shift from the beginning to the end (Rindsberger et al., 1990). Samples from the beginning of a rain shower show heavy isotope signature, moving to a lighter signature in the middle and ending with a heavy signature again. This effect with an often V-shaped curve over time can be explained by lower evaporation rates in the middle of the shower when it is most intensive (Hoefs, 2015, p. 240).

### *3.3.4 Deuterium excess (d-excess)*

Deuterium excess (d-excess) is a second-order stable isotope parameter (Bershaw, 2018). The GMWL intersects the $\delta^2H$ y-axis of a $\delta^2H$ - $\delta^{18}O$ diagram on the value of 10 ‰. This intercept was first described by W. Dansgaard (1964) as deuterium-excess (d-excess) and is driven by kinetic processes. It is a result of a slower movement of heavier water (see chapter 3.3.3) molecules like $^1H_2{}^{18}O$ in comparison with lighter $^1H^2H^{16}O$. While evaporation occurs, a strong gradient in relative humidity above the liquid surface in combination with advection by winds lead to an isotopic non-equilibrium which results in an excess of deuterium in the vapor phase (Bershaw, 2018; Pfahl & Sodemann, 2014). This mechanism is especially important while vapor genesis from the ocean. Similar processes occur on the evolution of vapor during transport and precipitation (Frohlich et al., 2002). Dependent on those processes occurring on the ocean surface, in clouds and while precipitation, it gives a characteristic signature which can be used as a tracer (Galewsky et al., 2016; Hager & Foelsche, 2015; Humer, 1995; Lewis et al., 2013; Sodemann & Zubler, 2010; Souchez et al., 2000; Uemura et al., 2005). Following Hager & Foelsche (2015), for Austria the re-evaporation of local water surfaces, the altitude of the sample station, seasonal shifts and the origin of the water vapor (Mediterranean, Atlantic) are particularly significant in summer. D-excess variations can be complex and the theoretical understanding of the controlling climatic factors has not been fully explored (Frohlich et al., 2002).

In mountainous regions like the Alps, d-excess values are usually higher in valleys than on summits since the distance to the cloud base is greater and thus, secondary evaporation of the raindrops can take place more intensively during their fall (Hager & Foelsche, 2015). Accordingly, the effect is more evident in summer and autumn due to

the undersaturated air layers below the cloud. In winter, smaller differences are expected due to snowfall, which is not affected by secondary evaporation processes during its fall (Clark & Fritz, 1997; Hager & Foelsche, 2015).

Since d-excess underlies seasonal and geographical variations, it reaches its highest monthly means in the northern hemisphere with the highest value of 12 ‰ in January and its lowest value of 7 ‰ in June (Frohlich et al., 2002). In the eastern Alps, summer values slightly increase from about 7.5 ‰ in July to 9.5 ‰ in September, whereby the GNIP station Villacher Alpe represents an outlier with a d-excess of 11-13 ‰ in long term monthly means (IAEA/WMO, 2022). Higher d-excess values in late summer are interpreted as a signal of permafrost internal ice melt (Munroe & Handwerger, 2022; Williams et al., 2006).

## 3.4 Iodine-129

Iodine is a trace element in the earth's crust with a mean concentration of 0.45 mg/kg (Salminen et al., 2005). Nearly 100 percent of iodine are iodine-127 ($^{127}$I). Iodine-129 ($^{129}$I) is only occurring in traces. It is the long-lived radioisotope of iodine with 76 neutrons. $^{129}$I is the radioisotope of iodine with the longest lifetime and the only naturally occurring isotope besides $^{127}$I. Its half-life time was first investigated in the 1950s and set to (1.72±0.09) × $10^7$ years (Katcoff et al., 1951). Later, the half-life period was refined to its actual value of (1.614) × $10^7$ years (García-Toraño et al., 2018). Its natural background is very low. At the beginning of the atomic age, humankind started to use the potential of nuclear reactions and thus, concentrations in the environment increased. The long lifetime of $^{129}$I equals about one third of earth's existence and the fact that recent human output exceeds the natural occurrence by far led to the assumption that the concentration of $^{129}$I in the environment can only rise over time (National Council on Radiation Protection and Measurements, 1983). The anthropogenic induced amount of $^{129}$I exceeds its natural occurrence by up to seven orders of magnitude. Anthropogenic output originates from nuclear weapons, nuclear accidents (e.g. Chernobyl) and a fast majority of the emissions is produced by nuclear fuel reprocessing plants (NFRP) (Ernst, 2003; Hou et al., 2009; Kadowaki et al., 2018; Osterc & Stibilj, 2011). Fig. 15 shows the different pathways of emissions caused by NFRPs. Since the behaviour of $^{129}$I in an environmental perspective is supposed to be

identical to other iodine isotopes, it is often considered in relation to the most dominant $^{127}I$ to observe its relative enrichment. Dependent on the area of application, $^{129}I$ is also considered in atoms/l as total content in water and air or in Becquerel [Bq] to express its emitted nuclear radiation. Therefore, it is not always easy to compare results.

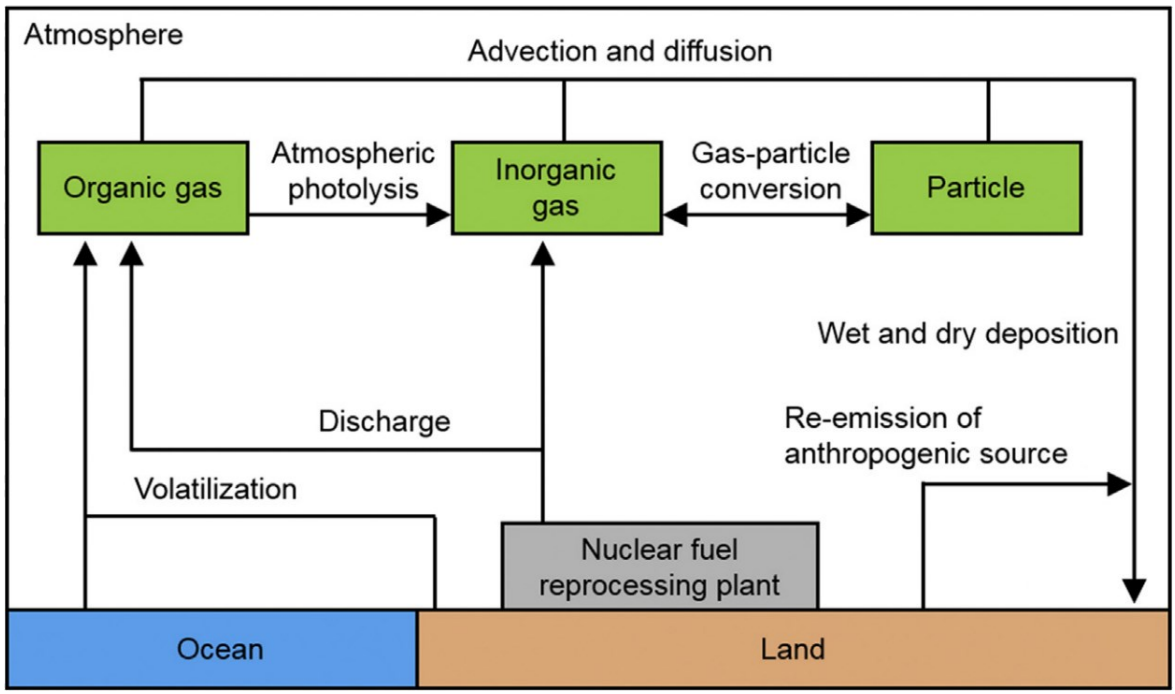


*Fig. 15: Sketch of processes and reservoirs in the $^{129}I$ cycle with the most important primary modern source NFRP in grey and secondary sources' re-emission from land and volatilization from oceans. Adapted from Kadowaki et al. (2018)*

### *3.4.1 Spreading, accumulation, and sinks*

Already in the early 1980s, Kocher (1981) released a dynamic model of the global iodine cycle with estimations of $^{129}I$ dose to the population based on calculations for the four compartments lithosphere, hydrosphere, atmosphere and biosphere. Despite research starting a long time ago, many questions regarding the quantitative distributions, quantities of chemical species and pathways of $^{129}I$ still stay unclear (Jabbar, Wallner, et al., 2012). Intensive research was done in the last decades and is still necessary to close these gaps bit by bit. According to Gilfedder et al. (2008), the major chemical species in aerosol, rain and snow is soluble organically bound iodine, whereas iodide and iodate are only minor fractions. In water, the dominant iodine species are iodide and iodate with minor organically bound iodine (Hou et al., 2009).

The major sink for iodine in the troposphere are iodine oxides such as iodate (Gilfedder et al., 2008).

The $^{129}$I-content of snow is about one order of magnitude lower than the content of rain (Buraglio et al., 2001; Dong et al., 2018). Surface air temperature and $^{129}$I is positively correlated in snow (Buraglio et al., 2001). $^{129}$I/$^{127}$I ratios in Tibetan snow are, in respect to prenuclear values, elevated about four orders of magnitude, European snow levels of $^{129}$I are still one to two orders of magnitude higher (Dong et al., 2018).

### *3.4.2 Natural background*

The natural background of $^{129}$I in surface waters lies in the magnitude of $10^5$ atoms/l (calculated by Kamleitner et al., 2019 after Snyder & Fabryka-Martin, 2007). Modern central European rainfall concentrations are with a magnitude of $10^{-12}$ g/l, what corresponds to 5 x $10^9$ atoms/l (Krupp & Aumann, 1999). Buraglio et al. (2001) gives central European rainfall values for $^{129}$I with $10^8$ – $10^9$ atoms/l. The calculated global inventory of $^{129}$I is about 250 kg in the hydrosphere, atmosphere and biosphere (Hou et al., 2009; Krupp & Aumann, 1999) or 1.2 x $10^{27}$ atoms in the hydrosphere as a steady state inventory (Fabryka-Martin et al., 1985). Although the total amount of 250 kg seems small, $^{129}$I can be utilized as a powerful tracer for hydrologic purposes in total amounts [atoms/l], as well as ratios in comparison with the naturally most often occurring isotope iodine-127 [c$^{129}$I /c$^{127}$I]. In the environment, naturally produced $^{129}$I stems primarily from cosmic rays' reactions in the atmosphere (cosmogenic $^{129}$I) and natural fission in the lithosphere (fissiogenic $^{129}$I) to sum up the natural background. This background is thought to be in a steady-state condition (Edwards, 1962). This naturally formed $^{129}$I is in equilibrium with $^{129}$I (Osterc & Stibilj, 2011). The spallation of xenon by cosmic rays in the atmosphere produces $^{129}$I as cosmogenic nuclides in the order of 5 mg/a (Fabryka-Martin et al., 1985). Spontaneous fission of primordial uranium is assumed to contribute 6 mg a $^{-1}$ to the natural background (Ernst, 2003). Other sources like muon reactions of tellurium 130 (Takagi et al., 1974) are of minor importance. Worldwide, there are about 256 kg of $^{129}$I in steady-state in soil and connected environmental compartments (Ernst, 2003). Based on these long-term stable contents and an equilibrium of $^{129}$I and the predominant iodine isotope $^{127}$I, there are constant $^{129}$I/$^{127}$I isotope ratios in all natural compartments between 5,6 × $10^{-13}$ und 1,5 × $10^{-12}$ (Fabryka-

Martin et al., 1985; X. Liu et al., 1997; Moran et al., 1998). Only in the stratosphere, uran-rich rocks, and the deep sea where production of $^{129}I$ takes place, the isotope ratios are slightly elevated (Ernst, 2003).

### *3.4.3 Anthropogenic emissions*

The origin of anthropogenic emitted $^{129}I$ is related to human activities such as nuclear weapons, accidents and nuclear fuel reprocessing. Hou et al. (2009) comprised many studies and show that nuclear weapon testing exceeds the natural background ratio $^{129}I/^{127}I$ of $10^{-12}$ by one to three magnitudes ($10^{-11}$ to $10^{-9}$). Marine discharge and the atmospheric release from European NFRP in form of rain exceeds the natural background by four to six magnitudes ($10^{-8}$ to $10^{-6}$); in close proximity to the facilities soil, grass and air were even more contaminated ($10^{-6}$ to $10^{-3}$). For comparison, in the contaminated area of Chernobyl, $^{129}I/^{127}I$ ratios of $10^{-8}$ to $10^{-6}$ were found (Hou et al., 2009). Following, most emissions are closely related to nuclear processing, especially to nuclear fuel reprocessing plants (NFRP) (Buraglio et al., 2001; Gómez-Guzmán et al., 2012; Hou et al., 2009; Salminen et al., 2005). There are three NFRP in western Europe, two of them still in use: La Hague in the Normandy (France) and Sellafield on the coast of the Irish Sea in England (Ernst, 2003; Kamleitner et al., 2019). Today, 99 % of European emissions are liquid emissions from those two facilities which end up in the Irish Sea and the British Cannel (Reithmeier et al., 2006). A third reprocessing plant in Marcoule near Marseille was a major emitter until its shutdown in 1997 (Jabbar, Wallner, et al., 2012). The major deposition mechanism of anthropogenic $^{129}I$ on continental surface is precipitation, while the impact of dry atmospheric deposition is of lower importance (Reithmeier et al., 2010). Specific data on speciation and distribution of $^{129}I$ is rare, but it is thought to be similar to $^{127}I$ since they have the same chemical properties (Hou et al., 2009). Also, exact values of $^{129}I$ emissions since the beginning of the nuclear age are hardly available, but reconstructions (see Fig. 16) give a good picture of their magnitude (Ernst, 2003). Other authors calculate the emitted $^{129}I$ as ten times higher (Reithmeier et al., 2006). Liquid emissions from European NFRP rose rapidly since 1990 with discharges of 250 kg/year in the late 1990s (Germain et al.,

1997). In total, the three European facilities emitted 0.44, 1.0 and 1.2 TBq of gaseous $^{129}$I until the year 2004 (Reithmeier et al., 2010). Calculations from Kadowaki et al. (2018) name La Hague and Sellafield as comparable emitters of five to ten GBq/a gaseous $^{129}$I in the years between 2006 and 2010. The major secondary source of anthropogenic $^{129}$I is the re-emission from earth's surface, most importantly from ocean surface water near NFRP. Through this pathway, also primarily liquid emissions from NFRP can be re-emitted by volatilized water and get into the atmosphere. Since 2000, emission rates of the European NFRP remain stable (Daraoui et al., 2012, 2016; Kadowaki et al., 2018).

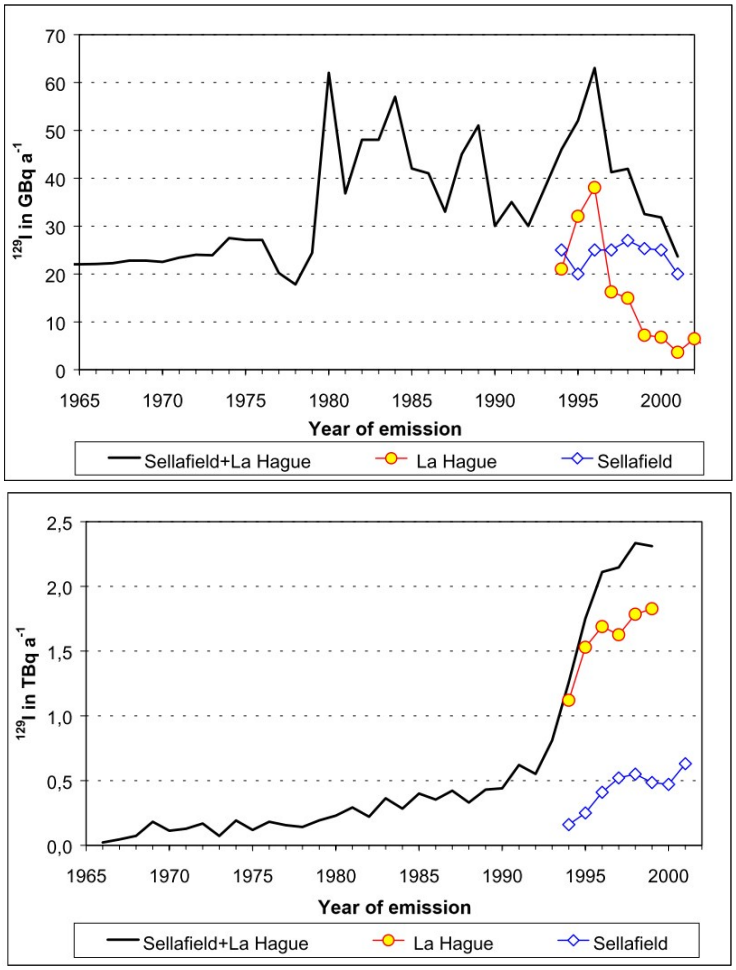


*Fig. 16: Above: Gaseous $^{129}$I-emissions from western European NFRP; below: Liquid $^{129}$I-emissions from western European NFRP; values before 1988 were reconstructed, values after 1988 were measured. Adapted from Ernst (2003), p. 13.*

### *3.4.4 Atmospheric distribution of anthropogenic $^{129}$I and modern concentrations*

$^{129}$I-emissions are spread by the air within the northern hemisphere. $^{129}$I can overcome thousands of kilometres after emission from a nuclear facility (Hasegawa et al., 2017). The residence time for particles is below 14 days and for gasses it does not exceed 19 days (Rahn et al., 1976). This distribution behaviour leads to a relatively homogeneous distribution in Europe but also to regional differences of 1-2 magnitudes between northern and southern parts of Europe (Kadowaki et al., 2018). These are the results of complex processes happening within the air by the latitude effect, the altitude effect,

the amount effect, the continental effect, and the seasonal effect (Dong et al., 2018; Gat et al., 2001). Importantly, there is a direct negative correlation of $^{129}$I-concentration with increasing distance to the emitter (sea or NFRP), increasing altitude in Europe, and time within a rain event (Fabryka-Martin et al., 1985; Jabbar, Steier, et al., 2012; Jabbar et al., 2013; Reithmeier et al., 2006).

Reithmeier et al. (2010) calculated the global distribution of $^{129}$I based on data from water samples, emissions from NFRP and re-emission from the ocean (see Fig. 17). Following the colour-code, there are two to three orders of magnitude higher pollutions in the northern hemisphere especially in Europa, the USA and Central Asia. Kadowaki et al. (2018) developed a more sophisticated distribution model by adding re-emission from land surface, atmospheric photolysis, but did not include water sample analysis. Their calculations were based on the Advanced Research Weather Research Forecast model (Skamarock et al., 2008) and extended by models for global forecasting (Richardson et al., 2007; Y. Zhang et al., 2012). The resulting so-called GEARN-FDM model is capable to simulate the natural and anthropogenic emissions, the distribution between chemical species, the spread in the atmosphere and the geographical distribution in rain waters. Still, their modelled distribution to the earth surface is comparable and validated the patterns of seasonal changes. More $^{129}$I is precipitating in the summer months which is dominated by atmospheric $^{129}$I, whereas winter precipitation of $^{129}$I is dominated by NFRP emissions (Kadowaki et al., 2018).

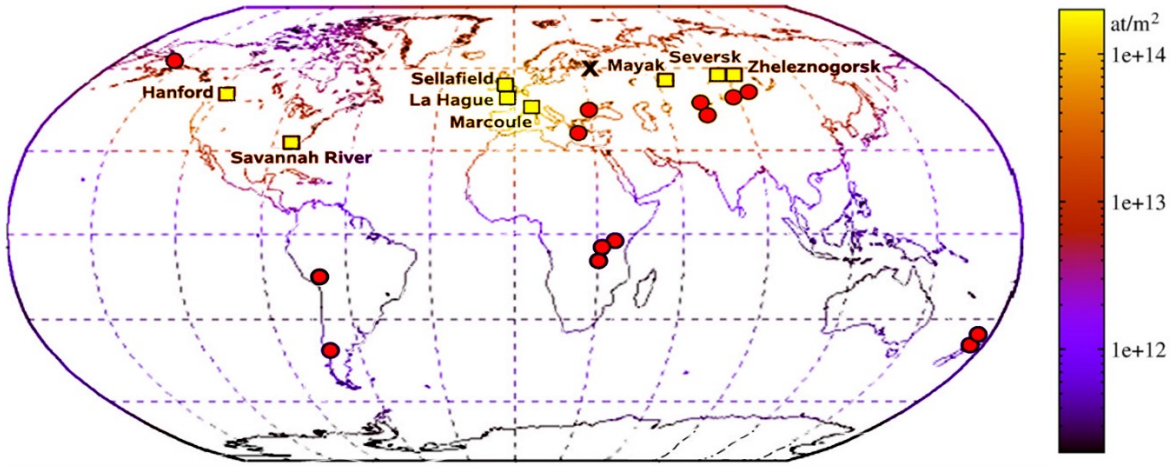


*Fig. 17: Major emitters of $^{129}$I: NFRP (yellow), water sampling sites for the distribution model (red); normalization point for the transport model (x). Calculated deposition fluences from marked NFRP, atomic explosions, and re-emissions of European NFRP from the ocean until the year 2004 are colour-coded in black to yellow. After Reithmeier et al. (2010)*

At a smaller scale, global models provide good data, but the reliability for complex orogenetic landscapes is still limited and regional to local studies are of relevance. $^{129}$I-distribution as particulate and gaseous matter is highly affected by regional meteorological and geographical patterns (Jabbar, Steier, et al., 2012). Precipitation measurements for $^{129}$I-concentration in northern Europe range from $10^8$ to $10^9$ atoms/l (Buraglio et al., 2001). Values for Bavaria, Germany, give a range from 21 x $10^7$ to 500 x $10^7$ atoms/l (Reithmeier et al., 2005). Jabbar, Steier, et al. (2012) found differences of $^{129}$I-concentrations in the meteorologically NW-dominated Zugspitze, compared to the SE-dominated Sonnblick, both detached peaks in the eastern Alps. Moreover, they observed a reduction in $^{129}$I-concentrations of about 1 magnitude in the air, $10^4$ atoms/m$^3$ at 3,000 m.a.s.l. to $10^5$ atoms/m$^3$ at 200 m.a.s.l., respectively as an altitude effect (Jabbar, Steier, et al., 2012). A big amount of $^{129}$I in the upper troposphere is resulting in a positive correlation of $^{129}$I with altitude in altitudes above 2,500 m.a.s.l., so, a reversed altitude effect in these regions can be observed (Dong et al., 2018). For the location of the Kaunertal Valley, close to the Kaiserbergtal Valley, an altitude effect was not found (Kamleitner et al., 2019). A timeline of airborne $^{129}$I-concentrations for Austria is directly correlated to emitted gaseous $^{129}$I by European NFRP Sellafield and Le Hague over the past decades (Jabbar, Wallner, et al., 2012).

Following, for the investigated area of the Kaiserbergtal Valley, there are two nuclear reprocessing facilities of special interest. First, there is the reprocessing plant of La Hague in the Normandy (France) and second, Sellafield on the coast of the Irish Sea in England (Ernst, 2003; Kamleitner et al., 2019).

### *3.4.5 Usage as a tracer*

Following its origin and behaviour in the environment, $^{129}$I is a tracer with great potential in various fields. It is one of the rare heavy cosmogenic isotopes that is utilisable as a tracer. It is a non-metal and forms good negative-ion beams in AMS (Dickin, 2005, p. 413). The idea of using iodine as an environmental tracer goes back some decades and first qualitative data was gained in 1984 by Fabryka-Martin “for hydrologic and geologic processes on a time scale up to 100 My” (Fabryka-Martin et al., 1985). It can be used as “a unique tracer of sources and for the temporal and spatial distribution of air and moisture masses” (Buraglio et al., 2001) and it has potential for distinguishing

water sources in discharge especially combined with other tracers like stable isotopes (Herod et al., 2016; Nimz, 1995). $^{129}I$ has been used to track the dispersion of radioiodine and brought new insights into athmosphere dynamics and the biogeochemical cycle (Jabbar, Steier, et al., 2012). $^{129}I$ is considered as a good tracer for global nuclear emissions, without being harmful to the biosphere (Alotaibi et al., 2021). Other studies calculated an elevated risk of one order of magnitude for thyroid cancer by the lifetime exposure of modern backgrounds of $^{129}I/^{127}I$ ratios of $10^{-8}$ in Austria (Jabbar, Wallner, et al., 2012).

Despite the problem of the very low half-life of tritium (12.3 years), analysis of tritium is still the common method for age determination of water (R. Bowen et al., 2012; Clark & Fritz, 1997; Kamleitner et al., 2019; Povinec et al., 2013). The low half-life of tritium will lead to a lower importance as a tracer, an alternative must be found. $^{129}I$ and tritium have comparable characteristics regarding genesis and distribution in the environment, but with the important difference that $^{129}I$ is continuously emitted and tritium is disappearing over time (Kamleitner et al., 2019). Nevertheless, the usage of $^{129}I$ as a tracer is a young field of application. Only little work is done in this field, but its potential to overcome the problem of tritium half time makes it an interesting alternative (Kamleitner et al., 2019).

As described above (see chapter 1.2) permafrost and rock glaciers developed hundreds and thousands of years ago and can be considered as being formed before nuclear age. Based on this fact, anthropogenic $^{129}I$ is a promising tracer to detect its degradation. So far, only few studies using $^{129}I$ for comparable purposes have been published. S. Kamleitner et al. (2019) analysed samples from rain, glacier ice and springs in a high alpine environment and validated them with simultaneously analysed tritium samples and existing $^{129}I$-studies from the alpine region of Reithmeier et al. (2006) and Wagner (1995). Herod et al. (2016) first combined $^{129}I$ with other environmental tracers to research discontinuous permafrost in the Yukon Territory, Canada. They distinguished between groundwater baseflow, spring freshet consisting of snowmelt and shallow groundwater, and active layer drainage. The highest values of $^{129}I$ were found at the onset of freshet and calculated 88 % of precipitated $^{129}I$ being kept in organic soil. Still, they claim its “behaviour, storage and transport within a watershed as poorly understood” (Herod et al., 2016).

### 3.4.6 Detection of $^{129}I$ in water

Since concentrations of $^{129}I$ are extremely low in the environment (see chapter 3.4.2), most methods of analysis are not suitable for measuring concentrations of $^{129}I$. Especially old groundwater and permafrost are supposed to only contain concentrations of pre-nuclear age. According to Hou et al. (2009), methods like X-γ spectrometry and ICP-MS have low detection limits for $^{129}I/^{127}I$ ratios and are only suitable for localities associated with nuclear waste and other polluted environments. The most accurate method is Accelerator Mass Spectrometry (AMS) because it counts every single atom in the sample (Dickin, 2005). It is the only method capable of detecting $^{129}I/^{127}I$ ratios of below $10^{-10}$, what is needed for permafrost analysis, since permafrost is considered to contain such pre nuclear contents of $^{129}I$ (Alotaibi et al., 2021; Hou et al., 2009).

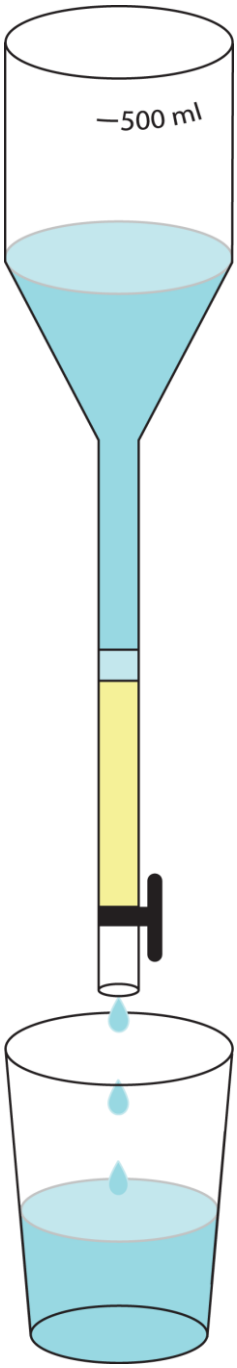


*Fig. 19: Sketch of iodine exchange column: 500 ml water sample reservoir, 1x8 100-200 mesh ion-exchange raisin (yellow)*

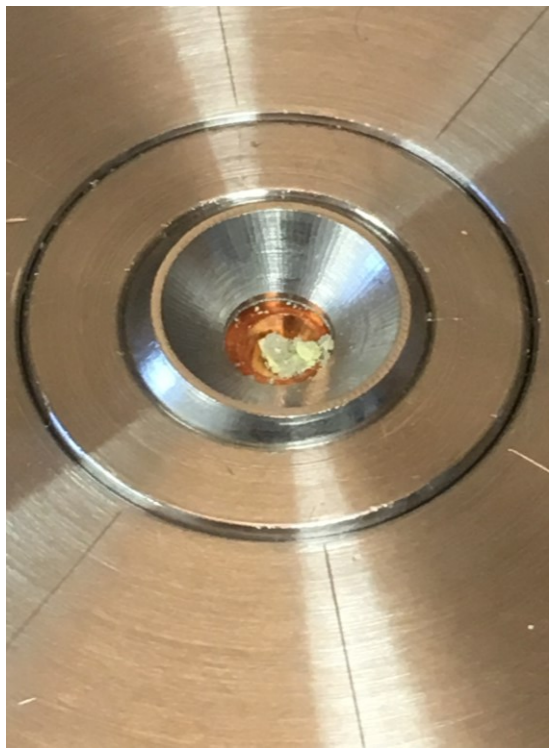

*Fig. 18: AgI-powder on top of a copper target prior to being pressed with a piston*

Deriving ratios of $^{129}I$ and $^{127}I$, multiple measurements would have been necessary. For practical reasons to save resources, it was decided not to measure $^{127}I$ contents and only work with $^{129}I$-contents. Sample preparation was done following Kamleitner et al. (2019) and L. Y. Zhang & Hou (2013). $^{129}I$-samples with 500 ml volume were spiked with NaI. $Ca(ClO)_2$, $NaHSO_3$, and $NH_2OHxHCl$ was added to bring all iodine in solution. $^{129}I$ was then kept in 1x8 100-200 mesh ion-exchange resin and flushed with $KNO_3$ (see sketch in Fig. 19). $AgNO_3$ was added to make Ag-compounds precipitate. The addition of $NH_3$ dissolves AgCl and only AgI stays precipitated. After repeated flushing with MilliQ-water, samples were centrifuged, and dried. The resulting AgI-powder was mixed with Ag in a ratio of 1:1 and pressed into copper targets for the measurement at the AMS (see Fig. 19). Those copper targets were placed in a target wheel and inserted into the atom accelerator. These measurements were done at the Vienna Environmental Research Accelerator (VERA) using 'Source 1' as sample input, a potential difference detector for $I^{127}$, and a Bragg-Type electron detector for $^{129}I$ (see Fig. 20). Some samples were treated with only half the volume (250 ml) or even one

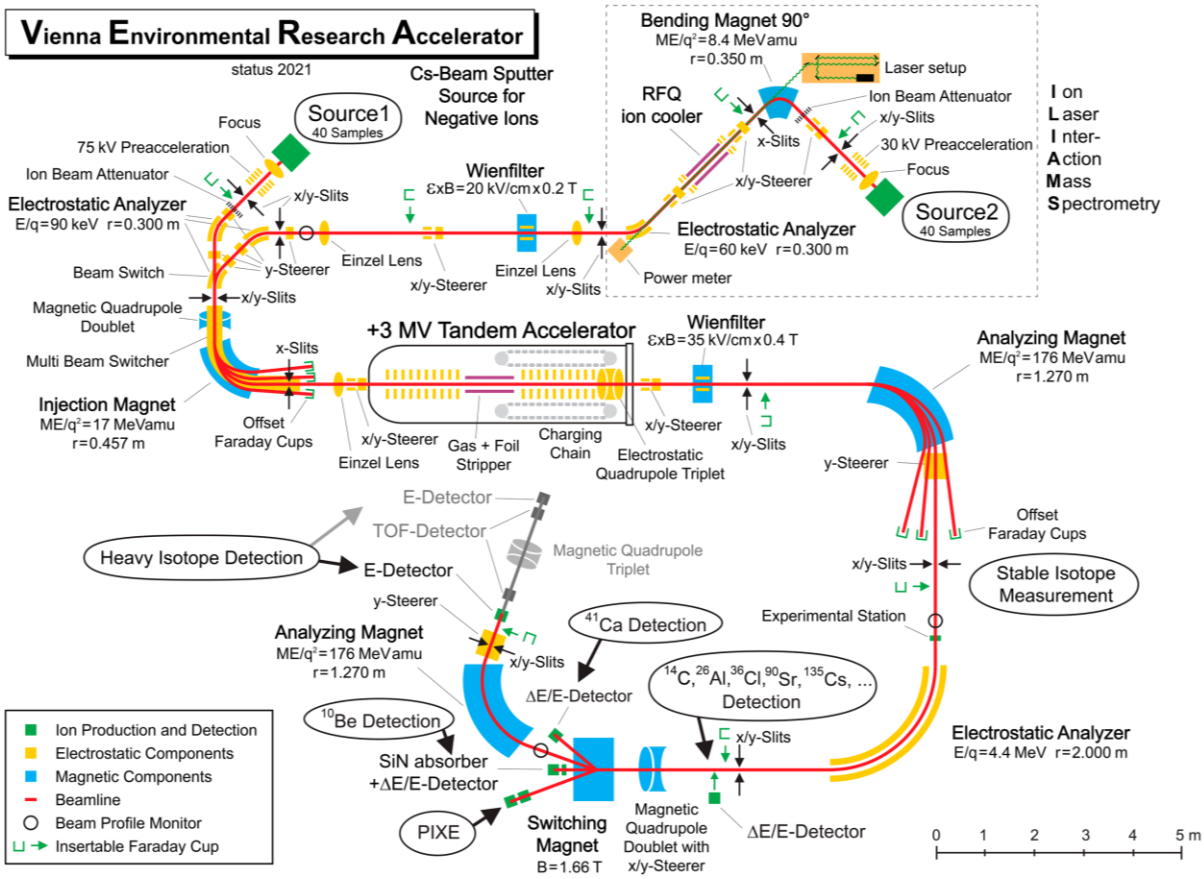


*Fig. 20: Detailed sketch of the VERA mass spectrometer from the Isotope Physics research group at the University of Vienna ("VERA", 2012)*

fifth of the standard volume (100 ml). This reduction in volume should only be applied to higher polluted samples (Hou et al., 2009, pp. 187-188).

## 3.5 Statistical analysis

All statistical analysis was done using R Studio 2022.07 (RStudio_Team, 2022) with the R version 4.2.1 (R_Core_Team, 2022) and several packages. Due to the effort of sample acquisition, the time-consuming sample preparation and analysation especially for $^{129}$I, sample size for this study was limited. This fact, however, can lead to a decrease of statistical power and potential misinterpretation of data especially in statistical analysis due to Type II errors (Button et al., 2013). Other researchers like Bacchetti (2013) relativize Button's argumentation. In order not to go too much into detail about the small sample size problem, we take our data trying to manage them in best manner to avoid misinterpretation. In the following statistical analysis, all tests were done with a significance level of $\alpha = 0.05$, unless marked otherwise. Basic statistical analysis of relevant parameters includes testing for normal distribution, variance analysis and post-hoc testing to find groups with significant differences. Data was always grouped by water origin.

For stable isotopes further investigations were done by plotting $\delta^{18}\mathrm{O}$-values against $\delta^{2}\mathrm{H}$-values (Dansgaard et al., 1960). This is the standard diagram to deriving a meteoric water line and putting the values in relation to other locations. Further investigations were done on $^{18}$O only, due to more common use than $^{2}$H (Hoffmann et al., 2005; Kamleitner et al., 2019; Thompson & Davis, 2005). There was no altitude effect correction applied to stable isotope values because earlier investigations in the area did not find a significant effect.

Deriving $^{129}$I-concentrations from AMS measurements is a delicate task and was done following Kamleitner et al. (2019) who based their procedure on Szidat (2000) and Klipsch (2005). Taking these values, descriptive statistics was done in the same way as other parameters. In addition, tests were done to find the best data for further analysis and calculations to address the research questions.

## 3.6 Intersection of data

Stable isotope signatures show whether water has experienced fractionation processes (see 3.3.3). Concentrations of $^{129}I$ give relative information on the age of waters (see 3.4.5). A combination of both can show old water which went through fractionation processes. Springs with these characteristics are interpreted as dominantly fed by permafrost water. In a last step, the percentage of prenuclear water is combined with information of discharge quantities of selected springs to calculate permafrost loss in volume per time.

# 4 Results

The full dataset contains in total 44 observations of 25 variables. Samples were taken from 5 different sources: glacier, springs, ponds, rain, and snow. This dataset contains more detailed information, which was not used for statistical analysis. They are attached in the appendix. The information includes standard deviation of SI-measurements, $^{129}$I relative error, exposition, ground material, inclination, vegetation, a description of the location, and additional notes.

## 4.1 Descriptive statistics

An overview for the most important variables is shown below in table 2. Not all parameters were measured at all locations. The most important parameters, stable isotopes (SI), and consequently deuterium excess (d-excess), were sampled in 41 cases, $^{129}$I was sampled in 38 cases. Temperature values from the EC/Temperature-meter for ice and snow were manually set to 0 prior to statistical analysis. Pond samples were included in the category spring because they are thought to be mainly by spring water, interflow, and groundwater.

*Table 2: Basic statistical values of the encompassing dataset for the most important variables stable isotopes ($\delta^{18}O$ and $\delta^{2}H$), deuterium excess, number of $^{129}$I-atoms, electrical conductivity (EC), temperature (T), and the elevation of the sampling location*

| $\delta^{18}O$ | $\delta^{2}H$ | d-excess | $^{129}$I [atoms/l] | EC [µS/cm] | T [°C] | elevation [m.a.s.l.] |
|---|---|---|---|---|---|---|
| Min. :-18.90 | Min. :-141.40 | Min. : 6.30 | Min. : 1115737 | Min. : 2.40 | Min. : 0.000 | Min. :2445 |
| 1st Qu.:-14.50 | 1st Qu.:-106.90 | 1st Qu.:10.10 | 1st Qu.: 17978001 | 1st Qu.: 12.32 | 1st Qu.: 1.400 | 1st Qu.:2585 |
| Median :-13.30 | Median : -94.70 | Median :11.40 | Median : 26118828 | Median : 35.00 | Median : 2.900 | Median :2636 |
| Mean :-13.29 | Mean : -94.84 | Mean :11.44 | Mean : 41125062 | Mean : 44.41 | Mean : 3.905 | Mean :2663 |
| 3rd Qu.:-12.40 | 3rd Qu.: -86.80 | 3rd Qu.:13.10 | 3rd Qu.: 40027542 | 3rd Qu.: 61.92 | 3rd Qu.: 4.975 | 3rd Qu.:2756 |
| Max. : -8.20 | Max. : -54.20 | Max. :15.80 | Max. :289508223 | Max. :215.00 | Max. :15.800 | Max. :2827 |
| NA's :3 | NA's :3 | NA's :3 | NA's :6 | NA | NA | NA |

In advance to the following statistical tests, it must be annotated that some groups of samples do not meet criteria of normal distribution. Statistical tests were done in all conscience. Some tests were done with the assumption that normal distribution would be achieved with higher sample numbers.

### *4.1.1 Temperature and electrical conductivity (EC)*

The dataset for temperature and EC was reduced to 36 by excluding outliers in temperature (n = 5) and EC (n = 1), as well as a glacier backup. Boxplots of all sources are shown in Fig. 21. A Shapiro-Wilk Test on electrical conductivity for springs show that the data do not meet the criteria of normal distribution (p = 0.039). Rain on the other side (p = 0.454) is normally distributed. The variables glacier and snow could not be tested due to small sample size (n=2). No parametric test can be applied to compare group means.

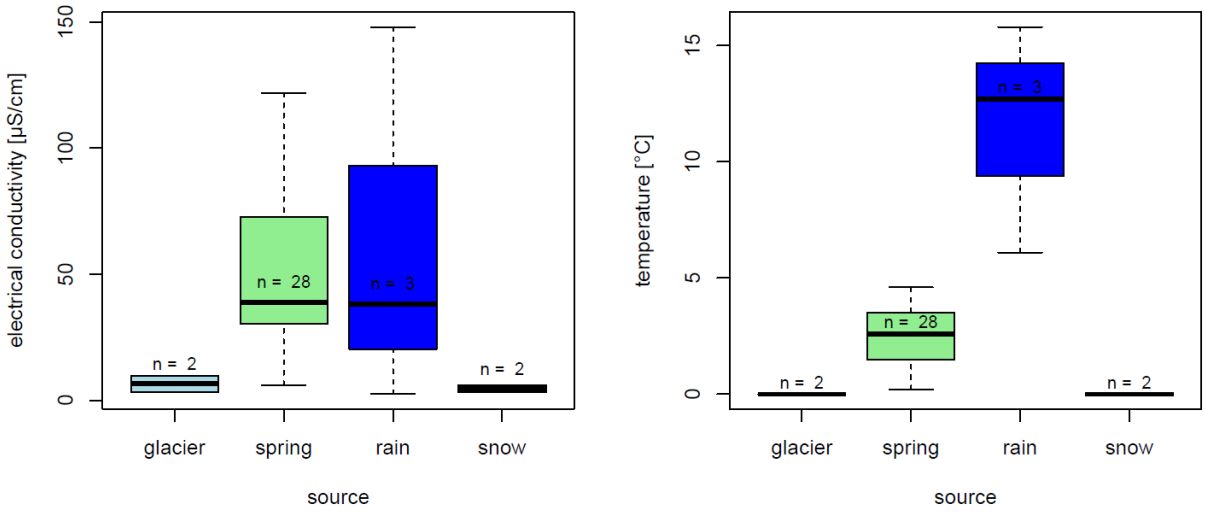


*Fig. 21: Boxplots of the variables electrical conductivity (left) and temperature (right), grouped by source; sample frequency is given for every group.*

The Kruskal-Wallis rank sum test as a non-parametric alternative to the ANOVA (Hollander et al., 2013) on EC shows a significant variation among different sources (p = 0.034). As a post hoc test Dunn Test with adjusted p-values was done (Dunn, 1961, 1964). No significant differences between the four groups were found (p < 0.05). The Kruskal-Wallis rank sum test on temperature shows a significant variation among different sources (p-value < 0.001). The post hoc Dunn test discovers significant differences between the groups glacier and rain (p = 0.0044), and rain and snow (p = 0.037). The mean difference of rain-spring (p = 0.051) missed the significance level of p = 0.05. The mean temperature of measured springs was 2.95 °C.

### *4.1.2 Stable isotopes ²H and ¹⁸O, and d-excess*

Following a Shapiro-Wilk Test for the overall dataset of $\delta^{18}O$ and $\delta^{2}H$, it is not normally distributed, whereas deuterium excess is normally distributed. At a closer look on the groups (see Fig. 22) of $\delta^{18}O$ data, spring (p = 0.051) and rain (p = 0.762) are normally distributed. Shapiro-Wilk Tests on the groups of $\delta^{2}H$ and deuterium excess show a normal distribution for both groups as well. The variables glacier and snow could not be tested due to small sample size (n=2).

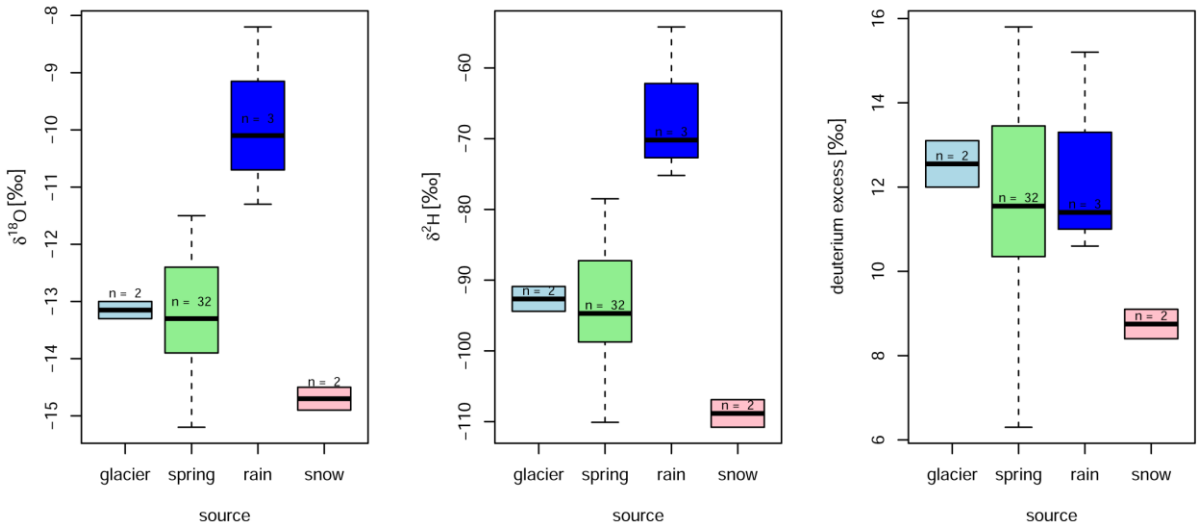


*Fig. 22: Boxplots of the variables $\delta^{18}O$ (left), $\delta^{2}H$ (centre), and deuterium excess (right) grouped by source; sample frequency is given for every group*

Analysis of variance (ANOVA) results on $\delta^{2}H$ and $\delta^{18}O$ look very similar. Significant variations were found within the whole dataset (F-values: 10.18 for $\delta^{2}H$ and 10.75 for $\delta^{18}O$ ($p < 0.001$). The post hoc Tukey test shows significant differences between the same groups for both parameters: rain and glacier (p = 0.014 for $\delta^{18}O$, p=0.018 for $\delta^{2}H$), rain and springs ($p < 0.001$), and snow and rain ($p < 0.001$). Mean values of $\delta^{2}H$ and $\delta^{18}O$ are -94.91 and -13.30, respectively. ANOVA results for deuterium excess are not as clear as those for stable isotopes. There is low variation between the sample means (F = 1.669, p = 0.191). Furthermore, no significant variance could be found with the post hoc Turkey test. The biggest differences are between snow and glacier (p = 0.241), snow and springs (p = 0.242), and snow and rain (p = 0.203), but still fail to meet the significance level of 0.05 by far. No differences in mean could be found for d-excess, the mean is 11.52.

An analytical duplicate was made once for verifying the accuracy of analytics. It was chosen to be a glacier ice sample (KB38). The results show differences in isotopic composition. KB38 shows a $\delta^{18}O$ value of -13.3 and a $\delta^{2}H$ value of -94.4, the analysis of the backup KB38b gives values of -14.4 and -107.5, respectively.

### *4.1.3 Local meteoric water line (LMWL)*

For the calculation of the local mean water line (Fig. 23), the number of 41 SI samples was reduced by a glacier backup (KB38b) and an outlier (KB10). KB 10 was excluded not only because of being a statistical outlier, but also because its sampling site was a insecure source. The sample was taken in July from water below a snow field relict with water from an unsecure source. A resulting dataset of 39 values has been used for the creation of the LMWL Kaiserbergtal Valley.

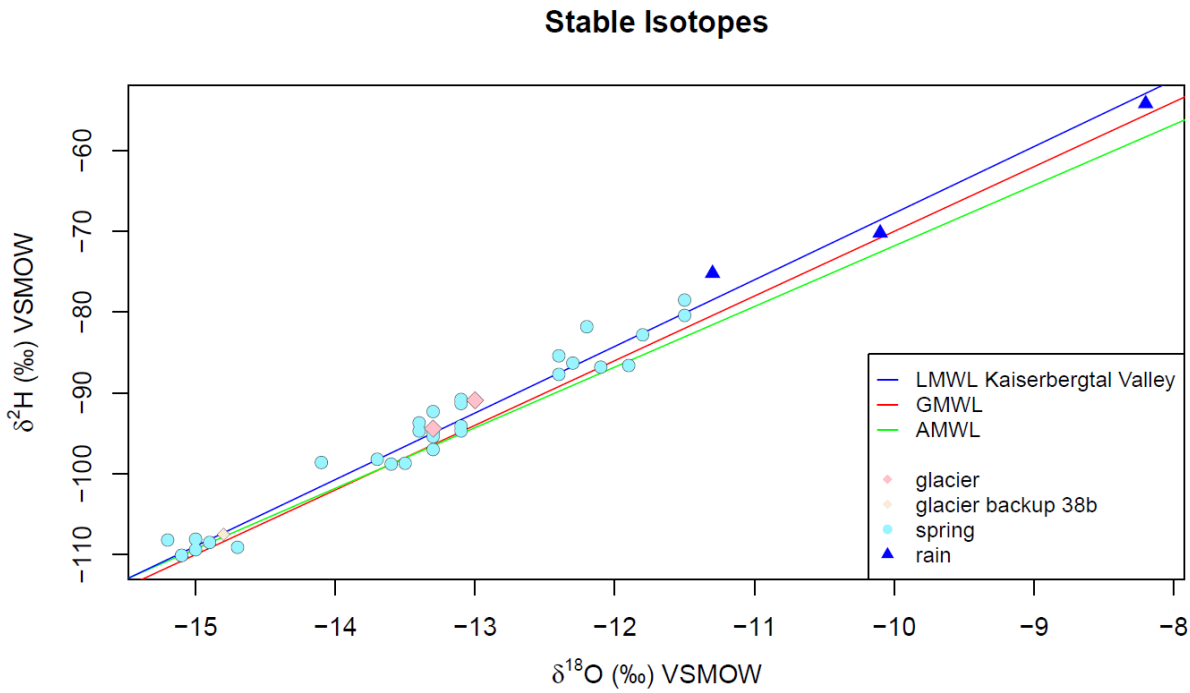


*Fig. 23: $\delta^{18}O$-values plotted against $\delta^{2}H$-values; sample types characterized by different symbols; including calculated local mean water line (LMWL) Kaiserbergtal Valley, global mean water line (GMWL) after W. Dansgaard (1964), and Austrian mean water line (AMWL) after Hager & Foelsche (2015)*

The values show a clear trend. A line of best fit for the investigated samples was calculated with $\delta^{2}H$ = 8.24 $\delta^{18}O$ + 14.66 ($R^2$ = 0.99; n = 39) and lies subparallel to the

GMWL, elevated in $\delta^2H$. Rain samples are clearly elevated in both, $\delta^2H$ and $\delta^{18}O$. Glacier samples are situated in between spring samples, the backup for the lower glacier sample plots far lower in both, $\delta^2H$ and $\delta^{18}O$.

### *4.1.4 Iodine-129*

A Shapiro-Wilk Test on $^{129}I$-concentration for springs (p = 0.044) shows that the data do not meet the criteria of normal distribution (p > 0.05). Only rain is normally distributed (p = 0.864). The variables glacier and snow could not be tested due to small sample size (n=2). The median of rain, snow, and glacier ice samples are 2.2 x $10^8$, 1.5 x $10^7$, and 1.5 x $10^6$ atoms/l, respectively. In a Kruskal-Wallis rank sum test on iodine, $^{129}I$ displays a significant variation among the various sources (p = 0.003). The post hoc Dunn test on the sources (see Fig. 24) shows significant differences between rain and glacier waters (p = 0.003), rain and spring waters (p = 0.047), and rain and melted snow (p = 0.046). Other groups, including the supposed difference between spring and glacier (p = 0.08) do not variate significantly. The mean concentration of $^{129}I$ of measured springs is 28.1 x $10^6$ [atoms/l]. Details on relations of variables from iodine sampling sites is given by a correlation plot in the appendix.

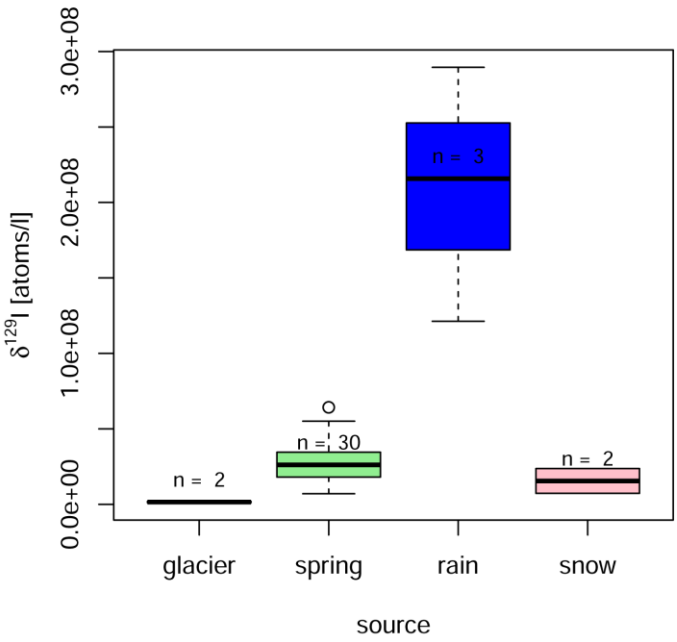


*Fig. 24: Boxplots of $^{129}I$-concentration grouped by source; sample number is given above each median line*

An analytical duplicate was taken once to control the accuracy of sample treatment and target measurement in the AMS. The difference between the two samples KB39 and KB39b taken at the same location (see Fig. 25) is 7.7 %. The relative measurement error of 3.4 % and 2.3 %, respectively.

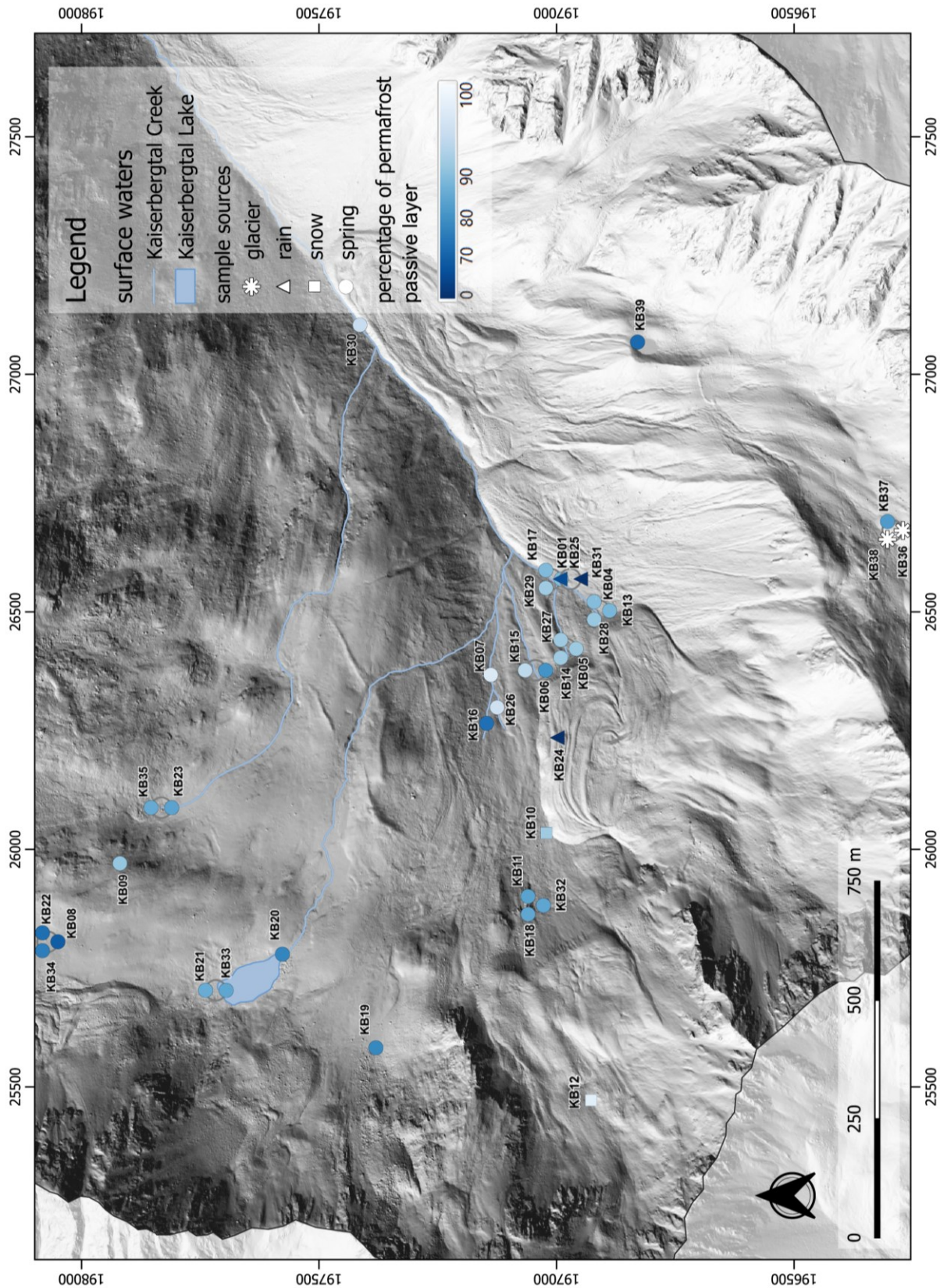


*Fig. 25: $^{129}I$ sampling points with permafrost content indicated with logarithmic increasing coloured to increase the visibility of differences. Coordinate Reference System: EPSG:31254 - MGI / Austria GK West*

## 4.2 September samples

To investigate a potential trend over the summer period and to find the most suitable month for further analysis, statistical tests were carried out. Six springs, which were tested on every field campaign (KB01, KB04, KB05, KB07, KB08, and KB11), were looked at in detail. The means for the summer months July to September are 2.7 x $10^7$, 3.2 x $10^7$, and 2.2 x $10^7$ atoms/l, respectively, and all are normal distributed (p-values: 0.09, 0.06, and 0.24). An ANOVA test found no evidence for significant variation in their means (F = 0.565; p = 0.58).

### *4.2.1 Iodine-129*

An illustrative way of showing iodine concentration, and following, prenuclear water proportions, is shown in Fig. 26. $^{129}$I-contents of spring samples from September were plotted in relation to glacier and rain. The mean concentration of $^{129}$I in rain samples (2.09 x $10^8$ atoms/l) is thought to represent 100 percent modern water (and consequently, 0 percent prenuclear water). The mean $^{129}$I-concentration of glacier samples (2.09 x $10^8$ atoms/l) is thought to be 100 percent pre nuclear water. A linear

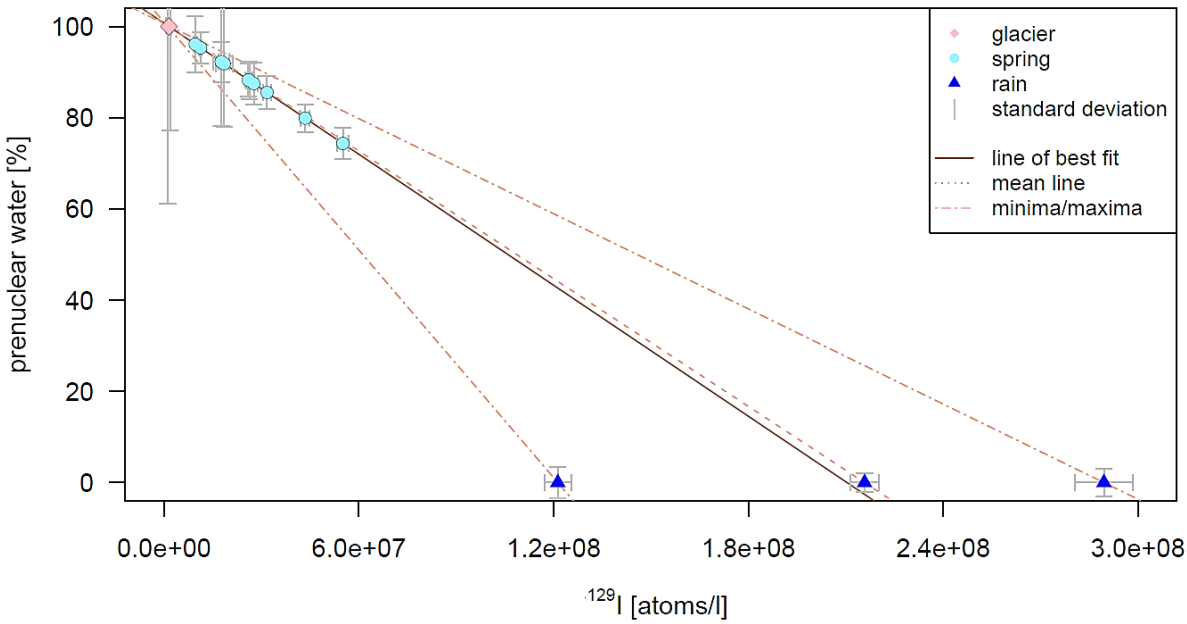


*Fig. 26: Proportions of prenuclear water in spring samples, calculated by its $^{129}$I-concentration in comparison to rain and glacier samples. The line of best fit was done by a linear regression of rain and glacier following Wilkinson & Rogers (1973), with sample numbers of 3 and 2, respectively*

regression model was calculated with spring samples (prenuclear water = 100.7 – 4.8 $*10^{-7}$ $^{129}I$, $R^2 = 1$) after Chambers & Hastie (1992) and Wilkinson & Rogers (1973). Fig. 26 shows all spring water samples are near to glacial concentrations of $^{129}I$ and less comparable to rain.

Standard errors in percentage are high in glacier samples (39.0 % and 22.5 %) which have low concentrations of $^{129}I$, and decrease towards rain samples (2.2 %, 3.1 %, 3.4 %) which show higher concentrations of $^{129}I$. The increase of $^{129}I$-concentration weakly negatively correlates with the relative error of the measurement, calculated for the whole dataset (Pearson's r = -0.27; p = 0.11; n = 37). With both variables log-transformed, a moderate negative correlation of the two variables could be found (Pearson's r = -0.75; p < 0.001; n =37). At a closer view on the plotted springs (Fig. 27 below), they all plot between 74.35 % (KB39) and 96.14 % (KB26) proportion of prenuclear water.

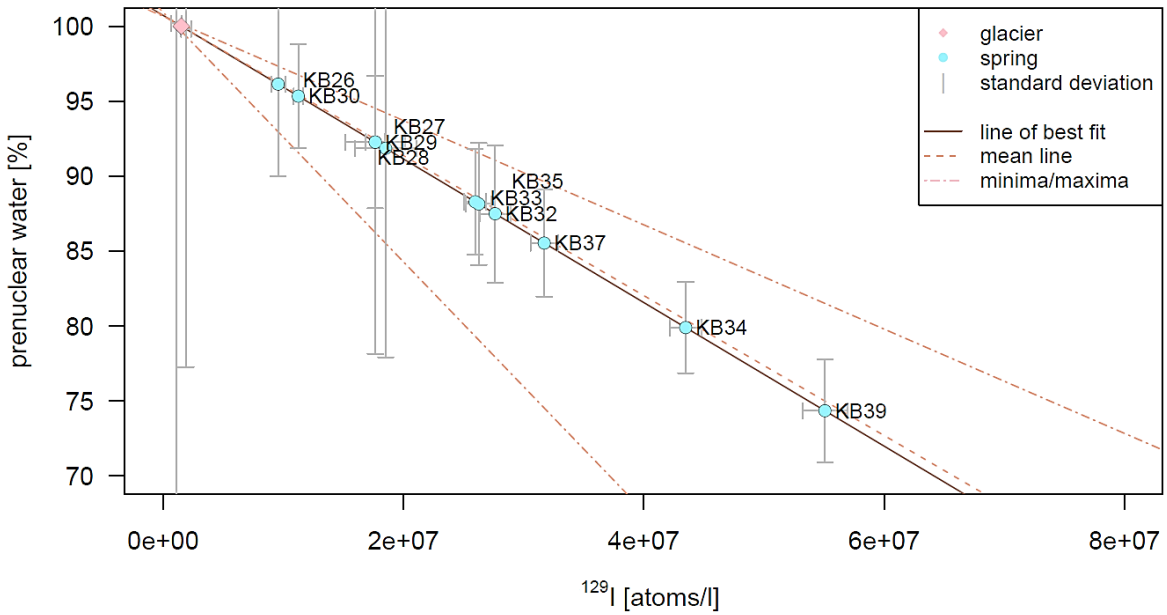


*Fig. 27: A closer look on Fig. 26; in this zoomed view all sampled springs can be shown with distinct labels. No rain sample can be plotted in this view. The three rain samples plot on the extensions of the mean, minima, and maxima lines at 0 % prenuclear water (y-axis).*

### 4.2.2 intersection of $^{129}I$ and $\delta^{18}O$

A combination of $^{129}$I-concentration in atoms/l and $\delta^{18}O$ in ‰ allows to combine the information of the two tracers. Waters with low $^{129}$I-concentrations are interpreted as mainly fed by old water sources, whereas high concentrations indicate recently formed waters (Kamleitner et al., 2019). Low $\delta^{18}O$ values indicate mainly ice melt fed sources, whereas high values can be seen as liquid water. Fig. 28 shows September spring samples in relation to rain and glaciers samples. All rain samples plot in the upper right field indicating post nuclear liquid water as a major source. All glacier samples plot in the lower left field, indicating prenuclear ice. All spring samples plot in the mixing zone described by Kamleitner et al. (2019) above and below the solid separation line for $^{129}$I by M. J. M. Wagner (1995).

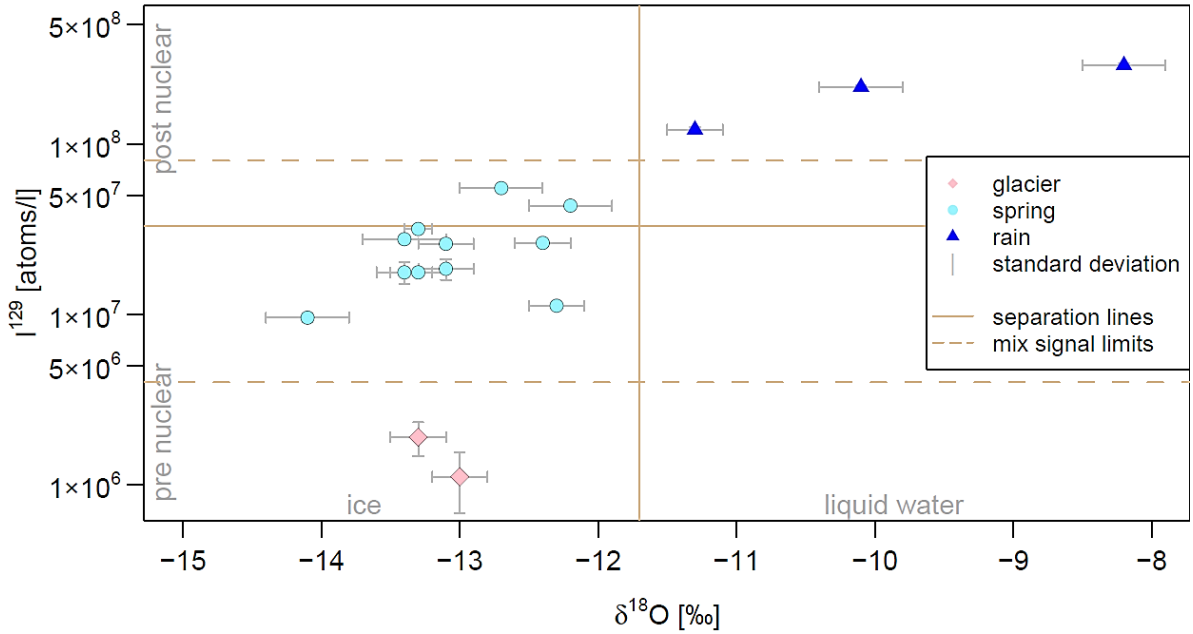


*Fig. 28: Concept graph of separation between ice/liquid and pre nuclear/post nuclear signature for September spring samples. Based on $\delta^{18}O$ signature on the x-axis and $^{129}$I-concentration on the logarithmic y-axis; x-axis is divided by a solid separation line based on data of the field campaign; y-axis separation lines for $^{129}$I-concentration are literature-based and divide pre/post nuclear signature (solid line) (M. J. M. Wagner, 1995b) with zones of mixture on both sides (dashed lines) (Kamleitner et al., 2019).*

## 4.3 Discharge in September

Salt tracer-based discharge measurements for distinct springs were done during the summer. Sampling sites were chosen for specific reasons like geographical distribution and feasibility of measurements (see 3.1). All springs were measured within the same hours in the afternoon (for more details on the selected samples see samples list in the Appendix). KB27 was measured on 27$^{th}$ of September, KB34 and KB35 were measured on 28$^{th}$ of September. KB34 and KB35 have already been measured on 30$^{th}$ of August with a discharge of 6.88 l/s (KB22) and 7.94 l/s (KB23), respectively. As discussed above, permafrost shares of all springs were calculated based on their $^{129}$I-content in relation to the endmembers glacier ice and rain water. By viewing the data in table 3, a weighted average of 91.6 % or 21.84 l/s discharge can be seen as permafrost fed.

*Table 3: Discharge of September measurements from spring KB27 on the 27$^{th}$ and the springs KB34 and KB35 on 28$^{th}$ of September. Permafrost melting rate is calculated based on salt tracer spring discharge measurements multiplied with prior calculated permafrost passive layer share.*

| Spring | measurement time | Discharge [l/s] | Permafrost share [%] | Permafrost melting rate [l/s] |
|---|---|---|---|---|
| KB27 | 16:15:00 | 20.542 | 92.3 | 18.954 |
| KB34 | 15:25:00 | 0.604 | 79.9 | 0.482 |
| KB35 | 16:20:00 | 2.728 | 88.1 | 2.404 |

A comprising view on results from the September campaign is shown in Fig 29. Twelve spring samples were taken during this field campaign, including one backup for $^{129}$I-measurement accuracy and sample treatment control. In addition to that, one rain sample from the rain sampler (KB31) and two glacier samples (KB36, KB38) were gathered.

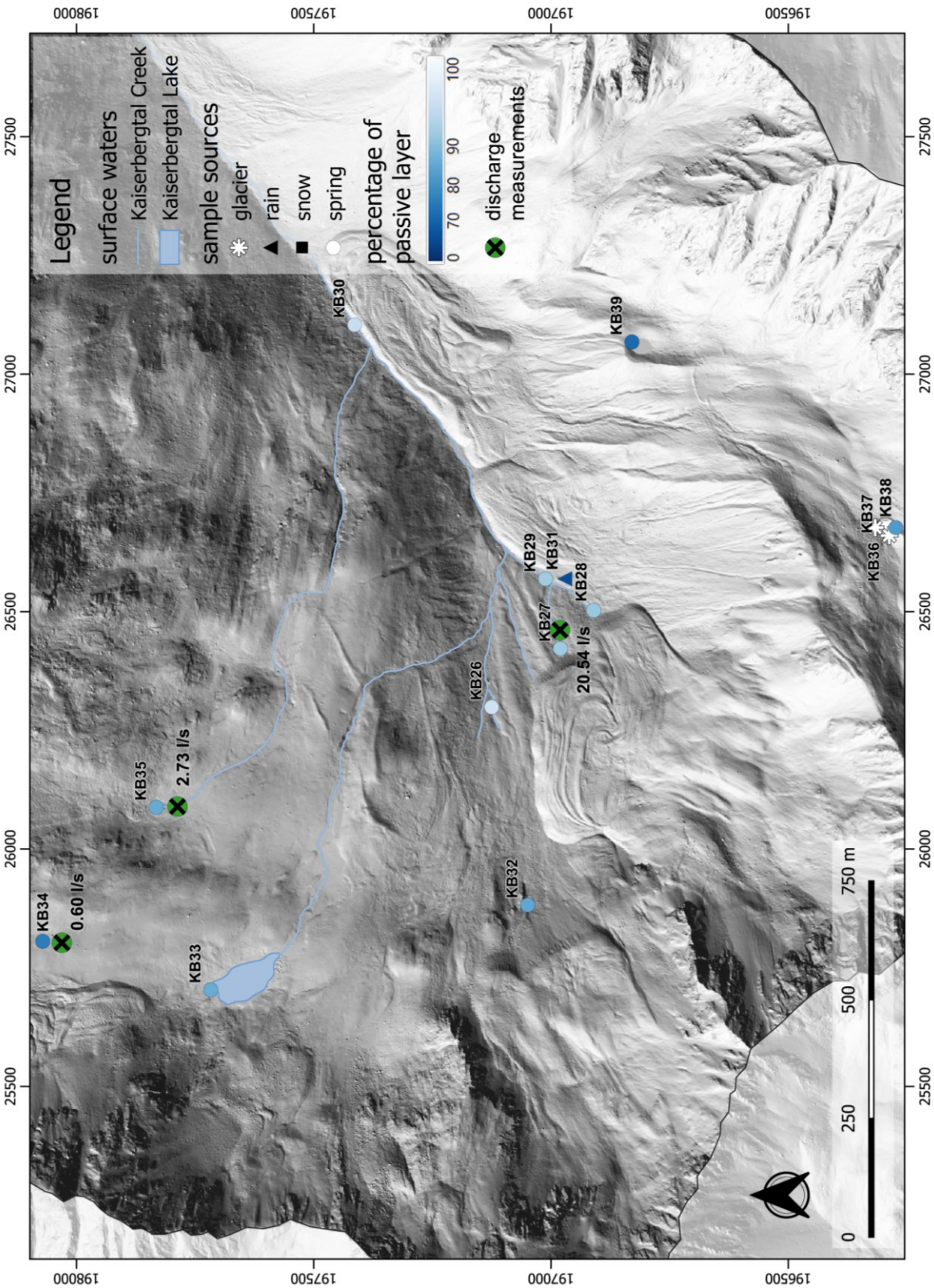


*Fig. 29: September sampling locations colour-coded in blue by permafrost passive layer shares based on $^{129}$I-concentrations and September spring measurement locations with discharge volumes*

# 5 Discussion

The following chapter is dedicated to the interpretation of study results based on state-of-the-art scientific knowledge. This is done by connecting the results of this study with findings and interpretations of the research presented in chapters 1 and 2. Starting with descriptive measures of water samples, this chapter aims to answer the research questions as defined in chapter 1.3 and present outcomes, which might be of additional value.

## 5.1 Conventional water parameters in a high alpine environment

Permafrost distribution in the valley as it is depicted in the Alpine Permafrost Index Map (APIM) (2018) is taken as fundamental information, and therefore, needs to be compared to field investigations. By combining the APIM-layer with a digital surface model (DSM) of the research area, which shows its geomorphological characteristics, a comparison with field observations can be done. The AMIP map glacier probability concurs with on-site found relicts of the Kaiserbergtal glacier in the southern part of the research area, which makes the APIM reliable also for other accessible information like permafrost. All active rock glaciers are colour-coded purple to blue, which means that, according to the authors, there is a high probability of permafrost occurrence in cold to all conditions (Boeckli et al., 2012). The lowest rock glacier of the valley is colour-coded orange and is therefore, in agreement with our field observation, most probably a relict rock glacier, overgrown by vegetation. The rock glacier following upstream, which was identified as relict rock glacier by Krainer (2011), is colour-coded as having high probability for permafrost occurrence in the APIM, what marks the biggest deviation from the APIM to field investigations.

### *5.1.1 Water temperature and EC*

The mean temperature of all measured water samples is 3.9 °C. This value can be explained by the higher number of spring samples (n=28), in contrast to samples of glacier (n=2) and rain (n=3) origin. Whereas rain samples are rather warm, the greater number of spring samples lower the overall average temperature to a value close to the spring samples' mean, which is 2.95 °C. Referring to Krainer & Mostler (2002), who

described rock glacier discharge as constantly being below 1 °C throughout the year, the average discharge temperature is exhibiting relict rock glacier characteristics, described as having temperatures up to 3 °C by Krainer & Mostler (2002). The water temperatures of two springs (KB16, KB09) are found to be near and slightly above 10 °C. Other springs (i.e. KB28, KB12) show temperatures below 1 °C. The mean spring temperature of 2.95 °C – just below the 3 °C upper end of permafrost spring temperatures described by Arenson et al. (2022) – can be explained by the fact that some springs could not be measured directly after the water reached the surface as it was covered by stones and boulders, and therefore inaccessible for tens of metres, or the discharge was so little that it was immediately warmed by surrounding dark gneiss gravel. The spring sample dataset also includes a small number of surface water sources in the valley including two samples from the Kaiserbergtalsee Lake, one from the terminal moraine pond and two from the Kaiserbergtalbach Creek, which are excluded from prior temperature analysis. Rain during the August campaign cannot account for the temperature increase, since other permafrost springs in Tyrol did not exceed 1 °C during or after heavy thunderstorms with considerable amounts of precipitation (Krainer & Mostler, 2002). The statistical analysis of temperatures shows significant differences between rain and ice. This difference could have resulted from the temperature measurement being made in the rain-sampler, representing more the ambient temperature of the measurement than the temperature of the rainfall, and therefore, cannot be interpreted as a valid finding. A significant difference between ice and spring water cannot be found, what however, can be interpreted as an indication for the origin of spring water from ice.

The mean EC of all measured samples is 44.41 µS and thus low in comparison with other high altitude alpine catchments (Cano-Paoli et al., 2019; Krainer & Mostler, 2002). Spring samples show a higher mean EC with 51.45 µS but are still low in comparison to alpine ground waters (Cano-Paoli et al., 2019). For rain samples, the two EC values measured in water from the monthly rain collector, 148.0 µS in August and 38.1 µS in September, exceed the range of 5 – 30 µS by Hölting & Coldewey (Hölting & Coldewey, 2013, pp. 161-164). This could be due to contamination of the water in the sampling container. Sediment could have been blown into the funnel by wind and then flushed by rain through the tube into the container. Alternatively, organisms like spiders or insects eighter crawled into the container or were flushed inside by rain. Spiderweb-like

material was indeed found in the August sample. The grouped measurements of glacier and snow demonstrate low mean EC values, 6.5 µS and 4.6 µS, respectively. These can be found even in the lower range of precipitation (Hölting & Coldewey, 2013, pp. 161-164) and indicate an uncontaminated source, which is preferred as an endpoint for further analysis.

Considering the two parameters – EC and Temperature – it can be concluded that there is a significant difference between glacier ice and rain. The two parameters show a considerable correlation (R = - 0.42), which is probably influenced by contamination. Rain does not contain electrically conductive material, therefore EC should be near 0. However, sample sizes are too small to determine significant differences between rain and springs, and springs and glacier ice, for both parameters. Same as for glacier samples is valid for snow samples. The results indicate differences between the end-members glacier ice and rain.

### *5.1.2 Stable isotopes*

Precipitation in the Kaunertal Valley generally exhibits some of the lightest signatures in Austria (Kralik et al., 2015). Stable isotope samples usually show an altitude effect, driven mainly by re-evaporation in summer and condensation in winter (Clark & Fritz, 1997; Jabbar, Steier, et al., 2012; Kern et al., 2020). However, studies on high alpine permafrost in the surrounding valleys have shown no significant altitude effect, and thus it is not considered in this study (Kamleitner et al., 2019).

As expected, and seen in various other environments, $\delta^{18}O$ and $\delta^{2}H$ values generally show similar patterns in distribution (Clark & Fritz, 1997). $\delta^{18}O$ values are considered as representative for both, as per common practice (Jasechko, 2019; Williams et al., 2006). Glacier samples and rock glacier outflow means are with -13.3 ‰ $\delta^{18}O$ and -13.2 ‰ $\delta^{18}O$, respectively, comparable in their stable isotope composition and in good alignment with previous reports (Miller et al., 2021). Rain samples on the other hand are comparably enriched in heavy isotopes, which is in agreement with findings of Williams et al. (2006). Rain values in the Kaiserbergtal Valley show a $\delta^{18}O$ mean of -10 ‰ and are slightly less negative than values measured in comparable altitudes in the Italian Alps, which are around -12 ‰ $\delta^{18}O$ as an annual mean (Giustini et al., 2016). The nearest GNIP stations in Austria (ANIP) is located at Patscherkofel (IAEA/WMO,

2022). The weighted annual precipitation mean of -13.5 ‰ $\delta^{18}O$ is far below the mean values of the Kaunertal Valley. An explanation for the difference could be found in the exposed position of Patscherkofel in comparison with the high alpine valley character of the upper Kaiserbergtal Valley (Hoefs, 2018, pp. 239).

Snow measurements show markedly more negative stable isotope values than rain, which is in line with findings of Williams et al. (2006). $\delta^{2}H$ snow values are heavy (mean = -110 ‰) compared to central alpine snow during the melting period, which are between -140 and -120 ‰ in comparable catchments and altitudes in Switzerland (Dietermann & Weiler, 2013). This difference could be attributed to melting and refreezing cycles of snow (Hürkamp et al., 2019), although samples were taken from layers with little assumed influence of these processes. A possible altitude effect is overlaid by various other effects and alterations in the snow pack (Dietermann & Weiler, 2013; Moser & Stichler, 1970). This was also stated in a study of permafrost springs in the nearby Kaunertal Valley (Kamleitner et al., 2019).

It can be stated that there is a significant difference in the means of both $\delta^{18}O$ and $\delta^{2}H$ between rain and spring samples. This fact and the more negative values for snow samples are in line with a previous report (Jones, Harrison, Anderson, et al. (2019)). The lack of significance of differences between glacier ice samples and spring samples, or more precisely, the fact that glacier samples in Fig. 23 plot in between a broader variation of spring sample values indicate a close relationship in formation history. Stable isotopes alone can only differentiate between water that has undergone freezing and melting cycles and water that has not. The broad variation of spring values indicates the different conditions of tested springs. Some samples of the lower quartile seem to contain melted snow of the previous winter season.

A backup sample of glacier water was taken to verify the accuracy of measurements in AgroIsoLab. Both samples were taken from the same flask of water mixture and treated in the same way before sending to the analysis laboratory. $\delta^{18}O$ values for sample KB38 and the backup KB38b are -13.3 ‰ and -14.8 ‰, respectively – with the 1st and 3rd quartile of the whole $\delta^{18}O$-dataset being -14.5 ‰ and -12.4 ‰, respectively. These apparently great differences raise doubts about the accuracy of sample treatment and/or measurements. $\delta^{2}H$ values show the same pattern. As KB38b is the only backup for stable isotopes (SI), no further investigation of the source can be made. Also, a mix-

up of this single sample is a possibility. Overall, the general trends of the SI results are assumed as being correct, since values and findings are similar to data from other reported studies conducted in comparable environments, such as those found in the comprehensive dataset of SI for Austria, complied by Krainer et al. (2007).

### *5.1.3 Mean Water Line (MWL)*

Further stable isotope data analysis includes a detailed elucidation of the relationship between $\delta^{18}O$ and $\delta^{2}H$. The calculated LMWL of the Kaiserbergtal Valley ($\delta^{2}H = 8.24 \times \delta^{18}O + 14.66$) is comparable with the LMWL in the Ötztal Valley ($\delta^{2}H = 8.5 \times \delta^{18}O + 12.6$) as calculated by Hager & Foelsche (2015). The steeper slope and higher intercept of the LMWL indicate a limited influence of secondary evaporation in the valley (Hager & Foelsche, 2015). The trend from the Ötztal Valley can also be found in spring samples of the Kaiserbergtal Valley. All samples plot above the GMWL and the AMWL. This can be explained by the high altitude of the sample area leading to a shift and a higher deuterium excess (Masiol et al., 2021) and can be further supported by J. R. Gat (1996), who stated that lower temperatures lead to a higher deuterium excess. All rain, snow, and spring samples used in this study were taken in the summer period. Therefore, the derived LMWL might not be representative.

In comparison to summer rain values in the eastern Alps, in which deuterium excess ranges between 7.5 ‰ and 9.5 ‰ (IAEA/WMO, 2022), Kaiserbergtal Valley samples show high deuterium excess values of between 11 ‰ and 13 ‰, which are comparable to the values reported by the Austrian meteorologic station of Villacher Alpe. The station of Villacher Alpe however marks an outlier for Austria's GNIP stations and is situated in the south of the alpine main ridge. A higher deuterium excess in rain samples was observed for the autumn period in northern Italy (Masiol et al., 2021). An older comprehensive study of 45 years by Froehlich et al. (2008) confirms the higher deuterium excess in September and October precipitation and comparable higher deuterium excess values at the locality of Patscherkofel near Innsbruck (12.1 ‰ in 2,245 m.a.s.l.) compared to the mean value of 11.4 ‰ in Kaiserbergtal Valley.

Spring samples have a higher mean deuterium excess (12.3 to 8.7) and heavier mean isotopic composition (- 13.1 ‰ to - 14.8 ‰) in comparison to snow, which suggests a dominance of permafrost melt in spring waters (Williams et al., 2006). The high

deuterium excess in the end of summer can be interpreted as permafrost internal ice melt (Munroe & Handwerger, 2022), which is in line with the local glacier ice values as the highest points. The stable isotope diagram (see Fig. 23) illustrates the situation. All spring and glacier samples have lighter isotope ratios than all rain samples. These findings support the validity of the data and sort out uncertainties about data quality arisen by the measurement of the backup sample KB38b.

## 5.2 Utilizing iodine-129 as a tracer for meltwater of old ice

The content of $^{129}I$ in water samples gives an indication of the age of waters. As stated by Hou et al. (2009), concentrations of $^{129}I$ can differ from $10^5$ atoms/l in surface waters to $10^9$ atoms/l (Kamleitner et al., 2019). The hereby used unit is atoms/l, which is independent of $^{127}I$ sample-contents and is commonly used for surface waters. Nevertheless, it makes comparison to other studies difficult. Publications about atmosphere and different compartments of hydrosphere, often use the unit µBq/l or the relative measurement of $^{129}I/^{127}I$.

A look on the iodine data shows that rain has highly accelerated contents of $^{129}I$ in comparison to all other sources. The mean value of summer precipitation (n=3) is with 2.1 x $10^9$ atoms/l. Glacier ice is much lower (1.5 x $10^6$ atoms/l) and represents more the natural background of water before the onset of the atomic age, which are postulated as $10^5$ atoms/l (Snyder & Fabryka-Martin, 2007). A mean value of 2.8 x $10^8$ atoms/l for springs is situated in between these two sources. An analytical duplicate for $^{129}I$-concentrations was taken from pond water at 2,830 m.a.s.l. The values show a difference of 7.7 %, whereby it must be noted that the backup was only done with a reduced sample volume of 100 ml in comparison to the normal 500 ml sample volume. However, the relative error of the measurement was with 2.2 % low and the result seems trustworthy.

Rain samples contents of $^{129}I$ in the Kaiserbergtal Valley reach from 1.2 x $10^8$ to 2.9 x $10^8$ atoms/l. These results for freshly formed precipitation are in line with the findings of Kamleitner et al. (2019), who measured a median concentration of 1.4 x $10^8$ atoms/l in the Kaunertal Valley. Buraglio et al. (2001) gives results for northern Italy with 0.3 to 9 x $10^8$ atoms/l. These comparable results in a region not far from the research area

support the accuracy of the new measurements of this study. Reithmeier et al. (2010) gives similar figures for Europe, which are about one or two orders of magnitude higher than those of the southern hemisphere (Reithmeier et al., 2010). The highest European values are measured in precipitation in Sweden and are about one order of magnitude higher than precipitation of the central and eastern Alps (Buraglio et al., 2001). The meteorological north-west influenced Zugspitze in the north of the research area and south-west influenced Sonnblick in the south-east show similar values to each other (Jabbar, Steier, et al., 2012). This supports the comparability of values taken north and south the Kaiserbergtal Valley, which is located near the alpine main ridge, which marks a meteorological divide (Hager & Foelsche, 2015). Jabbar, Steier et al. (2012) found a bigger difference in the altitude difference between Vienna and Sonnblick, leading to a concentration difference of one order of magnitude in $^{129}$I-concentration.

Considering the given altitude difference of 400 m for the research area and an even higher difference for the observed watershed, a potential altitude effect should be discussed. Based on previous studies on this concern it was decided not to do further investigations. Kamleitner et al. (2019) observed a slight increase of $^{129}$I-contents towards lower elevations, but quartiles overlap and therefore no statistically significant difference could be found. This finding is supported by Dong et al. (2018) who researched broad elevation differences in central Asia and found a negative correlation of altitude and $^{129}$I-contents in lower altitudes and a positive correlation for the higher troposphere. The investigated research area in the Kaiserbergtal Valley is exactly in between those two contrary trends. Following, the relatively strong correlation ($R = 0.45$) between $^{129}$I-concentrations and the sampling point altitude is thought to be a coincidence.

Snow, glacier melt waters, and spring waters are not as well investigated as rain waters. Snow sample measurements from Uppsala (Sweden) show $^{129}$I-concentrations which are one order of magnitude lower than summer rain samples (Buraglio et al., 2001). Still, $^{129}$I values from snow samples are more delicate to compare due to processes within the snow cover, which can influence the $^{129}$I-concentration considerably (Buraglio et al., 2001). For this study, samples from obviously low influenced layers in the snowpack were taken to minimize gathering snow exposed to alteration in regards of sunlight, temperature fluctuations, and atmospheric exposure. Following Buraglio et al. (2001), snow samples are one magnitude lower than rain samples. This shift can be

observed in samples from the Kaiserbergtal values, which show median values of 2.1 x $10^8$ atoms/l for rain and 1.5 x $10^7$ atoms/l for snow.

Glacier melt waters of the Kaiserbergtal Valley are comparable (median = 1.5 x $10^6$ atoms/l) to values from the nearby Gepatsch Ferner Glacier in Kaunertal Valley measured by (Kamleitner et al., 2019) (1.7 x $10^6$ to 3.2 x $10^6$ atoms/l) and are expectedly far below rain water concentrations (Hou et al., 2009). In regards to prenuclear water percentage, the big standard deviations observed especially in glacier samples (see Fig. 26), but also in some spring samples (KB29, KB28), can be linked to the low concentrations of $^{129}$I in the samples and the stretched range of the vertical axis.

Published $^{129}$I-concentrations for permafrost waters are rare, since it is a young field of application. For comparison, test results from the nearby Kaunertal Valley are therefore extremely valuable. Kamleitner et al. (2019) took spring water samples of 40 perennial springs. The results of their analysis done at the Vienna Environmental Research Accelerator (VERA) showed a range of 1.1 x $10^6$ to 5.5 x $10^8$ atoms/l and therefore a wide variety of concentrations. Results from permafrost springs in the Kaiserbergtal Valley show a comparably low variation between 7 x $10^6$ to 6.4 x $10^7$ atoms/l. This smaller range of values speaks for a more continuous composition of young and old waters throughout the valley.

Overall, test results from Kaiserbergtal Valley give a significantly positive answer to the applicability of the method to distinguish between rain and spring waters (p-value = 0.046). In contrast to the other postulated endmember, a significance in mean differences between spring waters and glacier waters could not be proven (p-value = 0.08) (see chapter 4.1.4). Possible reasons are the small size of glacier ice samples (n = 2) and/or a very high percentage of permafrost passive layer in spring samples, which might be a stronger explanation. And indeed, all spring samples reflect a close relationship to glacier water. All September spring samples plot between 74.4 % and 96.1 % old ice content (see Fig. 27**)**. A high impact of rock glacier melt in high altitudes in late summer was also observed by (Munroe & Handwerger, 2022), especially after a winter with little snow. When following the postulated idea of mixing the two sources precipitation and old (pre-nuclear) ice, it means all spring waters are mainly fed by old ice, and therefore, permafrost. In comparison to endmember mixing models which

normally also include a baseflow, this source of water is neglected here, because most springs in the valley are only periodically water-bearing.

Based on a monthly comparison of concentrations in six specific springs, mean $^{129}$I-concentrations slightly increased from July to August, and slightly fell from August to September. Samples were taken in the end of the months within three to four days. A comparison with precipitation data from HD-Tirol (2021) over time (see Fig. 10), does not point towards a higher input of rain in the catchment. Following, $^{129}$I should not be elevated due to recent water influence. For those samples no clear trend of $^{129}$I-concentrations throughout the summer season could be seen. Unfortunately, there is no data on seasonal trends available in literature. A dryer first half of August would point towards the opposite. In a dryer period a higher fraction of permafrost melt could be assumed due to a lack of precipitation, leading to lower $^{129}$I-concentrations. Such a negative trend over the summer period could not be found. In comparison with an end-member mixing study in an comparable high altitude permafrost influenced catchment in the Wolf Creek Basin in Canada of (Herod et al., 2016), this study's investigations show similarities and a point of reference within the scarcity of studies in this field of application. Signs for a correlation of precipitation and elevated $^{129}$I-concentrations in the creek could be found.

Geographical trends become visible in Fig. 25. Spring samples on more elevated or exposed sites on slopes show higher $^{129}$I-concentrations and therefore, a lower percentage of supposed permafrost passive layer melt. Samples in the northernmost sampling point (KB08, KB22, KB34) all have relatively low percentage of passive layer melt (around 80 %) in comparison to samples near the thalweg (line of lowest points in the valley) like those near the main rock glacier in the centre of the research area (i.a. KB05, KB26, and many others). The same trend of slightly elevated $^{129}$I-levels on elevated parts of slopes can be observed in the west (KB19) and the south (KB37), as well as for the pond sample KB39, which, however, is directly influenced by precipitation. Maybe higher parts of slopes do not contain that much old ice, or the permafrost passive layer does not melt in these locations. KB09 with a very high passive layer percentage near hundred percent marks an exceptional case of this assumed trend.

Interestingly, spring sample KB07 from July, situated in the north of the main rock glacier, which does not represent a direct discharge beneath a rock glacier shows one of the highest percentages of passive layer melt. This small creek carried much more water in August (KB16), which was enriched in $^{129}$I. In September (KB26), this creek carried less water again with a lower $^{129}$I-concentration. This vastly different iodine concentrations throughout the summer season might indicate a baseflow of old water in July.

## 5.3 View on a snow-free environment

Thawed snow can influence the results and make the interpretation of the data more complicated (see chapter 3.3.3, 3.3.4, and 3.4.1). In the end of the snow-free season, a minimum of influence can be assumed. Therefore, the following analyses focus on September samples. Snow samples were omitted from further investigations.

As a dataset for further investigations, the month September was selected. This decision was made because of multiple reasons: In September, all relicts of snowfields from the previous winter season in the research area were melted. In September, the influence and therefore proportion of snowfield meltwaters on springs can be assumed to be as little as possible in the course of a year (Krainer & Mostler, 2002; T. Wagner et al., 2020). The September-dataset is the biggest (n = 11) and the experience of two previous sampling routines are considered as beneficial background knowledge. Glacier ice and rain samples were, as well, taken in this field campaign.

By combining information from the two major tracers $^{129}$I and $\delta^{18}O$ used in this study, a clearer picture about the character of spring waters can be drawn (see Fig. 28). On a logarithmic scale, Kaiserbergtal Valley glacier samples plot clearly below the separation value of 3.3 x $10^7$ atoms/l (M. J. M. Wagner, 1995a) as well as beneath the lower mixing signal limit calculated by Kamleitner et al. (2019). All spring samples show a mixing signal of pre nuclear and post nuclear $^{129}$I-concentrations, and only two (KB39, KB34) indicate modern water. KB39 shows the highest iodine value (5.5 x $10^7$ atoms/l), it represents water from an end-moraine pond and is therefore directly influenced by precipitation. KB34 is situated in the uppermost part of the valley. In September it carried the smallest discharge (0.6 l/s) of all measured springs and only 10 % of August

discharge. All rain samples show clearly post nuclear concentrations of $^{129}I$ and are the only samples showing liquid water (not showing fractionation by freezing) as a source.

EC as a proxy for the salt concentration in waters (Leibundgut et al., 2009, p107) is the basis for discharge measurements. Due to fluctuations of spring discharge in the course of a day (Krainer & Mostler, 2002), all springs were measured on the same time of the day during afternoon hours. Creek beds were not perfectly shaped to conduct discharge measurements, since the basement in many areas is blocky and a considerable part of the water discharges in the subsurface between rocks and boulders. It cannot be precluded that some parts leave the visible creek between input location of the salt tracer and electrical conductivity measurement. Still, it is the best practice for this kind of environment, but can only give a minimum value for discharge (Bolognesi et al., 2006). In total, discharge was measured five times. Two springs were measured in late August (KB22, KB23) and resampled in late September (KB34, KB35). September discharge was measured for an additional spring (KB27), which is the biggest and in terms of a distinct creek bed the best measurable spring of the main rock glacier. In August it was raining during the field campaign. In September, the last precipitation at the Gepatsch Reservoir was observed on the 22$^{nd}$ of September. Until the measurements on 27$^{th}$ and 28$^{th}$ of September, there was a period of four and five days without rain before the discharge measurements were done. The influence of precipitation on September measurements is therefore unlikely (T. Wagner, Kainz, Krainer, et al., 2021). For the two repeatedly measured springs, a much higher discharge was observed in August compared to September (6.88l/s to 0.60 l/s for KB34 and 7.94 l/s to 2.73 l/s for KB35). The decrease in discharge is in line with daily mean discharges of other rock glacier springs in Tyrol measured by Krainer & Mostler (2002) and can be explained by the missing drainage of permafrost active layer thaw and recent rain (Jones, Harrison, Anderson, et al., 2019; Krainer et al., 2007). The majority of the annual snow cover, however, is already thawed and drained by August (T. Wagner, Kainz, Krainer, et al., 2021), so both August measurements can already be assumed to have been made without snowmelt influence. The difference between August and September measurements can be explained only by missing recent precipitation or the lack of permafrost melt. Regarding permafrost passive layer share, the observed decrease of $^{129}I$-concentrations from higher slope locations towards the thalweg can also be seen in the smaller September dataset (see Fig. 29). Sample

locations farther uphill show passive layer shares around 80 percent, whereas the Kaiserbergtal creek seems to be fed by around 95 % permafrost passive layer meltwater in two locations (KB26, KB30).

## 5.4 Quantification of permafrost passive layer melting rates

As there is information on the percentage of permafrost passive layer melt of every single spring and discharge measurements of distinct springs, calculations of passive layer melting rates can be performed. The three springs KB27, KB34, and KB35 are situated in locations where discharge measurements could be operated. KB27 is probably the most valuable source because it is one of the springs surfacing just beneath the main rock glacier, which was subject of several studies in past decades (Groh & Blöthe, 2019; Krainer, 2011, 2015a; Krainer & Ribis, 2009; Wälder et al., 2004). It also represents the biggest spring at that timepoint with a salt-tracer-test resulting in 20.54 l/s of discharge volume. A water sample for the measurement of $^{129}$I-concentration showed 1.77 x $10^7$ atoms/l, what corresponds to 92.3 % passive layer share for the measurement (see Fig. 27). As a result, 18.95 l/s discharge can be seen as thawed passive layer water. Similar to these calculations, two more rates for passive layer loss were calculated, resulting in 0.48 l/s (79.9 % of 0.60 l/s) for KB34 (88.1 % of 2.73 l/s) and 2.4 l/s for KB35. These passive layer runoff volumes can be seen as maximum values, as $^{129}$I can be retarded by organic matter (Herod et al., 2016). This fact can influence the overall $^{129}$I-content, although September samples were taken in a dry period and surface runoff and interflow, which might be influenced by organic matter, is thought to be extremely limited due to the geomorphological situation of especially KB27 and KB34. The catchment of KB35 might also include water that has been in contact with soil, comparably rich in organic matter. There is a slope in the north-west of KB35, which is partly overgrown by pioneer plants and grass, which is a typical flora for the area (Zangerl et al., 2022) and can be seen as a source for organic matter potentially interacting with surface runoff and interflow.

# 6 Conclusion

Since the role of permafrost as a mountain ridge's water tower will increase with progressing global warming and the resulting glacier melt, every aspect of its behaviour is of importance for future estimations of downstream water resources. Thus, for years, researchers have called for further hydrological studies on the topic. This thesis responds to these calls: It contributes to filling some research gaps in terms of identifying old ice beneath mountain slopes and quantifying rates of its loss. More specifically, a dry alpine mountain catchment dominated by rock glaciers, as was the chosen research area for this study, can be seen as an environment similar to Southern American mountainous areas, which are already dependent on rock glacier ice melt as the major water source and will be even more so in the future. The relevance of this study, though conducted in a small valley in the Tyrolean Alps, lies on the applicability of its findings to other areas around the globe and the potential benefits the investigated methods could bring along for future research in the field of cryogenic bound water.

The aim of this study was the investigation of combined information from water samples' $^{129}$I-concentrations and stable isotopes ($^{18}$O and $^{2}$H) as a method to measure the content of permafrost melt water in alpine springs. Stable isotope (SI) values alone can only be used to differentiate between water that did undergo freezing and thawing and water that did not. To retrieve information about passive layer contributions in discharge, information about the age of water is needed. $^{129}$I can be utilized for this purpose. Moreover, it bears the potential to overcome the problem of a short half-life of tritium (12.3 a), which is regularly used for dating waters in the environment. With the help of $^{129}$I as a tracer, the age of permafrost can be determined relatively. The share of old water in a spring can be determined, which can either be stored in ice for a long time or as old ground water. The latter is assumed to be absent in a high alpine catchment.

This was done by addressing the question in what ways glacier ice, rain waters and spring waters in a small alpine catchment differ from each other regarding the footprint of the tracers $^{18}$O, $^{2}$H and $^{129}$I as well as other parameters like temperature, electric conductivity and deuterium excess. Further questions of interest were the locations of permafrost fed springs in the valley, seasonal trends in $^{129}$I-concentrations, as well as the amount of permafrost melt in runoff.

As study area, a small alpine valley, named Kaiserbergtal, near Gepatsch Reservoir in Tyrol, Austria, was chosen, since it was already subject of earlier studies, mainly by Karl Krainer (Hausmann et al., 2012; Krainer, 2015b, 2015a; Krainer & Ribis, 2009). The field work consisted of field investigations, searching for sampling points, three field campaigns, including numerous samplings each. Sample preparation and analysis was done in Vienna, followed by various statistical analytics and tests. Both the design of the study as well as the discussion of the results was embedded in state-of-the-art theory to ensure the scientific value and validity of both the measurements and the final results of the study.

In conclusion, the findings of this study enable an answer to almost all research questions set in the beginning of this thesis. In order to give a clear overview of those answers, findings are summarized chronologically.

Differences in the footprint of $\delta^{18}\mathrm{O}$ and $\delta^{2}\mathrm{H}$ can be found between rain and glacier ice as well as rain water and spring water, but not between glacier ice and spring water. Both spring water and especially glacier ice have lighter isotope ratios than rain water, which itself has one of the lightest SI-signatures in Austria (Hager & Foelsche, 2015). Moreover, SI analysis show an ice-origin character for all spring samples. Regarding the radionuclide $^{129}$I, similar statistical findings were noticed. All spring samples show higher contents of $^{129}$I than glacier ice and far lower contents of $^{129}$I than rain water, only the former not being statistically significant. Differences of mean between spring waters and glacier ice could not be found for both main tracers of the study (SI and $^{129}$I), what points towards a high share of old formerly ice bound water in the samples, and thus indicating mainly permafrost passive layer melt. There is a mixed picture for other parameters. Samples of glacier ice, rain waters and spring waters do not differ significantly from each other in regards of EC, temperature and d-excess. Only the difference in mean temperature between rain and glacier differ significantly. No other group-pair of glacier, spring, and rain shows differences of those three parameters. A look on the relation between the two stable isotopes underlines these missing differences of groups for d-excess. In comparison to rock glacier spring measurements in the nearby valleys (Krainer & Mostler, 2002), discharges in the Kaiserbergtal Valley have a lower EC, whereby they show typical rock glacier spring temperatures (Arenson et al., 2022).

A seasonal trend of $^{129}$I-concentrations became visible insofar as that there is an increase from July to August and a slight decrease from August to September, but no statistical significance was found for the observation. According to a study in Canada (Herod et al., 2016), concentrations of $^{129}$I are the highest in late May, a period that was not covered in this study. This shows that further studies about the seasonal trends of $^{129}$I-concentrations would be preferable. Fig. 25 pictures permafrost passive layer percentages of springs and their geographical relations. All of the springs in the small mountain catchment show a mixture of pre- and post-nuclear $^{129}$I-concentrations, meaning all springs contain to some part water originating from pre-nuclear ice, most of them to a large extent. Especially high percentages of permafrost passive layer melt of up to 95 % can be found in springs located in the lowest points of the valley cross section, for instance KB26, KB27, and KB30 near the main rock glacier, while springs located in exposed or elevated sites have a comparably lower percentage of passive layer melt with around 80 %. Altogether, this numbers seem to be really high, considering them as selected time point measurements throughout the summer period. Iodine might be captured in the system within its way to the sampling points, although attention was paid to take samples as near to the spring as possible. Nevertheless, all 30 investigated springs are situated between pre- and post-nuclear mix-sample-boundaries stated by Kamleitner et al. (2019). In total, 74.4 % to 96.1 % of all the water in samples, gathered throughout the study can be considered as permafrost fed. Snow measurements were not included in further analysis because their interpretation was controversial. For excluding potential difficulties in data interpretation, September as a period thought to be free from snow melt influence was chosen for a detailed look into a two-end-member-system. All permafrost springs plot in the two-dimensional space between mean rain water and mean glacier ice.

Spring discharges were measured for three springs in this September-dataset. They were determined for three springs in the research area by instantaneous injection of NaCl and recalculation of discharge rates from EC changes over time. As a result, a total melt rate of 18.95 l/s passive layer could be determined for the central spring of the main rock glacier in the centre of the research area. Two smaller springs in the upper part of the valley discharge 0.48 l/s and 2.40 l/s melted passive layer in the end of September. Together, for the three springs a weighted 91.6 % or 21.84 l/s of their

combined runoff (23.7 l/s) is seen as permafrost passive layer melt. This also marks the rate of permafrost passive layer loss at an afternoon in late September.

Findings which were retrieved by this non-invasive method proved to be easily applicable in the field. A big advantage of the here presented method in comparison to conservative methods like bore hole drilling, ERT, or excavations is the small amount of equipment in the field. No heavy devices must be carried to the often pathless terrain of permafrost research areas. The process of sample collecting is time efficient, and further treatment easy. The here presented results and findings can be used on their own or as a basis for further analysis.

The data gathered in this study has high potential for further research. One way to retrieve further information are multiple statistics. For instance, a PCA analysis with all parameters could be done for a more comprehensive evaluation including all parameters. A first attempt of retrieving chemical groupings for potential further analysis can be found in the appendix. These results could then be further utilized for an EMMA model and finally result in a hydrograph separation between end-members. For a better picture and more robust findings, a larger number of samples is recommended.

The described workflow so far has been followed with conventional water parameters, but without information from $^{129}$I. Based on Klaus & McDonnell (2013), the differentiation of water origins in a high alpine catchment can be done with a hydrograph separation approach. This is commonly done by using conservative tracers (Boucher & Carey, 2010; Williams et al., 2006). Water isotopes ($\delta^{18}O, \delta^{2}H$) and major solute chemistry ($Ca_2$+, $Mg_2$+, Na+, $SO_4^{2-}$, acid neutralizinig capacity, and SiO) as input parameters were used by Williams et al. (2006) to devide water origins. With a principal component analysis (PCA) three end-members represent the edges of a triangle. Their approach results in the estimation that spring water in the early summer is fed by snow, in mid-summer by soil water, and late summer measurements represent the base flow. However, not all rock glacier discharge fits in. $^{129}$I-measurements have the potential to add direct information from the passive layer to differentiate between waters formed before and after the beginning of the nuclear age (Buraglio et al., 2001; Fabryka-Martin et al., 1985; Hou et al., 2009; Osterc & Stibilj, 2011; L. Y. Zhang & Hou, 2013). An investigation on the influence of the here presented tracer $^{129}$I can be considered as promising to refine EMMA, as it is common practice for untangling the origin of surface

waters (L. E. Brown et al., 2006; Dwivedi et al., 2019; Engel et al., 2016; Gui et al., 2019; Jódar et al., 2017; Markovich, Dahlke, et al., 2019; Penna et al., 2014). In case it shows evidence, it can refine the picture of runoff characteristics in similar catchments.

By investigating this comparatively little used method of using $^{129}I$ for endmember-mixing, not only opportunities and possibilities for future research became clear, but also some limitations and challenges became evident. For instance, for further studies on the topic, sample processing in the laboratory could be improved to be more time-efficient. Refining the procedure to extract iodine from water samples bears the biggest potential to accelerate the measurement process and thus make it more applicable. Efforts in this direction are already in progress (Alotaibi et al., 2021). What also became obvious while working with the iodine isotope 129 is that there are different uses of units in different scientific fields, even within the use as a tracer for similar purposes. While it makes sense to investigate ratios of the relative enrichment of $^{129}I$ and $^{127}I$, the measurement of two isotopes instead of just one also doubles the effort. Other studies, for instance, use the radiation unit Bp. Therefore, the establishment of a standards for communication might be worthwhile.

The presented study concentrated on a snow free environment in the late summer season. 2018 This simplifies interpretation, as there are research gaps in the understanding of processes within the snow layer. Investigations on effects of these processes on $^{129}I$ are of immense value in the field: Research on glaciers and rock glaciers would benefit enormously from this as snow is present in mountainous areas for the most part throughout a year.

Finally, as was discussed earlier, a possible weakness of this study might be the low quantity of samples taken. A larger sample number would make the arguments stronger and statistically more valid. Thus, further research in this field in the future could add value to this study by increasing the sample size.

In a bigger context, all efforts to refine investigation methods on mountains' water towers in general and permafrost passive layer in this particular field contribute to a better understanding on the dynamic of water sources and their future use – something that becomes increasingly important with ongoing global warming and subsequent drinking water shortages. This study contributes to the team effort that has to be made

globally to gain a better understanding of climate change and to be better prepared for the many challenges that it will bring along.

# References

Aggarwal, P. K., Gat, J. R., & Froehlich, K. F. O. (2005). *Isotopes in the water cycle : past, present and future of a developing science*. Springer.

Alotaibi, F. A., Cornett, R. J., & Herod, M. N. (2021). Rapid and efficient autoclave digestion for the extraction of iodine-129 from urine samples. *Journal of Environmental Radioactivity*, *228*. https://doi.org/10.1016/J.JENVRAD.2020.106528

*Alpine Permafrost Index Map (APIM)*. (2018). Retrieved from https://www.geo.uzh.ch/microsite/cryodata/PF_map_explanation.html

Anderson, R. S., Anderson, L. S., Armstrong, W. H., Rossi, M. W., & Crump, S. E. (2018). Glaciation of alpine valleys: The glacier – debris-covered glacier – rock glacier continuum. *Geomorphology*, *311*, 127–142. https://doi.org/10.1016/j.geomorph.2018.03.015

Andrianova, M., Bondarenko, E., Reinikainen, S.-P., & Cheremisin, A. (2019). Study of urban river water chemical and optical parameters using PCA. *IOP Conference Series: Earth and Environmental Science*, *390*(1), 012006. https://doi.org/10.1088/1755-1315/390/1/012006

Arenson, L. U., Harrington, J. S., Koenig, C. E. M., & Wainstein, P. A. (2022). Mountain Permafrost Hydrology—A Practical Review Following Studies from the Andes. *Geosciences (Switzerland)*, *12*(2), 48. https://doi.org/10.3390/geosciences12020048

*AuWiPot – Windatlas und Windpotentialstudie Österreich*. (2011). Retrieved from https://www.windatlas.at/

Azócar, G. F., & Brenning, A. (2010). Hydrological and geomorphological significance of rock glaciers in the dry Andes, Chile (27°-33°s). *Permafrost and Periglacial Processes*, *21*(1), 42–53. https://doi.org/10.1002/ppp.669

Bacchetti, P. (2013). Small sample size is not the real problem. *Nature Reviews Neuroscience 2013 14:8*, *14*(8), 585–585. https://doi.org/10.1038/nrn3475-c3

Baertschi, P. (1976). Absolute18O content of standard mean ocean water. *Earth and Planetary Science Letters*, *31*(3), 341–344. https://doi.org/10.1016/0012-821X(76)90115-1

Bao, H., Thiemens, M. H., Farquhar, J., Campbell, D. A., Lee, C. C.-W., Heine, K., & Loope, D. B. (2000). Anomalous 17O compositions in massive sulphate deposits on the Earth. *Nature*, *406*(6792), 176–178.

Bao, H., Thiemens, M. H., & Heine, K. (2001). Oxygen-17 excesses of the Central Namib gypcretes: spatial distribution. *Earth and Planetary Science Letters*, *192*(2), 125–135.

Barry, R. G. (2008). Changes in mountain climates. In R. G. Barry (Ed.), *Mountain Weather and Climate* (3rd ed., pp. 474–494). Cambridge: Cambridge University Press. https://doi.org/DOI: 10.1017/CBO9780511754753.008

Beniston, M. (2006). Mountain Weather and Climate: A General Overview and a Focus on Climatic Change in the Alps. *Hydrobiologia 2006 562:1*, *562*(1), 3–16. https://doi.org/10.1007/S10750-005-1802-0

Bershaw, J. (2018). Controls on Deuterium Excess across Asia. *Geosciences 2018, Vol. 8, Page 257*, *8*(7), 257. https://doi.org/10.3390/GEOSCIENCES8070257

Biskaborn, B. K., Smith, S. L., Noetzli, J., Matthes, H., Vieira, G., Streletskiy, D. A., … Lantuit, H. (2019). Permafrost is warming at a global scale. *Nature Communications*, *10*(1), 1–11. https://doi.org/10.1038/s41467-018-08240-4

Blöthe, J. H., Halla, C., Schrott, L., Götz, J., & Trombotto, D. (2016). Spatial distribution of rock glaciers in the semi-arid Andes of Argentina. In *Geophysical Research Abstracts EGU General Assembly*.

Boeckli, L., Brenning, A., Gruber, S., & Noetzli, J. (2012). Permafrost distribution in the European Alps: Calculation and evaluation of an index map and summary statistics. *Cryosphere*, *6*(4), 807–820. https://doi.org/10.5194/tc-6-807-2012

Bolognesi, A., Gottardi, G., & Maglionico, M. (2006). Discharge measurements in a small ungauged river: Comparison between conventional current-meter and tracer dilution methods. *Proceedings of the River Flow*, *2*. https://doi.org/10.1201/9781439833865.ch200

Bosco, C., Rusco, E., Montanarella, L., & Panagos, P. (2009). Soil erosion in the Alpine area: risk assessment and climate change. *Studi Trent. Sci. Nat*, *85*, 119–125.

Boucher, J. L., & Carey, S. K. (2010). Exploring runoff processes using chemical, isotopic and hydrometric data in a discontinuous permafrost catchment. *Hydrology Research*, *41.6*, 508–519. https://doi.org/10.2166/nh.2010.146

Bowen, G. J., Cai, Z., Fiorella, R. P., & Putman, A. L. (2019). Isotopes in the Water Cycle: Regional- to Global-Scale Patterns and Applications. *Annual Review of Earth and Planetary Sciences*, *47*, 453–479. https://doi.org/10.1146/annurev-earth-053018-060220

Bowen, R., London, H., & York, N. (2012). *Isotopes in the earth sciences*. Retrieved from https://books.google.com/books?hl=en&lr=&id=ztPsCAAAQBAJ&oi=fnd&pg=PR13&ots=NxxYHzeew5&sig=gvDWYimUT67U7nLlnDJ1QDCpb7c

Brardinoni, F., Scotti, R., Sailer, R., & Mair, V. (2019). Evaluating sources of uncertainty and variability in rock glacier inventories. *Earth Surface Processes and Landforms*. https://doi.org/10.1002/esp.4674

Brighenti, S., Tolotti, M., Bruno, M. C., Wharton, G., Pusch, M. T., & Bertoldi, W. (2019). Ecosystem shifts in Alpine streams under glacier retreat and rock glacier thaw: A review. *Science of The Total Environment*, *675*, 542–559. https://doi.org/10.1016/J.SCITOTENV.2019.04.221

Brown, J., Ferrians Jr, O. J., Heginbottom, J. A., & Melnikov, E. S. (1997). *Circum-Arctic map of permafrost and ground-ice conditions*. US Geological Survey Reston, VA.

Brown, L. E., Hannah, D. M., Milner, A. M., Soulsby, C., Hodson, A. J., & Brewer, M. J. (2006). Water source dynamics in a glacierized alpine river basin (Taillon-Gabiétous, French Pyrénées). *Water Resources Research*, *42*(8), 8404. https://doi.org/10.1029/2005WR004268

Buba Seli, A., Obiefuna, G. I., Gomes, C., Sperandio, D., Borges, N., Barbosa, A., … Pazinato Dias, G. (2019). Water Quality Assessment through PCA Analysis Related papers Physicochemical Charact erist ics of Groundwat er Qualit y of Dumne Area NE Nigeria Water Quality Assessment through PCA Analysis. *International Journal of Advanced Engineering Research and Science (IJAERS)*, *6*(3), 1469. https://doi.org/10.22161/ijaers.6.3.26

Buraglio, N., Aldahan, A., Possnert, G., & Vintersved, I. (2001). 129I from the nuclear reprocessing facilities traced in precipitation and runoff in Northern Europe. *Environmental Science and Technology*, *35*(8), 1579–1586. https://doi.org/10.1021/es001375n

Buttle, J. M. (1994). Isotope hydrograph separations and rapid delivery of pre-event water from drainage basins. *Progress in Physical Geography: Earth and Environment*, *18*(1), 16–41. https://doi.org/10.1177/030913339401800102

Button, K. S., Ioannidis, J. P. A., Mokrysz, C., Nosek, B. A., Flint, J., Robinson, E. S. J., & Munafò, M. R. (2013). Power failure: why small sample size undermines the reliability of neuroscience. *Nature Reviews Neuroscience 2013 14:5*, *14*(5), 365–376. https://doi.org/10.1038/nrn3475

Camargo, A. (2022). PCAtest: testing the statistical significance of Principal Component Analysis in R. *PeerJ*, *10*. https://doi.org/10.7717/peerj.12967

Cano-Paoli, K., Chiogna, G., & Bellin, A. (2019). Convenient use of electrical conductivity measurements to investigate hydrological processes in Alpine headwaters. *Science of The Total Environment*, *685*, 37–49. https://doi.org/10.1016/J.SCITOTENV.2019.05.166

Cazenave, A., & Cozannet, G. Le. (2014). Sea level rise and its coastal impacts. *Earth's Future*, *2*(2), 15–34.

Chadburn, S. E., Burke, E. J., Cox, P. M., Friedlingstein, P., Hugelius, G., & Westermann, S. (2017). An observation-based constraint on permafrost loss as a function of global warming. *Nature Climate Change*, *7*(5), 340–344.

Chambers, J. M., & Hastie, T. (1992). Linear models. Chapter 4. In *Statistical models in S* (p. 608). Wadsworth & Brooks/Cole Advanced Books & Software.

Christophersen, N., & Hooper, R. P. (1992). Multivariate analysis of stream water chemical data: The use of principal components analysis for the end-member mixing problem. *Water Resources Research*, *28*(1), 99–107. https://doi.org/10.1029/91WR02518

Cicoira, A., Beutel, J., Faillettaz, J., & Vieli, A. (2019). Water controls the seasonal rhythm of rock glacier flow. *Earth and Planetary Science Letters*, *528*. https://doi.org/10.1016/j.epsl.2019.115844

Clark, I. D., & Fritz, P. (1997). *Environmental Isotopes in Hydrogeology*. *Environmental Isotopes in Hydrogeology*. CRC Press. https://doi.org/10.1201/9781482242911

Clayton, R. N., Mayeda, T. K., & Hurd, J. M. (1974). Loss of oxygen, silicon, sulfur, and potassium from the lunar regolith. In *Lunar and Planetary Science Conference Proceedings* (Vol. 5, pp. 1801–1809).

Clayton, R. N., & Steiner, A. (1975). Oxygen isotope studies of the geothermal system at Wairakei, New Zealand. *Geochimica et Cosmochimica Acta*, *39*(8), 1179–1186. https://doi.org/10.1016/0016-7037(75)90059-9

Cochand, M., Christe, P., Ornstein, P., & Hunkeler, D. (2019). Groundwater Storage in High Alpine Catchments and Its Contribution to Streamflow. *Water Resources Research*. https://doi.org/10.1029/2018WR022989

Craig, H. (1961). Isotopic variations in meteoric waters. *Science*, *133*(3465), 1702–1703. https://doi.org/10.1126/science.133.3465.1702

Craig, H., & Gordon, L. I. (1965). Deuterium and oxygen 18 variations in the ocean and the marine atmosphere.

Cremonese, E., Gruber, S., Phillips, M., Pogliotti, P., Boeckli, L., Noetzli, J., … Zischg, A. (2011). “An inventory of permafrost evidence for the European Alps.” *The Cryosphere*, *5*, 651–657. https://doi.org/10.5194/tc-5-651-2011

Czarnowsky, V. (2016). *Isotopenchemische und hydrologische Untersuchungen an perennierenden und episodischen Quellen zum Nachweis von Untergrundeis an den Seitenmoränen im Gletschervorfeld des Gepatschferners (Tirol ,Österreich )*. Leipzig.

Dansgaard, W. (1953). The Abundance of O18 in Atmospheric Water and Water Vapour. *Tellus*, *5*(4), 461–469. https://doi.org/10.1111/j.2153-3490.1953.tb01076.x

Dansgaard, W. (1954). Oxygen-18 abundance in fresh water. *Nature*, *174*(4422), 234–235. https://doi.org/10.1038/174234a0

Dansgaard, W. (1959). The content of heavy oxygen isotope in the water masses of the Philippine Trench. *Deep Sea Research (1953)*, *6*, 346–350. https://doi.org/10.1016/0146-6313(59)90094-2

Dansgaard, W. (1964). Stable isotopes in precipitation. *Tellus*, *16*(4), 436–468. https://doi.org/10.1111/j.2153-3490.1964.tb00181.x

Dansgaard, W., Nief, G., & Roth, E. (1960). Isotopic Distribution in a Greenland Iceberg. *Nature*, *185*(4708), 232–232. https://doi.org/10.1038/185232a0

Daraoui, A., Michel, R., Gorny, M., Jakob, D., Sachse, R., Tosch, L., … Alfimov, V. (2012). *Iodine-129 and iodine-127 in seawater of the North Sea and precipitation from northern Germany*.

Daraoui, A., Riebe, B., Walther, C., Wershofen, H., Schlosser, C., Vockenhuber, C., & Synal, H. A. (2016). Concentrations of iodine isotopes (129I and 127I) and their isotopic ratios in aerosol samples from Northern Germany. *Journal of Environmental Radioactivity*, *154*, 101–108. https://doi.org/10.1016/j.jenvrad.2016.01.021

Day, T. J., & Day, T. T. (1977). Field procedures and evaluation of a slug dilution gauging method in mountain streams. *Journal of Hydrology (New Zealand)*, *16*, 113–133. https://doi.org/10.2307/43944411

Defant, F. (1951). Local winds. In *Compendium of meteorology* (pp. 667–669). Springer.

Dickin, A. P. (2005). Radiogenic Isotope Geology, *2*. https://doi.org/10.1017/CBO9781139165150

Dietermann, N., & Weiler, M. (2013). Spatial distribution of stable water isotopes in alpine snow cover. *Hydrology and Earth System Sciences*, *17*(7), 2657–2668. https://doi.org/10.5194/hess-17-2657-2013

Dong, Z., Shao, Y., Qin, D., Zhang, L., Hou, X., Wei, T., … Qin, X. (2018). Insight Into Radio-Isotope 129I Deposition in Fresh Snow at a Remote Glacier Basin of Northeast Tibetan Plateau, China. *Geophysical Research Letters*, *45*(13), 6726–6733. https://doi.org/10.1029/2018GL078480

Driesner, T. (1997). The Effect of Pressure on Deuterium-Hydrogen Fractionation in High-Temperature Water. *Science*, *277*(5327), 791–794. https://doi.org/10.1126/SCIENCE.277.5327.791

Dunn, O. J. (1961). Multiple Comparisons among Means. *Journal of the American Statistical Association*, *56*(293), 52–64. https://doi.org/10.1080/01621459.1961.10482090

Dunn, O. J. (1964). Multiple Comparisons Using Rank Sums. *Technometrics*, *6*(3), 241. https://doi.org/10.2307/1266041

Dwivedi, R., Meixner, T., McIntosh, J. C., Ferré, P. A. T., Eastoe, C. J., Niu, G. Y., … Chorover, J. (2019). Hydrologic functioning of the deep critical zone and contributions to streamflow in a high-elevation catchment: Testing of multiple conceptual models. *Hydrological Processes*, *33*(4), 476–494. https://doi.org/10.1002/HYP.13363

Edwards, R. R. (1962). Iodine-129: Its occurrence in nature and its utility as a tracer. *Science*, *137*(3533), 851–853. https://doi.org/10.1126/science.137.3533.851

EEA. (2021). *Water resources across Europe - confronting water stress: an updated assessment*.

Elder, K., Kattelmann, R., & Ferguson, R. (1990). Refinements in dilution gauging for mountain streams. *Hydrology in Mountainous Regions I. IAHS Publication*, *193*, 247–254.

Engel, M., Penna, D., Bertoldi, G., Dell'Agnese, A., Soulsby, C., & Comiti, F. (2016). Identifying run-off contributions during melt-induced run-off events in a glacierized alpine catchment. *Hydrological Processes*, *30*(3), 343–364. https://doi.org/10.1002/HYP.10577

Ernst, T. (2003). *Anthropogenes Iod-129 als Tracer für Umweltprozesse Ein Beitrag zum Verhalten von Spurenstoffen bei der Migration in Böden und beim atmosphärischen Transport*. Universität Hannover.

Fabryka-Martin, J., Bentley, H., Elmore, D., & Airey, P. . L. (1985). Natural iodine-129 as an environmental tracer. *Geochimica et Cosmochimica Acta*, *49*(2), 337–347. https://doi.org/10.1016/0016-7037(85)90027-4

Fischer, B. M. C., van Meerveld, H. J. (Ilja), & Seibert, J. (2017). Spatial variability in the isotopic composition of rainfall in a small headwater catchment and its effect on hydrograph separation. *Journal of Hydrology*, *547*, 755–769. https://doi.org/10.1016/J.JHYDROL.2017.01.045

Fleischer, F., Haas, F., Piermattei, L., Pfeiffer, M., Heckmann, T., Altmann, M., … Becht, M. (2021). Multi-decadal (1953--2017) rock glacier kinematics analysed by high-resolution topographic data in the upper Kaunertal, Austria. *The Cryosphere*, *15*(12), 5345–5369. https://doi.org/10.5194/tc-15-5345-2021

Förstel. (2006, September 7). Isotopen-Analyse, Herkunftsüberprüfung, Rückverfolgbarkeitssysteme. Retrieved March 11, 2019, from http://www.agroisolab.de/

Frauenfelder, R., & Kääb, A. (2000). Towards a palaeoclimatic model of rock glacier formation in the Swiss Alps. *Annals of Glaciology*. https://doi.org/10.3189/172756400781820264

Fritz, P., Cherry, J. A., Weyer, K. U., & Sklash, M. (Waterloo U. . O. (Canada). D. of E. S. (1976). Storm runoff analyses using environmental isotopes and major ions. *Panel Proceedings Series - International Atomic Energy Agency (IAEA)*.

Retrieved from http://agris.fao.org/agris-search/search.do?recordID=XF7602740

Froehlich, K., Kralik, M., Papesch, W., Rank, D., Scheifinger, H., & Stichler, W. (2008). Deuterium excess in precipitation of Alpine regions - Moisture recycling. *Isotopes in Environmental and Health Studies*, *44*(1), 61–70. https://doi.org/10.1080/10256010801887208

Frohlich, K., Gibson, J. J., & Aggarwal, P. K. (2002). DEUTERIUM EXCESS IN PRECIPITATION AND ITS CLIMATOLOGICAL SIGNIFICANCE. In *IAEA-CN-80/104* (pp. 54–66). IAEA.

Galewsky, J., Steen-Larsen, H. C., Field, R. D., Worden, J., Risi, C., & Schneider, M. (2016). Stable isotopes in atmospheric water vapor and applications to the hydrologic cycle. *Reviews of Geophysics*, *54*(4), 809–865. https://doi.org/10.1002/2015RG000512

García-Toraño, E., Altzitzoglou, T., Auerbach, P., Bé, M. M., Bobin, C., Cassette, P., … Sochorová, J. (2018). The half-life of 129I. *Applied Radiation and Isotopes*, *140*, 157–162. https://doi.org/10.1016/j.apradiso.2018.06.007

Gat, J. R. (1996). Oxygen and hydrogen isotopes in the hydrologic cycle. *Annual Review of Earth and Planetary Sciences*, *24*(1), 225–262. https://doi.org/10.1146/annurev.earth.24.1.225

Gat, J. R. (2000). Atmospheric water balance-the isotopic perspective. In *Hydrological Processes*. https://doi.org/10.1002/1099-1085(20000615)14:8<1357::AID-HYP986>3.0.CO;2-7

Gat, J. R., Mook, W. G., & Meijer, H. A. J. (2001). Environmental isotopes in the hydrological cycle Principles and applications Atmospheric water United Nations Educational, International Atomic Energy Agency Scientific and Cultural Organization. *Technical Documents in Hydrology I No*, *39*.

Geboy, N. J., & Engle, M. A. (2011). *Quality assurance and quality control of geochemical data: A primer for the research scientist*. US Department of the Interior, US Geological Survey.

Germain, P., Nuclear Safety and Protection Institute. Marine Radioecological Laboratory., & Great Britain. Ministry of Agriculture, F. and F. (1997). *Radionuclides in the oceans : RADOC 96-97 : Cherbourg-Octevill, France, 7-11 October, 1996 : proceedings part 1 : inventories, behaviour and processes*. Les Editions de Physique.

Gilfedder, B. S., Lai, S. C., Petri, M., Biester, H., Hoffmann, T., Beister, H., … Hoffmann, T. (2008). Iodine speciation in rain, snow and aerosols. *Atmospheric Chemistry and Physics*, *8*(20), 6069–6084. https://doi.org/10.5194/acp-8-6069-2008

Giustini, F., Brilli, M., & Patera, A. (2016). Mapping oxygen stable isotopes of

precipitation in Italy. *Journal of Hydrology: Regional Studies*, *8*, 162–181. https://doi.org/10.1016/J.EJRH.2016.04.001

Gobiet, A., Kotlarski, S., Beniston, M., Heinrich, G., Rajczak, J., & Stoffel, M. (2014). 21st century climate change in the European Alps—A review. *Science of the Total Environment*, *493*, 1138–1151. https://doi.org/10.1016/J.SCITOTENV.2013.07.050

Gómez-Guzmán, J. M., Enamorado-Báez, S. M., Pinto-Gómez, A. R., Abril-Hernández, J. M., López-Gutiérrez, J. M., & García-León, M. (2012). Anthropogenic 129I concentration and 129I/127I ratio in rainwater from Seville (Spain) in the period 2005–2008 as affected by airborne releases from Sellafield and La Hague facilities. *Atmospheric Environment*, *56*, 26–32. https://doi.org/10.1016/J.ATMOSENV.2012.03.075

Gressel, W. (1973). Die europäische Wetterentwicklung und ihr Einfluß auf den Südalpenraum. *Carinthia II*, *163_83*, 253–265.

Groh, T., & Blöthe, J. H. (2019). Rock glacier kinematics in the kaunertal, Ötztal alps, Austria. *Geosciences (Switzerland)*, *9*(9). https://doi.org/10.3390/geosciences9090373

Gröning, M., Lutz, H. O., Roller-Lutz, Z., Kralik, M., Gourcy, L., & Pöltenstein, L. (2012). A simple rain collector preventing water re-evaporation dedicated for δ18O and δ2H analysis of cumulative precipitation samples. *Journal of Hydrology*, *448–449*, 195–200. https://doi.org/10.1016/j.jhydrol.2012.04.041

Gruber, S. (2012). Derivation and analysis of a high-resolution estimate of global permafrost zonation. *Cryosphere*, *6*(1), 221–233. https://doi.org/10.5194/TC-6-221-2012

Gui, J., Li, Z., Yuan, R., & Xue, J. (2019). Hydrograph separation and the influence from climate warming on runoff in the north-eastern Tibetan Plateau. *Quaternary International*, *525*, 45–53. https://doi.org/10.1016/J.QUAINT.2019.09.002

Haeberli, W., Hallet, B., Arenson, L., Elconin, R., Humlum, O., Kääb, A., … Vonder Mühll, D. (2006). Permafrost Creep and Rock Glacier Dynamics z. *Permafrost and Periglacial Processes*, *17*, 189–214. https://doi.org/10.1002/ppp.561

Hagemann, R., Nief, G., & Roth, E. (1970). Absolute isotopic scale for deuterium analysis of natural waters. Absolute D/H ratio for SMOW. *Tellus*, *22*(6), 712–715. https://doi.org/10.1111/j.2153-3490.1970.tb00540.x

Hager, B., & Foelsche, U. (2015). Stable isotope composition of precipitation in Austria. https://doi.org/10.17738/ajes.2015.0012

Haid, M., Gohm, A., Umek, L., Ward, H. C., & Rotach, M. W. (2022). Cold-Air Pool Processes in the Inn Valley During Föhn: A Comparison of Four Cases During the PIANO Campaign. *Boundary-Layer Meteorology*, *182*(3), 335–362.

Halla, C., Henrik Blöthe, J., Tapia Baldis, C., Trombotto Liaudat, D., Hilbich, C., Hauck, C., & Schrott, L. (2021). Ice content and interannual water storage changes of an active rock glacier in the dry Andes of Argentina. *Cryosphere*, *15*(2), 1187–1213. https://doi.org/10.5194/TC-15-1187-2021

Hammer, W. (1923). Geologische Spezialkarte der Republik Österreich - Nauders. Verlag der Geologischen Bundesanstalt.

Hasegawa, H., Kakiuchi, H., Akata, N., Ohtsuka, Y., & Hisamatsu, S. (2017). Regional and global contributions of anthropogenic iodine-129 in monthly deposition samples collected in North East Japan between 2006 and 2015. *Journal of Environmental Radioactivity*, *171*, 65–73. https://doi.org/10.1016/j.jenvrad.2017.01.027

Hauck, C., Böttcher, M., & Maurer, H. (2011). A new model for estimating subsurface ice content based on combined electrical and seismic data sets. *The Cryosphere*, *5*(2), 453–468.

Hausmann, H., Krainer, K., Brückl, E., & Mostler, W. (2007). Internal Structure and Ice Content of Reichenkar Rock Glacier (Stubai Alps, Austria). *Permafrost and Periglacial Processes*, *18*(18), 351–367. https://doi.org/10.1002/ppp

Hausmann, H., Krainer, K., Brückl, E., & Ullrich, C. (2012). Internal structure, ice content and dynamics of Ölgrube and kaiserberg rock glaciers (Ötztal Alps, Austria) determined from geophysical surveys. *Austrian Journal of Earth Sciences*, *105*(2), 12–31.

HD-Tirol. (2021). Precipitation data for Kaiserbergtal Valley, Gepatsch Dam.

Herod, M. N., Li, T., Pellerin, A., Kieser, W. E., & Clark, I. D. (2016). The seasonal fluctuations and accumulation of iodine-129 in relation to the hydrogeochemistry of the Wolf Creek Research Basin, a discontinuous permafrost watershed. *Science of the Total Environment*, *569–570*, 1212–1223. https://doi.org/10.1016/J.SCITOTENV.2016.06.196

Herrmann, A., Martinec, J., & Stichler, W. (1978). Study of snowmelt-runoff components using isotope measurements. *Modeling of Snow Cover Runoff, US Army Cold Regions Research and Engineering Laboratory, Hanover, New Hampshire*, 26–28.

Herrmann, A., & Stichler, W. (1980). Groundwater-runoff relationships. *CATENA*, *7*(2–3), 251–263. https://doi.org/10.1016/0341-8162(80)90011-9

Hoefs, J. (2015). *Stable Isotope Geochemistry*. Cham: Springer International Publishing. https://doi.org/10.1007/978-3-319-19716-6

Hoefs, J. (2018). Stable Isotope Geochemistry. https://doi.org/10.1007/978-3-319-78527-1

Hofem, S. (2018). Autentizität von Wasser (Proben von Jacob [sic!] Müller).

Agroisolab GmbH.

Hoffmann, G., Cuntz, M., Jouzel, J., & Werner, M. (2005). How much climatic information do water isotopes contain? A systematic comparison between the IAEA/GNIP isotope network and the ECHAM 4 atmospheric general circulation model. *Isotopes in the Water Cycle: Past, Present and Future of a Developing Science*, 303–320. https://doi.org/10.1007/1-4020-3023-1_19/COVER

Hoinkes, G., Koller, F., Rantitsch, G., Dachs, E., Höck, V., Neubauer, F., & Schuster, R. (1999). Alpine metamorphism of the Eastern Alps. *Schweizerische Mineralogische Und Petrographische Mitteilungen*, (79), 155–181.

Hoinkes, G., Thöni, M., Bernhard, F., Kaindl, R., Lichem, C., Schweigl, J., … Cosca, M. (1997). Metagranitoids and associated metasediments as indicators for the pre-Alpine magmatic and metamorphic evolution of the Western Austroalpine Ötztal Basement (Kaunertal, Tirol). *Schweizerische Mineralogische Petrographische Mitteilungen*, *77*, 299–314.

Holden, N. E., de Laeter, J. R., Tepper, D. H., Yoneda, S., Walczyk, T., Roth, E., … O'Connor, G. (2018). IUPAC Periodic Table of the Elements and Isotopes (IPTEI) for the Education Community (IUPAC Technical Report). *Pure and Applied Chemistry*, *90*(12), 1833–2092. https://doi.org/10.1515/pac-2015-0703

Hollander, M., Wolfe, D. A., & Chicken, E. (2013). Nonparametric statistical methods, Wiley Series in Probability and Statistics, 848. Retrieved from https://www.wiley.com/en-us/Nonparametric+Statistical+Methods%2C+3rd+Edition-p-9780470387375

Hölting, B., & Coldewey, W. G. (2013). *Hydrogeologie: Einführung in die Allgemeine und Angewandte Hydrogeologie*. Springer Verlag Berlin Heidelberg. https://doi.org/10.1007/978-3-8274-2354-2

Holzhauser, H. (1982). Neuzeitliche Gletscherschwankungen. *Geographica Helvetica*, *37*(2), 115–126. https://doi.org/10.5194/gh-37-115-1982

Hooper, R., & Christophersen, N. (1990). Modelling streamwater chemistry as a mixture of soilwater end-members—An application to the Panola Mountain catchment, Georgia, USA. *Hydrology*. Retrieved from https://www.sciencedirect.com/science/article/pii/002216949090131G

Hou, X., Hansen, V., Aldahan, A., Possnert, G., Lind, O. C., & Lujaniene, G. (2009). A review on speciation of iodine-129 in the environmental and biological samples. *Analytica Chimica Acta*, *632*(2), 181–196. https://doi.org/10.1016/j.aca.2008.11.013

Hubert, P., Marin, E., & Meybeck, M. (1969). *Aspects hydrologique, géochimique et sédimentologique de la crue exceptionnelle de la Dranse du Chablais du 22 septembre 1968*.

Hudson, R., & Fraser, J. (2008). Introduction to Salt Dilution Gauging for Streamflow

Measurement Part IV : The Mass Balance ( or Dry Injection ) Method. Retrieved from https://www.semanticscholar.org/paper/Introduction-to-Salt-Dilution-Gauging-for-Part-IV-%3A-Hudson-Fraser/2ca8a8883f5598b68dd7909fe3dbb4dc8ff37d75

Humer, G. (1995). Niederschlagsisotopenmessnetz Österreich. Retrieved from http://www.umweltbundesamt.at/fileadmin/site/publikationen/M052.pdf

Hürkamp, K., Zentner, N., Reckerth, A., Weishaupt, S., Wetzel, K. F., Tschiersch, J., & Stumpp, C. (2019). Spatial and temporal variability of snow isotopic composition on Mt. Zugspitze, Bavarian Alps, Germany. *Journal of Hydrology and Hydromechanics*, *67*(1), 49–58. https://doi.org/10.2478/johh-2018-0019

Hydrographischer_Dienst_Tirol. (2013). Klimadiagramme Land Tirol, Südtirol (Periode 1980-2000) (Tirol Atlas Kartenset »Klimadiagramme«) - Climate Chart Feichten - Kaunertal. Retrieved June 30, 2022, from https://tirolatlas.uibk.ac.at/graphics/lieth/diag.py/chart?lang=de;id=1390128

IAEA/WMO. (2022). Global Network of Isotopes in Precipitation. The GNIP Database. Retrieved March 14, 2022, from http://www.iaea.org/water

IAEA. (2022). IAEA Website. Retrieved March 15, 2022, from https://www.iaea.org/

Ikeda, A., & Matsuoka, N. (2002). Degradation of talus-derived rock glaciers in the Upper Engadin, Swiss Alps. *Permafrost and Periglacial Processes*, *13*(2), 145–161.

Immerzeel, W. W., Lutz, A. F., Andrade, M., Bahl, A., Biemans, H., Bolch, T., … Baillie, J. E. M. (2020). Importance and vulnerability of the world's water towers. *Nature*, *577*(7790), 364–369. https://doi.org/10.1038/s41586-019-1822-y

Ingraham, N. L., & Criss, R. E. (1993). Effects of surface area and volume on the rate of isotopic exchange between water and water vapor. *Journal of Geophysical Research*, *98*(D11), 20547. https://doi.org/10.1029/93JD01735

Ingraham, N. L., & Criss, R. E. (1998). The effect of vapor pressure on the rate of isotopic exchange between water and water vapor. *Chemical Geology*. https://doi.org/10.1016/S0009-2541(98)00109-0

Jabbar, T., Steier, P., Wallner, G., Priller, A., Kandler, N., & Kaiser, A. (2012). Iodine isotopes (127I and 129I) in aerosols at high altitude alp stations. *Environmental Science and Technology*, *46*(16), 8637–8644. https://doi.org/10.1021/es300948t

Jabbar, T., Wallner, G., & Steier, P. (2013). A review on 129I analysis in air. *Journal of Environmental Radioactivity*, *126*, 45–54. https://doi.org/10.1016/J.JENVRAD.2013.07.013

Jabbar, T., Wallner, G., Steier, P., Katzlberger, C., & Kandler, N. (2012). Retrospective measurements of airborne 129Iodine in Austria. *Journal of*

*Environmental Radioactivity*, *112*, 90–95. https://doi.org/10.1016/J.JENVRAD.2012.05.010

Jasechko, S. (2019, September 1). Global Isotope Hydrogeology—Review. *Reviews of Geophysics*. Blackwell Publishing Ltd. https://doi.org/10.1029/2018RG000627

Jin, H., Huang, Y., Bense, V. F., Ma, Q., Marchenko, S. S., Shepelev, V. V, … Jin, X. (2022). Permafrost Degradation and Its Hydrogeological Impacts. *Water*, *14*(3), 372.

Jódar, J., Cabrera, J. A., Martos-Rosillo, S., Ruiz-Constán, A., González-Ramón, A., Lambán, L. J., … Custodio, E. (2017). Groundwater discharge in high-mountain watersheds: A valuable resource for downstream semi-arid zones. The case of the Bérchules River in Sierra Nevada (Southern Spain). *Science of The Total Environment*, *593–594*, 760–772. https://doi.org/10.1016/J.SCITOTENV.2017.03.190

Johnstone, D. E. (1988). Some recent developments of constant-injection salt dilution gauging in rivers. *Journal of Hydrology (New Zealand)*, *27*, 128–153. https://doi.org/10.2307/43944616

Jones, D. B., Harrison, S., & Anderson, K. (2019). Mountain glacier-to-rock glacier transition. *Global and Planetary Change*, *181*, 13. https://doi.org/10.1016/J.GLOPLACHA.2019.102999

Jones, D. B., Harrison, S., Anderson, K., & Whalley, W. B. (2019). Rock glaciers and mountain hydrology: A review. *Earth-Science Reviews*, *193*, 66–90. https://doi.org/10.1016/J.EARSCIREV.2019.04.001

Jouzel, J., Merlivat, L., & Roth, E. (1975). Isotopic study of hail. *Journal of Geophysical Research*, *80*(36), 5015–5030. https://doi.org/10.1029/JC080i036p05015

Kääb, A. (2013). Rock Glaciers and Protalus Forms. In *Encyclopedia of Quaternary Science: Second Edition* (pp. 535–541). Elsevier Inc. https://doi.org/10.1016/B978-0-444-53643-3.00104-7

Kääb, Andreas, & Weber, M. (2004). Development of transverse ridges on rock glaciers: Field measurements and laboratory experiments. *Permafrost and Periglacial Processes*. https://doi.org/10.1002/ppp.506

Kadowaki, M., Katata, G., Terada, H., Suzuki, T., Hasegawa, H., Akata, N., & Kakiuchi, H. (2018). Impacts of anthropogenic source from the nuclear fuel reprocessing plants on global atmospheric iodine-129 cycle: A model analysis. *Atmospheric Environment*, *184*, 278–291. https://doi.org/10.1016/j.atmosenv.2018.04.044

Kaindl, R., Hoinkes, G., Knoll, P., & Abart, R. (1999). Fluid inclusions related to Variscan and Alpine metamorphism in the Austroalpine Ötztal Basement,

Eastern Alps. *Mineralogy and Petrology*, *65*(1–2), 29–49. https://doi.org/10.1007/BF01161575

Kamleitner, S. (2017). *Is there still dead ice in the Little Ice Age lateral moraine?* University of Vienna.

Kamleitner, S., Lachner, J., Steier, P., Weise, S. M., & Kraushaar, S. (2019). 129I concentration in a high-mountain environment. *Nuclear Instruments and Methods in Physics Research, Section B: Beam Interactions with Materials and Atoms*, *456*(January 2018), 193–202. https://doi.org/10.1016/j.nimb.2019.05.003

Katcoff, S., Schaeffer, O. A., & Hastings, J. M. (1951). Half-Life of I 129 and the Age of the Elements. *Physical Review*, *82*(5), 688–690. https://doi.org/10.1103/PhysRev.82.688

Kern, Z., Hatvani, I. G., Czuppon, G., Fórizs, I., Erdélyi, D., Kanduč, T., … Vreča, P. (2020). Isotopic 'altitude'and 'continental'effects in modern precipitation across the Adriatic–Pannonian Region. *Water*, *12*(6), 1797.

Kerschner, H. (1978). Paleoclimatic Inferences from Late Würm Rock Glaciers , Eastern Central Alps , Western Tyrol. *Arctic and Alpine Research*, *10*(3), 635–644. https://doi.org/10.1080/00040851.1978.12004000

Kerschner, H., & Ivy-Ochs, S. (2008). Palaeoclimate from glaciers: Examples from the Eastern Alps during the Alpine Lateglacial and early Holocene. *Global and Planetary Change*, *60*(1–2), 58–71. https://doi.org/10.1016/J.GLOPLACHA.2006.07.034

Klaus, J., & McDonnell, J. J. (2013). Hydrograph separation using stable isotopes: Review and evaluation. *Journal of Hydrology*, *505*, 47–64. https://doi.org/10.1016/j.jhydrol.2013.09.006

Klipsch, K. (2005). Bestimmung von 129I und 127I in Umweltproben zwecks der Ermittlung radioökologischer Parameter des 129I auf seinem Weg von Quellen durch die Nahrungskette bis zum Menschen. Hannover: Universität.

Kocher, D. C. (1981). A dynamic model of the global iodine cycle and estimation of dose to the world population from releases of iodine-129 to the environment. *Environment International*, *5*(1), 15–31. https://doi.org/10.1016/0160-4120(81)90110-0

Krainer, K. (2011). Blockgletscherinventar Tirol. *Mitteilungsblatt Des Hydrographischen Dienstes in Österreich*, (87), 67–87.

Krainer, K. (2015a). Blockgletscher in den Ötztaler und Stubaier Alpen: Eine Überischt. In *Forschung am Blockgletscher: Methoden und Ergebnisse* (pp. 33–54). Innsbruck University Press.

Krainer, K. (2015b). Blockgletscher in Tirol. Bozen: Permaqua.

Krainer, K., Bressan, D., Dietre, B., Haas, J. N., Hajdas, I., Lang, K., … Tonidandel, D. (2015). A 10,300-year-old permafrost core from the active rock glacier Lazaun, southern Ötztal Alps (South Tyrol, northern Italy). *Quaternary Research (United States)*, *83*(2), 324–335. https://doi.org/10.1016/j.yqres.2014.12.005

Krainer, K., & He, X. (2006). Flow velocities of active rock glaciers in the Austrian Alps. *Geografiska Annaler, Series A: Physical Geography*. https://doi.org/10.1111/j.0435-3676.2006.00300.x

Krainer, K., & Mostler, W. (2002). Hydrology of active rock glaciers: Examples from the Austrian Alps. *Arctic, Antarctic, and Alpine Research*, *34*(2), 142. https://doi.org/10.2307/1552465

Krainer, K., Mostler, W., & Chrisoph, S. (2007). Discharge from active rock glaciers, Austrian Alps: a stable isotope approach. *Austrian Journal of Earth Sciences*, *100*, 102–112. Retrieved from www.geol-ges.at/undwww.biologiezentrum.at

Krainer, K., & Ribis, M. (2009). Blockgletscher und ihre hydrologische Bedeutung im Hochgebirge. *Mitteilungsblatt Des Hydrographischen Dienstes in Österreich*, *86*(86), 65–78.

Krainer, K., & Ribis, M. (2012). A rock glacier inventory of the tyrolean alps (Austria). *Austrian Journal of Earth Sciences*.

Kralik, M. (2018). *280096 VU Tracer Hydrology*.

Kralik, M., Benischke, R., Wyhlidal, S., & Philippitsch, R. (2015). *Erläuterungen zur Wasserisotopenkarte Österreichs*. Wien.

Kralik, M., Benischke, R., Wyhlidal, S., & Philippitsch, R. (2017). First Water-Isotope-Map (δ18O, δ2H, 3H) of Austria: Applications, Extremes and Trends. *Procedia Earth and Planetary Science*, *17*, 924–927. https://doi.org/10.1016/j.proeps.2017.01.021

Kraushaar, S., & Blöthe, J. H. (2022). Towards deciphering the contribution of permafrost and active layer to summer runoff in a small alpine catchment. In *EGU* (p. 10). Vienna.

Krenmayr, H. G. (2016). Geofast 1:50.000 - 172 - Weißkugel. Geologische Bundesanstalt.

Krugger, M. I., & Stern, H. P. (2009). *New permafrost and glacier research*. New York : Nova Science Publishers,. Retrieved from http://search.ebscohost.com/login.aspx?direct=true&scope=site&db=nlebk&AN=315734

Krupp, G., & Aumann, D. C. (1999). Iodine-129 in rainfall over Germany. *Journal of Environmental Radioactivity*, *46*(3), 287–299. https://doi.org/10.1016/S0265-931X(98)00148-9

Leibundgut, C., Maloszewski, P., & Külls, C. (2009). *Tracers in Hydrology*. Wiley-Blackwell. Retrieved from http://lib1.org/_ads/2C6B23D59C547D0970BC1A5D6AD90A7A

Leibundgut, C., & Seibert, J. (2011). Tracer Hydrology. In *Treatise on Water Science* (Vol. 2, pp. 215–236). Elsevier. https://doi.org/10.1016/B978-0-444-53199-5.00036-1

Lewis, S. C., Legrande, A. N., Kelley, M., & Schmidt, G. A. (2013). Modeling insights into deuterium excess as an indicator of water vapor source conditions. *Journal of Geophysical Research: Atmospheres*, *118*(2), 243–262. https://doi.org/10.1029/2012JD017804

Liu, J., Fu, G., Song, X., Charles, S. P., Zhang, Y., Han, D., & Wang, S. (2010). Stable isotopic compositions in Australian precipitation. *Journal of Geophysical Research Atmospheres*. https://doi.org/10.1029/2010JD014403

Liu, X., Fehn, U., & Teng, R. T. D. (1997). Oil formation and fluid convection in Railroad Valley, NV: a study using cosmogenic isotopes to determine the onset of hydrocarbon migration. *Nuclear Instruments and Methods in Physics Research Section B: Beam Interactions with Materials and Atoms*, *123*(1–4), 356–360. https://doi.org/10.1016/S0168-583X(96)00631-3

Markovich, K. H., Dahlke, H. E., Arumí, J. L., Maxwell, R. M., & Fogg, G. E. (2019). Bayesian hydrograph separation in a minimally gauged alpine volcanic watershed in central Chile. *Journal of Hydrology*, *575*, 1288–1300. https://doi.org/10.1016/J.JHYDROL.2019.06.014

Markovich, K. H., Manning, A. H., Condon, L. E., & McIntosh, J. C. (2019). Mountain-Block Recharge: A Review of Current Understanding. *Water Resources Research*, *55*(11), 8278–8304. https://doi.org/10.1029/2019WR025676

Masiol, M., Zannoni, D., Stenni, B., Dreossi, G., Zini, L., Calligaris, C., … Treu, F. (2021). Spatial distribution and interannual trends of δ18O, δ2H, and deuterium excess in precipitation across North-Eastern Italy. *Journal of Hydrology*, *598*. https://doi.org/10.1016/j.jhydrol.2020.125749

Mergili, M., Jaboyedoff, M., Pullarello, J., & Pudasaini, S. P. (2020). Back calculation of the 2017 Piz Cengalo–Bondo landslide cascade with r. avaflow: what we can do and what we can learn. *Natural Hazards and Earth System Sciences*, *20*(2), 505–520.

Merlivat, L., & Jouzel, J. (1979). Global climatic interpretation of the deuterium-oxygen 16 relationship for precipitation. *Journal of Geophysical Research*. https://doi.org/10.1029/JC084iC08p05029

Miller, S. A., Mercer, J. J., Lyon, S. W., Williams, D. G., & Miller, S. N. (2021). Stable isotopes of water and specific conductance reveal complimentary information on streamflow generation in snowmelt-dominated, seasonally arid watersheds.

*Journal of Hydrology*, *596*. https://doi.org/10.1016/j.jhydrol.2021.126075

Monnier, S., & Kinnard, C. (2015). Internal Structure and Composition of a Rock Glacier in the Dry Andes, Inferred from Ground-penetrating Radar Data and its Artefacts. *Permafrost and Periglacial Processes*, *26*(4), 335–346. https://doi.org/10.1002/ppp.1846

Mook, W. G., Groeneveld, D. J., Brouwn, A. E., & Ganswijk, A. J. van. (1974). *Analysis of a run-off hydrograph by means of natural 18O*. International Atomic Energy Agency (IAEA): IAEA. Retrieved from http://inis.iaea.org/search/search.aspx?orig_q=RN:38048671

Moore, R. D. D. D. (2003). Introduction to salt dilution gauging for streamflow measurement: part 1. *Streamline Watershed Management Bulletin*, *7*(2), 20–23. https://doi.org/10.1592/phco.23.9.1S.32890

Moran, J. E., Fehn, U., & Teng, R. T. D. (1998). Variations in 129I/127I ratios in recent marine sediments: evidence for a fossil organic component. *Chemical Geology*, *152*(1–2), 193–203. https://doi.org/10.1016/S0009-2541(98)00106-5

Morche, D., Schuchardt, A., Dubberke, K., & Baewert, H. (2014). Channel morphodynamics on a small proglacial braid plain (Fagge River, Gepatschferner, Austria). *IAHS-AISH Proceedings and Reports*, *367*(December 2014), 109–116. https://doi.org/10.5194/piahs-367-109-2015

Moser, H., & Stichler, W. (1970). Verwendung des Deuterium-und Sauerstoff-18-Gehalts bei hydrologischen Untersuchungen. In *Isotope Hydrology 1970* (pp. 43–54). Geol. Bavarica.

Muller, S. W. (1943). Permafrost or permanently frozen ground and related engineering problems. Special Report, Strategic Engineering Study no. 62. *Intelligence Branch, Office of the Chief of Engineers*.

Munroe, J. S., & Handwerger, A. L. (2022). Contribution of Rock Glacier Discharge to Late-Summer and Fall Streamflow in the Uinta Mountains , Utah , USA, (September), 1–25.

National Council on Radiation Protection and Measurements. (1983). *Iodine-129, evaluation of releases from nuclear power generation*. The Council.

Nicolussi, K., Lumassegger, G., Patzelt, G., Pindur, P., & Schiessling, P. (2001). Aufbau einer holozänen Hochlagen-Jahrring-Chronologie für die zentralen Ostalpen: Möglichkeiten und erste Ergebnisse. *Innsbrucker Geographische Gesellschaft (Hrsg.): Innsbrucker Jahresbericht*, *2*(16), 114–136.

Nimz, G. J. (1995). Lithogenic and Cosmogenic Tracers in Catchment Hydrology.

Olivieri, L., & Bettanini, C. (2022). Preliminary observation of Marmolada glacier collapse of July 2022 with space-based cameras. *Https://Doi.Org/10.1080/2150704X.2022.2152754*, *14*(1), 21–29.

https://doi.org/10.1080/2150704X.2022.2152754

Osterc, A., & Stibilj, V. (2011). The Potential Of I-129 as an Environmental Tracer. *Radioisotopes - Applications in Physical Sciences*. https://doi.org/10.5772/23711

Patzelt, G., Bortenschlager, S., & Frenzel, B. (1976). Spät-und Postglazial im Ötztal und Inntal (Ostalpen, Tirol). *Frenzel, B*, 5–13.

Pearson, K. (1901). On lines and planes of closest fit to systems of points in space. *Philosophical Magazine*, *2*(11), 559–572. https://doi.org/10.1080/14786440109462720

Penna, D., Engel, M., Mao, L., Dell'agnese, A., Bertoldi, G., & Comiti, F. (2014). Tracer-based analysis of spatial and temporal variations of water sources in a glacierized catchment. *Hydrology and Earth System Sciences*, *18*(12), 5271–5288. https://doi.org/10.5194/HESS-18-5271-2014

Pfahl, S., & Sodemann, H. (2014). Climate of the Past What controls deuterium excess in global precipitation? *Climate of the Past*, *10*, 771–781. https://doi.org/10.5194/cp-10-771-2014

Pfiffner, O. A. (2014). *Geology of the Alps*. (John Wiley & Sons, Ed.) (2nd editio). UTB. Retrieved from http://www.ghbook.ir/index.php?name=فرهنگ و رسانه های نوین&option=com_dbook&task=readonline&book_id=13650&page=73&chkhashk=ED9C9491B4&Itemid=218&lang=fa&tmpl=component

Pokrovsky, O. S. (2014). *Permafrost: Distribution, composition and impacts on infrastructure and ecosystems*. *Permafrost: Distribution, Composition and Impacts on Infrastructure and Ecosystems*.

Potter, N. (1972). Ice-cored rock glacier, Galena Creek, northern Absaroka Mountains, Wyoming. *Bulletin of the Geological Society of America*, *83*(10), 3025–3058. https://doi.org/10.1130/0016-7606(1972)83[3025:IRGGCN]2.0.CO;2

Povinec, P. P., Aoyama, M., Biddulph, D., Breier, R., Buesseler, K., Chang, C. C., … Zhang, L. Y. (2013). Climate of the Past Geoscientific Instrumentation Methods and Data Systems Cesium, iodine and tritium in NW Pacific waters-a comparison of the Fukushima impact with global fallout. *Biogeosciences*, *10*, 5481–5496. https://doi.org/10.5194/bg-10-5481-2013

Pruessner, L., Huss, M., Phillips, M., & Farinotti, D. (2021). A Framework for Modeling Rock Glaciers and Permafrost at the Basin-Scale in High Alpine Catchments. *Journal of Advances in Modeling Earth Systems*, *13*(4), e2020MS002361. https://doi.org/10.1029/2020MS002361

Purtscheller, F., & Sassi, F. P. (1975). Some thoughts on the pre-Alpine metamorphic history of the Austridic basement of the Eastern Alps. *Tschermaks Mineralogische Und Petrographische Mitteilungen*, *22*(3), 175–

199.

Putman, A. L., Fiorella, R. P., Bowen, G. J., & Cai, Z. (2019). A Global Perspective on Local Meteoric Water Lines: Meta-analytic Insight Into Fundamental Controls and Practical Constraints. *Water Resources Research*, *55*(8), 6896–6910. https://doi.org/10.1029/2019WR025181

R_Core_Team. (2022). R: A Language and Environment for Statistical Computing. Vienna, Austria: R Foundation for Statistical Computing. Retrieved from https://www.r-project.org/

Rahn, K. A., Borys, R. D., & Duce, R. A. (1976). Tropospheric halogen gases: Inorganic and organic components. *Science*, *192*(4239), 549–550. https://doi.org/10.1126/science.192.4239.549

Ralf, B., Benischke, R., & Harum, T. (1990). Hydrology in Mountainous Regions. Hydrological Measurements; the Water Cycle (proceedings of two Lausanne Symposia). *Research Gate*, (193). Retrieved from https://www.researchgate.net/publication/242569468

Reithmeier, H., Lazarev, V., Kubo, F., Rühm, W., & Nolte, E. (2005). 129I in precipitation using a new TOF system for AMS measurements. *Nuclear Instruments and Methods in Physics Research Section B: Beam Interactions with Materials and Atoms*, *239*(3), 273–280. https://doi.org/10.1016/J.NIMB.2005.04.070

Reithmeier, H., Lazarev, V., Rühm, W., & Nolte, E. (2010). Anthropogenic 129I in the atmosphere: Overview over major sources, transport processes and deposition pattern. *Science of The Total Environment*, *408*(21), 5052–5064. https://doi.org/10.1016/J.SCITOTENV.2010.07.015

Reithmeier, H., Lazarev, V., Rühm, W., Schwikowski, M., Gäggeler, H. W., & Nolte, E. (2006). Estimate of European129I releases supported by129I analysis in an alpine ice core. *Environmental Science and Technology*, *40*(19), 5891–5896. https://doi.org/10.1021/es0605725

Richardson, M. I., Toigo, A. D., & Newman, C. E. (2007). PlanetWRF: A general purpose, local to global numerical model for planetary atmospheric and climate dynamics. *Journal of Geophysical Research E: Planets*, *112*(9), E09001. https://doi.org/10.1029/2006JE002825

Rindsberger, M., Jaffe, S., Rahamim, S., & Gat, J. R. (1990). Patterns of the isotopic composition of precipitation in time and space: data from the Israeli storm water collection program. *Tellus B*, *42*(3), 263–271.

Rozanski, K, Araguás-Araguás, L., Gonfiantini, R., Swart, P. K., Lohmann, K. C., McKenzie, J. A., & Savin, S. (1993). Climate change in continental isotopic records. *Climate Changes in Continental Isotopic Records*, *78*, 1–36.

Rozanski, Kazimierz, Araguás-Araguás, L., & Gonfiantini, R. (1992). Isotopic

Patterns in Modern Global Precipitation. *Journal of Geophysical Research Atmospheres*, (January), 1–36. https://doi.org/10.1029/gm078p0001

RStudio_Team. (2022). RStudio: Integrated Development Environment for R. Boston, MA: RStudio, Inc. Retrieved from http://www.rstudio.com/

Rutzinger, M., Heinrich, K., Borsdorf, A., & Stötter, J. (2014). *permAfrost, Austrian Permafrost Initiative. Final Report*.

Salminen, R. (Chief-editor), Batista, M. J., Bidovec, M., Demetriades, A., De Vivo, B., De Vos, W., … Tarvainen, T. (2005). Geochemical Atlas of Europe. *Geochemical Atlas of Europe. Part 1: Background Information, Methodology and Maps*. Espoo, Geological Survey of Finland. Retrieved from http://weppi.gtk.fi/publ/foregsatlas/

Santin, I., Colucci, R. R., Žebre, M., Pavan, M., Cagnati, A., & Forte, E. (2019). Recent evolution of Marmolada glacier (Dolomites, Italy) by means of ground and airborne GPR surveys. *Remote Sensing of Environment*, *235*, 111442. https://doi.org/10.1016/J.RSE.2019.111442

Scandroglio, R., Draebing, D., Offer, M., & Krautblatter, M. (2021). 4D quantification of alpine permafrost degradation in steep rock walls using a laboratory-calibrated electrical resistivity tomography approach. *Near Surface Geophysics*, *19*(2), 241–260. https://doi.org/10.1002/NSG.12149/CITE/REFWORKS

Schmidt, R. (2009). *Klimawandel in Österreich : die letzten 20.000 Jahre ... und ein Blick voraus*. *Report* (1. Aufl..). Innsbruck: IUP - Innsbruck Univ. Press. Retrieved from https://ubdata.univie.ac.at/AC07606825

Schrott, L., Otto, J., & Keller, F. (2012). Modelling alpine permafrost distribution in the Hohe Tauern region, Austria. *Austrian Journal of Earth Sciences*, *105*(2), 169–183.

Schuster, R., Egger, H., Krenmayr, H. G., Linner, M., Mandl, W. G., Matura, A., … Schnabel, W. (2015). Geologische Übersichtskarte der Republik Österreich1:1.500.000 (ohne Quartär). Wien: Geologische Bundesanstalt.

Schweizer, V. (2012). *Wörterbuch der Geologie / Dictionary of Geology*. *Wörterbuch der Geologie / Dictionary of Geology* (Vol. 59). Springer Verlag Berlin Heidelberg. https://doi.org/10.1007/978-3-8274-2262-0

Scotti, R., Brardinoni, F., Alberti, S., Frattini, P., & Crosta, G. B. (2013). A regional inventory of rock glaciers and protalus ramparts in the central Italian Alps. *Geomorphology*, *186*, 136–149. https://doi.org/10.1016/j.geomorph.2012.12.028

Shannon, S., Smith, R., Wiltshire, A., Payne, T., Huss, M., Betts, R., … Harrison, S. (2019). Global glacier volume projections under high-end climate change scenarios. *The Cryosphere*, *13*(1), 325–350.

Skamarock, W. C., Klemp, J. B., Dudhia, J., Gill, D. O., Barker, D. M., Duda, M. G., … Powers, J. G. (2008). A description of the advanced research WRF version 3, NCAR Technical Note. *National Center for Atmospheric Research, Boulder, Colorado, USA*.

Sklash, M. G., Farvolden, R. N., & Fritz, P. (1976). A conceptual model of watershed response to rainfall, developed through the use of oxygen-18 as a natural tracer. *Canadian Journal of Earth Sciences*, *13*(2), 271–283. https://doi.org/10.1139/e76-029

Slater, C., Preston, T., & Weaver, L. T. (2001). Stable isotopes and the international system of units. *Rapid Communications in Mass Spectrometry*, *15*(15), 1270–1273. https://doi.org/10.1002/rcm.328

Snyder, G. T., & Fabryka-Martin, J. T. (2007). 129I and 36Cl in dilute hydrocarbon waters: Marine-cosmogenic, in situ, and anthropogenic sources. *Applied Geochemistry*, *22*(3), 692–714. https://doi.org/10.1016/j.apgeochem.2006.12.011

Sodemann, H., & Zubler, E. (2010). Seasonal and inter-annual variability of the moisture sources for Alpine precipitation during 1995–2002. *International Journal of Climatology*, *30*(7), 947–961. https://doi.org/10.1002/JOC.1932

Souchez, R. A., Jouzel, J., Lorrain, R., Sleewaegen, S., Stiévenard, M., & Verbeke, V. (2000). A kinetic isotope effect during ice formation by water freezing. *Geophysical Research Letters*, *27*(13), 1923–1926.

Souchez, R. A., & Lorrain, R. D. (2012). *Ice composition and glacier dynamics* (Vol. 8). Springer Science & Business Media.

Spinoni, J., Vogt, J. V, Naumann, G., Barbosa, P., & Dosio, A. (2018). Will drought events become more frequent and severe in Europe? *International Journal of Climatology*, *38*(4), 1718–1736.

Sternai, P., Sue, C., Husson, L., Serpelloni, E., Becker, T. W., Willett, S. D., … Castelltort, S. (2019). Present-day uplift of the European Alps: Evaluating mechanisms and models of their relative contributions. *Earth-Science Reviews*, *190*, 589–604. https://doi.org/10.1016/j.earscirev.2019.01.005

Strauhal, T., Zangerl, C., Fellin, W., Holzmann, M., Engl, D. A., Brandner, R., … Tessadri, R. (2017). Structure, Mineralogy and Geomechanical Properties of Shear Zones of Deep-Seated Rockslides in Metamorphic Rocks (Tyrol, Austria). *Rock Mechanics and Rock Engineering*, *50*(2), 419–438. https://doi.org/10.1007/s00603-016-1113-y

Szidat, S., Schmidt, A., Handl, J., Jakob, D., Botsch, W., Michel, R., … Städe, W. (2000). Iodine-129: Sample preparation, quality control and analyses of pre-nuclear materials and of natural waters from Lower Saxony, Germany. *Nuclear Instruments and Methods in Physics Research Section B: Beam Interactions with Materials and Atoms*, *172*(1–4), 699–710. https://doi.org/10.1016/S0168-

583X(00)00377-3

Szidat, Sönke. (2000). Iod-129: Probenvorbereitung, Qualitätssicherung und Analyse von Umweltmaterialien. Hannover: Gottfried Wilhelm Leibniz Universität Hannover.

Tabari, H. (2020). Climate change impact on flood and extreme precipitation increases with water availability. *Scientific Reports 2020 10:1*, *10*(1), 1–10. https://doi.org/10.1038/s41598-020-70816-2

Takagi, J., Hampel, W., & Kirsten, T. (1974). Cosmic-ray muon-induced 129I in tellurium ores. *Earth and Planetary Science Letters*, *24*(1), 141–150. https://doi.org/10.1016/0012-821X(74)90019-3

Tappa, D. J., Kohn, M. J., McNamara, J. P., Benner, S. G., & Flores, A. N. (2016). Isotopic composition of precipitation in a topographically steep, seasonally snow-dominated watershed and implications of variations from the global meteoric water line. *Hydrological Processes*, *30*(24), 4582–4592. https://doi.org/10.1002/hyp.10940

Theurillat, J.-P., & Guisan, A. (2001). Potential impact of climate change on vegetation in the European Alps: a review. *Climatic Change*, *50*(1), 77–109.

Thomas, C. D., Cameron, A., Green, R. E., Bakkenes, M., Beaumont, L. J., Collingham, Y. C., … Williams, S. E. (2004). Extinction risk from climate change. *Nature 2003 427:6970*, *427*(6970), 145–148. https://doi.org/10.1038/nature02121

Thompson, L. G., & Davis, M. E. (2005). Stable isotopes through the holocene as recorded in low-latitude, high-altitude ice cores. *Isotopes in the Water Cycle: Past, Present and Future of a Developing Science*, 321–339. https://doi.org/10.1007/1-4020-3023-1_20/COVER

Tian, C., Wang, L., Kaseke, K. F., & Bird, B. W. (2018). Stable isotope compositions (δ2H, δ18O and δ17O) of rainfall and snowfall in the central United States. *Scientific Reports 2018 8:1*, *8*(1), 1–15. https://doi.org/10.1038/s41598-018-25102-7

Tollmann, A. (1985). Geologie von Österreich, Band 1. Wien (Deuticke).

Tropper, P., & Hoinkes, G. (1996). Geothermobarometry of Al2SiO5-bearing metapelites in the western Austroalpine Ötztal-basement. *Mineralogy and Petrology*, *58*(3--4), 145–170. https://doi.org/10.1007/BF01172094

Uemura, R., Matsui, Y., Yoshida, N., Abe, O., & Mochizuki, S. (2005). Isotopic fractionation of water during snow formation: Experimental evidence of kinetic e#ect. *Polar Meteorological Glaciology*, *19*, 1–14.

UNEP. (2022). Climate change, water scarcity and security. Retrieved August 20, 2022, from https://www.unep.org/news-and-stories/speech/climate-change-

water-scarcity-and-security

Van Huissteden, J. (2020). *Thawing permafrost: Permafrost Carbon in a Warming Arctic*. Springer International Publishing.

Vehling, L., Baewert, H., Glira, P., Moser, M., Rohn, J., & Morche, D. (2017). Quantification of sediment transport by rockfall and rockslide processes on a proglacial rock slope (Kaunertal, Austria). *Geomorphology*, *287*, 46–57. https://doi.org/10.1016/J.GEOMORPH.2016.10.032

Vehling, Lucas. (2016). Gravitative Massenbewegungen an alpinen Felshängen-Quantitative Bedeutung in der Sedimentkaskade proglazialer Geosysteme. Friedrich-Alexander-Universität Erlangen-Nürnberg (FAU).

Veit, H. (2002). *Die Alpen–Geoökologie und Landschaftsentwicklung* (Vol. 2327). Eugen Ulmer.

VERA. (2022). Retrieved June 14, 2022, from https://isotopenphysik.univie.ac.at/en/vera/

Viviroli, D., Dürr, H. H., Messerli, B., Meybeck, M., & Weingartner, R. (2007). Mountains of the world, water towers for humanity: Typology, mapping, and global significance. *Water Resources Research*, *43*(7).

Wagner, M. J. M. (1995a). *Intermediate mass range radionuclides: new detection methods and applications of nickel-59, tin-126 and iodine-129; Mittelschwere Radionuklide: neue Nachweismethoden und Anwendungen von Nickel-59, Zinn-126 und Iod-129*. Zurich (Switzerland).

Wagner, M. J. M. (1995b). Mittelschwere Radionuklide. Neue Nachweismethode und Anwendungen von Nickel-59, Zinn-126 und Iod-129. https://doi.org/10.3929/ETHZ-A-001516112

Wagner, M. J. M., Dittrich-Hannen, B., Synal, H. A., Suter, M., & Schotterer, U. (1996). Increase of 129I in the environment. *Nuclear Instruments and Methods in Physics Research Section B: Beam Interactions with Materials and Atoms*, *113*(1–4), 490–494. https://doi.org/10.1016/0168-583X(95)01348-2

Wagner, T., Brodacz, A., Krainer, K., & Winkler, G. (2020). Active rock glaciers as shallow groundwater reservoirs, Austrian Alps. *Grundwasser*, *25*(3), 215–230. https://doi.org/10.1007/s00767-020-00455-x

Wagner, T., Kainz, S., Helfricht, K., Fischer, A., Avian, M., Krainer, K., & Winkler, G. (2021). Assessment of liquid and solid water storage in rock glaciers versus glacier ice in the Austrian Alps. *Science of the Total Environment*, *800*, 149593. https://doi.org/10.1016/j.scitotenv.2021.149593

Wagner, T., Kainz, S., Krainer, K., & Winkler, G. (2021). Storage-discharge characteristics of an active rock glacier catchment in the Innere Ölgrube, Austrian Alps. *Hydrological Processes*, *35*(5), 1–16.

https://doi.org/10.1002/hyp.14210

Wahrhaftig, C., & Cox, A. (1959). Rock glaciers in the Alaska Range. *Geological Society of America Bulletin*, *70*(4), 383–436.

Wälder, O., Krainer, K., & Mostler, W. (2004). *Praktische Anwendung von speziellen Spline-Verfahren zur Gletscherkinematik am Beispiel eines aktiven Blockgletschers (Tirol)*.

Whalley, W. B., & Martin, H. E. (1992). Rock glaciers : II models and mechanisms. *Progress in Physical Geography*, *16*(2), 127–186. https://doi.org/10.1177/030913339201600201

Wilkinson, G. N., & Rogers, C. E. (1973). Symbolic Description of Factorial Models for Analysis of Variance. *Journal of Applied Statistics*, *22*(3), 392–399. https://doi.org/10.2307/2346786

Williams, M. W., Knauf, M., Caine, N., Liu, F., & Verplanck, P. L. (2006). Geochemistry and source waters of rock glacier outflow, Colorado Front Range. *Permafrost and Periglacial Processes*, *17*(1), 13–33. https://doi.org/10.1002/ppp.535

Woo, M.-K. (2012). *Permafrost hydrology*. Springer.

Yang, Y., Wu, Q., Jin, H., Wang, Q., Huang, Y., Luo, D., … Jin, X. (2019). Delineating the hydrological processes and hydraulic connectivities under permafrost degradation on Northeastern Qinghai-Tibet Plateau, China. *Journal of Hydrology*, *569*, 359–372. https://doi.org/10.1016/j.jhydrol.2018.11.068

Zangerl, U., Haselberger, S., & Kraushaar, S. (2022). Classifying Sparse Vegetation in a Proglacial Valley Using UAV Imagery and Random Forest Algorithm. *Remote Sensing*, *14*(19). https://doi.org/10.3390/rs14194919

Zhang, L. Y., & Hou, X. L. (2013). Speciation analysis of 129I and its applications in environmental research. *Radiochimica Acta*, *101*(8), 525–540. https://doi.org/10.1524/ract.2013.2077

Zhang, Y., Hemperly, J., Meskhidze, N., & Skamarock, W. C. (2012). The Global Weather Research and Forecasting (GWRF) Model: Model Evaluation, Sensitivity Study, and Future Year Simulation. *Atmospheric and Climate Sciences*, *02*(03), 231–253. https://doi.org/10.4236/acs.2012.23024

## Eidesstattliche Erklärung

Ich versichere:

- dass ich die Masterarbeit selbstständig verfasst, andere als die angegebenen Quellen und Hilfsmittel nicht benutzt und mich auch sonst keiner unerlaubten Hilfe bedient habe.
- dass alle Stellen, die wörtlich oder sinngemäß aus veröffentlichten und nicht veröffentlichten Publikationen entnommen sind, als solche kenntlich gemacht sind.
- dass ich dieses Masterarbeitsthema bisher weder im In- noch im Ausland (einer Beurteilerin/ einem Beurteiler zur Begutachtung) in irgendeiner Form als Prüfungsarbeit vorgelegt habe.
- dass diese Arbeit mit der vom Begutachter beurteilten Arbeit übereinstimmt.

| Datum | Unterschrift |
| --- | --- |
| 25.01.2023 | 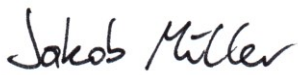 |

# Appendix

## I. detailed sample sheet

| Sample ID | sample reference | date | time | $\delta^{18}O$ | SD O | $\delta^{2}H$ | SD H | excess (Formel | I129 [atoms/l] | rel error | PL [%] | Q [l/s] | inclination [%] | source | exposition | GPS lat | GPS long | GPS ele |
|---|---|---|---|---|---|---|---|---|---|---|---|---|---|---|---|---|---|---|
| KB01 | KB01 | 24/07/18 | 13:00 | -15.0 | 0.3 | -108.1 | 1.0 | 11.9 | 2.20E+07 | 3.6% | 90.18 | | 7 | spring | NO | 46.911629 | 10.681797 | 2550 |
| KB02 | KB02 | 24/07/18 | 13:45 | -14.9 | 0.4 | -108.5 | 0.6 | 10.7 | | | | | 10 | spring | ONO | 46.910732 | 10.681355 | 2581 |
| KB03 | KB03 | 24/07/18 | 14:00 | -14.7 | 0.2 | -109.1 | 0.8 | 8.5 | | | | | 15 | spring | NO | 46.910495 | 10.680938 | 2574 |
| KB04 | KB04 | 24/07/18 | 14:15 | -15.2 | 0.2 | -108.2 | 1.2 | 13.4 | 2.29E+07 | 3.8% | 89.74 | | 10 | spring | NO | 46.910717 | 10.68092 | 2568 |
| KB05 | KB05 | 24/07/18 | 15:00 | -15.0 | 0.3 | -109.4 | 0.8 | 10.6 | 1.80E+07 | 5.1% | 92.08 | | 13 | spring | ONO | 46.911352 | 10.67987 | 2587 |
| KB06 | KB06 | 24/07/18 | 15:30 | | | | | | | | | | 15 | spring | O | 46.91193 | 10.679279 | 2600 |
| KB06 | KB06 | 25/07/18 | 11:00 | -13.6 | 0.3 | -98.8 | 0.9 | 10.0 | 3.45E+07 | 2.1% | 84.20 | | 11 | spring | O | 46.91193 | 10.679279 | 2600 |
| KB07 | KB07 | 25/07/18 | 11:30 | -15.1 | 0.3 | -110.1 | 0.9 | 10.7 | 7.00E+06 | 8.2% | 97.37 | | 17 | spring | OSO | 46.912775 | 10.679159 | 2602 |
| KB08 | KB08 | 25/07/18 | 13:00 | -13.1 | 0.2 | -94.7 | 0.9 | 10.1 | 6.43E+07 | 2.0% | 69.96 | | 14 | spring | WSW | 46.92119 | 10.671837 | 2827 |
| KB09 | KB09 | 25/07/18 | 13:50 | -13.1 | 0.2 | -94.1 | 1.2 | 10.7 | 1.91E+07 | 2.2% | 91.57 | | 35 | spring | SO | 46.919814 | 10.673995 | 2794 |
| KB10 | KB10 | 26/07/18 | 11:30 | -18.9 | 0.2 | -141.4 | 2.1 | 9.8 | | | | | 10 | spring | - | 46.911737 | 10.674783 | 2623 |
| KB10 | KB10 | 26/07/18 | 11:30 | -14.9 | 0.2 | -110.8 | 1.6 | 8.4 | 2.37E+07 | 2.8% | 89.38 | | 10 | snow | SO | 46.911737 | 10.674783 | 2623 |
| KB11 | KB11 | 26/07/18 | 13:30 | -15.1 | 0.3 | -110.1 | 0.9 | 10.7 | 2.79E+07 | 4.7% | 87.38 | | 40 | spring | OSO | 46.911992 | 10.672785 | 2697 |
| KB12 | KB12 | 26/07/18 | 15:00 | | | | | | | | | | 40 | spring | - | 46.910913 | 10.667393 | 2817 |
| KB12 | KB12 | 26/07/18 | 15:00 | -14.5 | 0.3 | -106.9 | 0.8 | 9.1 | 7.27E+06 | 33.2% | 97.24 | | 40 | snow | O | 46.910913 | 10.667393 | 2817 |
| KB13 | KB04 | 29/08/18 | 14:20 | -13.5 | 0.3 | -98.7 | 0.8 | 9.3 | 2.14E+07 | 3.5% | 90.50 | | 10 | spring | NO | 46.910717 | 10.68092 | 2568 |
| KB14 | KB05 | 29/08/18 | 15:20 | -13.7 | 0.2 | -98.2 | 0.7 | 11.4 | 1.80E+07 | 4.7% | 92.13 | | 13 | spring | ONO | 46.911352 | 10.67987 | 2587 |
| KB15 | KB06 | 29/08/18 | 16:00 | -11.9 | 0.2 | -86.6 | 1.9 | 8.6 | 1.31E+07 | 9.3% | 94.44 | | 11 | spring | O | 46.91193 | 10.679279 | 2600 |
| KB16 | KB07 | 29/08/18 | 16:40 | -12.1 | 0.3 | -86.8 | 1.2 | 10.0 | 5.09E+07 | 5.2% | 76.36 | | 17 | spring | OSO | 46.912859 | 10.677819 | 2633 |
| KB17 | KB01 | 30/08/18 | 11:50 | -13.3 | 0.2 | -97.0 | 0.8 | 9.4 | 2.20E+07 | 3.6% | 90.18 | | 7 | spring | NO | 46.911629 | 10.681797 | 2550 |
| KB18 | KB11 | 30/08/18 | 13:10 | -13.3 | 0.1 | -95.4 | 0.8 | 11.0 | 2.87E+07 | 3.1% | 86.96 | | 40 | spring | OSO | 46.911992 | 10.672785 | 2697 |
| KB19 | KB19 | 30/08/18 | 14:20 | -11.8 | 0.3 | -82.8 | 0.9 | 11.6 | 3.88E+07 | 2.6% | 82.15 | | 3 | spring | | 46.914982 | 10.668867 | 2763 |
| KB20 | KB20 | 30/08/18 | 14:20 | -12.6 | 0.2 | -88.8 | 1.1 | 12.0 | 4.04E+07 | 3.1% | 81.36 | | 0 | spring | OSO | 46.916745 | 10.671466 | 2755 |
| KB21 | KB21 | 30/08/18 | 15:25 | -12.4 | 0.2 | -87.7 | 0.9 | 11.5 | 2.81E+07 | 3.4% | 87.26 | | 3 | spring | SO | 46.918008 | 10.670474 | 2750 |
| KB22 | KB08 | 30/08/18 | 16:05 | -11.5 | 0.3 | -78.5 | 0.8 | 13.5 | 5.20E+07 | 2.3% | 75.80 | 6.88 | 14 | spring | WSW | 46.92119 | 10.671837 | 2827 |
| KB23 | KB23 | 30/08/18 | 17:10 | -11.5 | 0.2 | -80.4 | 1.5 | 11.6 | 2.88E+07 | 2.8% | 86.92 | 7.94 | 10 | spring | SSW | 46.919025 | 10.675529 | 2739 |
| KB24 | KB24 | 31/08/18 | 09:40 | -10.1 | 0.3 | -70.2 | 1.3 | 10.6 | 2.16E+08 | 2.1% | -2.59 | | 0 | rain | - | 46.911524 | 10.677414 | 2649 |
| KB25 | KB25 | 31/08/18 | Aug | -8.2 | 0.3 | -54.2 | 0.7 | 11.4 | 2.90E+08 | 3.1% | -37.89 | | 0 | rain | - | 46.911262 | 10.681798 | 2551 |
| KB26 | KB07 | 27/09/18 | 15:30 | -14.1 | 0.3 | -98.6 | 2.6 | 14.2 | 9.58E+06 | 6.1% | 96.14 | | 18 | spring | O | 46.912658 | 10.678259 | 2622 |
| KB27 | KB05 | 27/09/18 | 16:15 | -13.4 | 0.2 | -94.7 | 0.8 | 12.5 | 1.77E+07 | 14.1% | 92.27 | 20.54 | 13 | spring | ONO | 46.911352 | 10.67987 | 2587 |
| KB28 | KB04 | 27/09/18 | 16:45 | -13.1 | 0.2 | -91.3 | 0.6 | 13.5 | 1.85E+07 | 13.9% | 91.86 | | 10 | spring | NO | 46.910717 | 10.68092 | 2568 |
| KB29 | KB01 | 27/09/18 | 17:15 | -13.3 | 0.2 | -94.8 | 0.9 | 11.6 | 1.77E+07 | 4.4% | 92.27 | | 7 | spring | NO | 46.911629 | 10.681797 | 2550 |
| KB30 | KB30 | 28/09/18 | 10:00 | -12.3 | 0.2 | -86.3 | 1.3 | 12.1 | 1.13E+07 | 3.5% | 95.34 | | 11 | spring | NO | 46.915225 | 10.688844 | 2445 |
| KB31 | KB25 | 28/09/18 | Sept | -11.3 | 0.2 | -75.2 | 1.2 | 15.2 | 1.21E+08 | 3.4% | 42.65 | | 0 | rain | - | 46.911262 | 10.681798 | 2551 |
| KB32 | KB11 | 28/09/18 | 13:30 | -13.4 | 0.3 | -93.7 | 1.0 | 13.5 | 2.76E+07 | 4.6% | 87.49 | | 40 | spring | OSO | 46.911992 | 10.672785 | 2697 |
| KB33 | KB21 | 28/09/18 | 15:00 | -13.1 | 0.2 | -90.8 | 0.6 | 14.0 | 2.60E+07 | 3.5% | 88.29 | | 3 | spring | SO | 46.918008 | 10.670474 | 2750 |
| KB34 | KB08 | 28/09/18 | 15:25 | -12.2 | 0.3 | -81.8 | 1.1 | 15.8 | 4.35E+07 | 3.0% | 79.90 | 0.60 | 14 | spring | WSW | 46.92119 | 10.671837 | 2827 |
| KB35 | KB23 | 28/09/18 | 16:20 | -12.4 | 0.2 | -85.4 | 0.8 | 13.8 | 2.63E+07 | 4.1% | 88.14 | 2.73 | 10 | spring | SSW | 46.919025 | 10.675529 | 2739 |
| KB36 | KB36 | 29/09/18 | 13:45 | -13.0 | 0.2 | -90.9 | 0.8 | 13.1 | 1.12E+06 | 39.0% | 100.19 | | 0 | ice | - | 46.905106 | 10.682954 | 2769 |
| KB37 | KB37 | 29/09/18 | 14:00 | -13.3 | 0.1 | -92.3 | 0.8 | 14.1 | 3.17E+07 | 3.6% | 85.54 | | 8 | spring | NO | 46.905179 | 10.68315 | 2758 |
| KB38 | KB38 | 29/09/18 | 14:15 | -13.3 | 0.2 | -94.4 | 0.6 | 12.0 | 1.91E+06 | 22.6% | 99.81 | | 0 | ice | - | 46.905177 | 10.683195 | 2758 |
| KB38b | KB38 | 29/09/18 | 14:15 | -14.8 | 0.2 | -107.5 | 0.9 | 10.9 | | | | | 0 | ice | - | 46.905177 | 10.683195 | 2758 |
| KB39 | KB39 | 29/09/18 | 15:00 | -12.7 | 0.3 | -95.3 | 1.1 | 6.3 | | | | | 0 | spring | - | 46.909968 | 10.688337 | 2638 |
| KB39b | KB39 | 29/09/18 | 15:00 | | | | | | 5.51E+07 | 3.4% | 74.35 | | 0 | spring | - | 46.909968 | 10.688337 | 2638 |
| | | | | | | | | | 5.93E+07 | 2.3% | 72.34 | | | | | | | |

~aprox

iod-analyse mit 500 ml
iod-analyse mit 250 ml
iod-analyse mit 100 ml

## II. Correlation plot of spring sample data

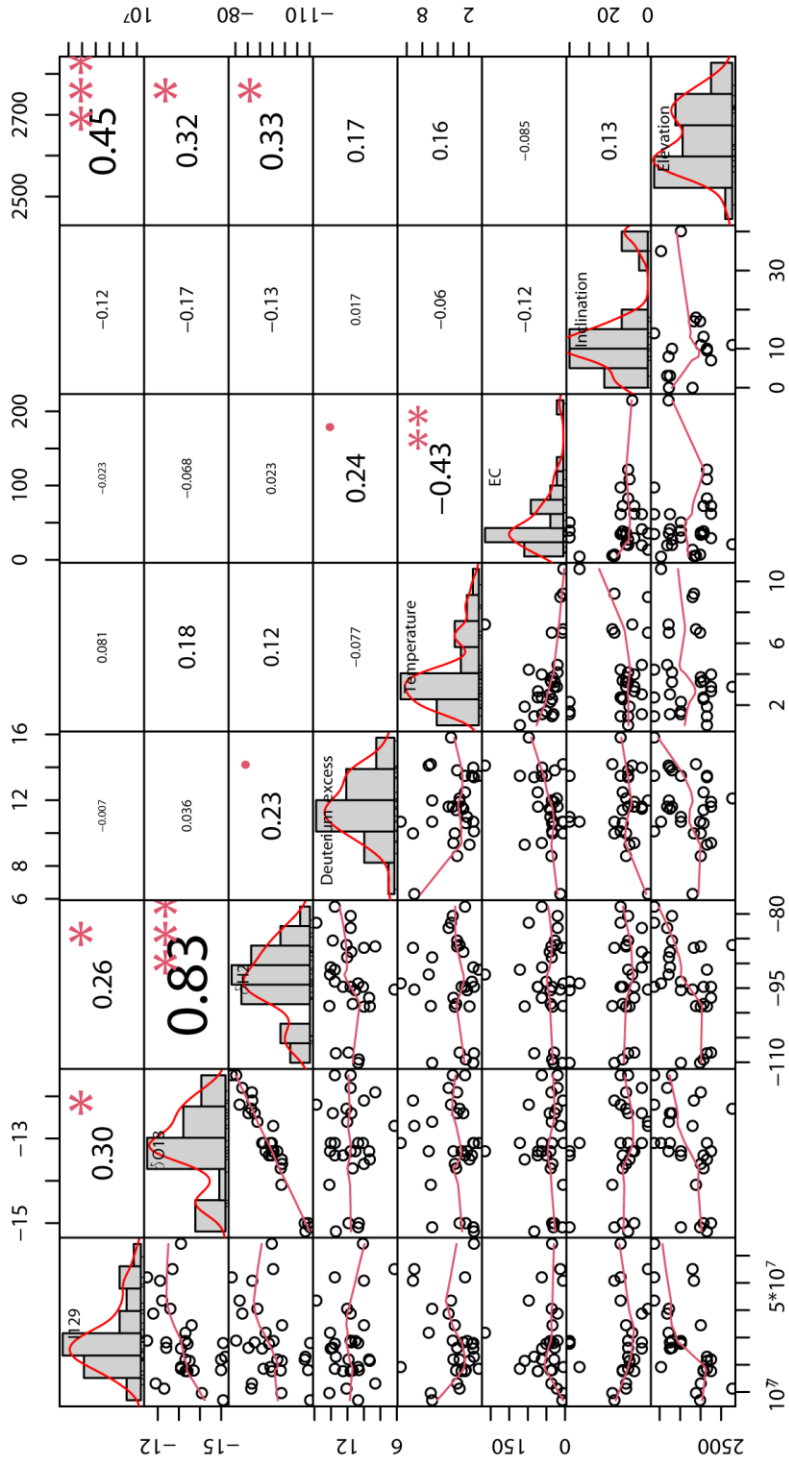

## III. PCA - Groupings

The four spring water origins are plotted in a two-dimensional room of principal component 1 (PC1) and principal component 2 (PC2)

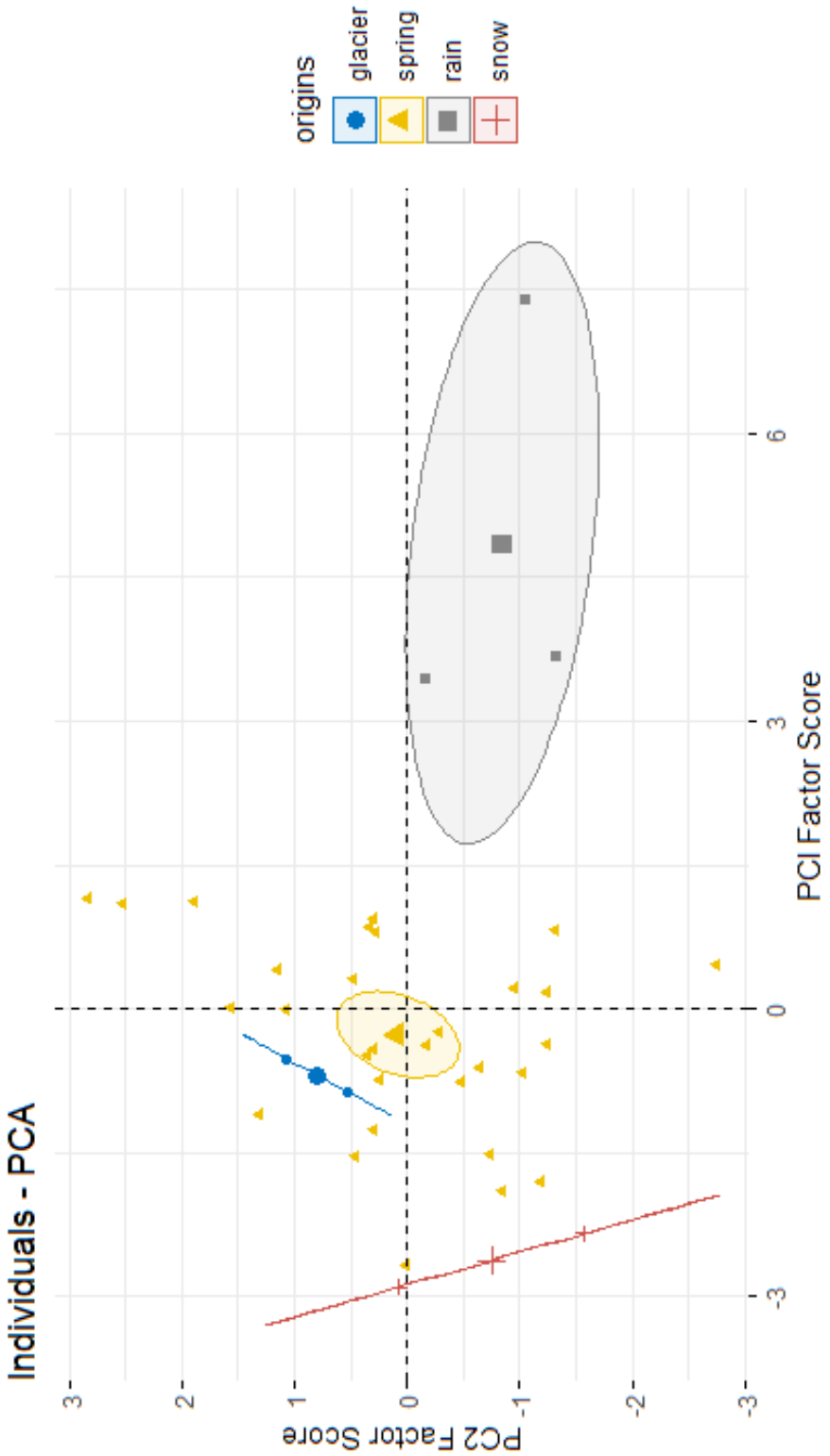

## IV. PCA - Biplot

Spring water sample variables and their contributions to PCA dimensions colour-coded, and table of Eigenvalues, Individuals, and variables

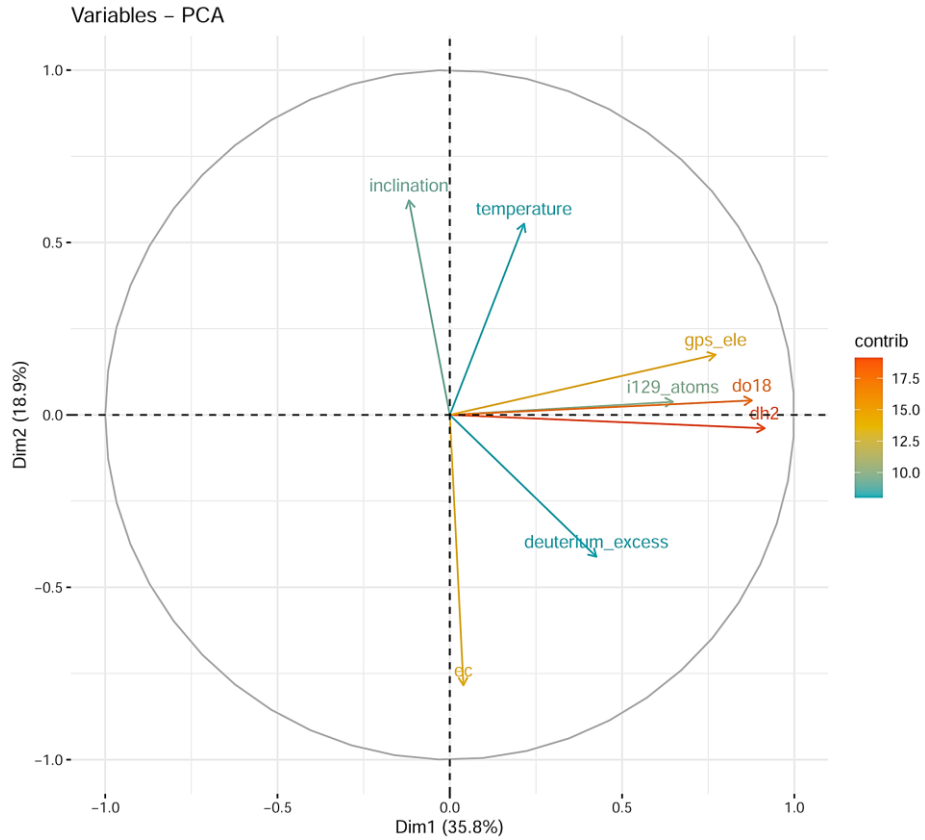


Eigenvalues

| | Dim.1 | Dim.2 | Dim.3 | Dim.4 | Dim.5 | Dim.6 | Dim.7 | Dim.8 |
|---|---|---|---|---|---|---|---|---|
| Variance | 3.431 | 1.358 | 1.160 | 0.825 | 0.575 | 0.403 | 0.248 | 0.000 |
| % of var. | 42.885 | 16.980 | 14.503 | 10.316 | 7.184 | 5.034 | 3.099 | 0.000 |
| Cumulative % of var. | 42.885 | 59.864 | 74.367 | 84.683 | 91.867 | 96.901 | 100.000 | 100.000 |

Individuals (the 10 first)

| | Dist | Dim.1 | ctr | cos2 | Dim.2 | ctr | cos2 | Dim.3 | ctr | cos2 |
|---|---|---|---|---|---|---|---|---|---|---|
| 1 | 2.293 | -0.520 | 0.213 | 0.051 | 1.067 | 2.267 | 0.217 | 0.513 | 0.614 | 0.050 |
| 2 | 2.189 | -0.859 | 0.581 | 0.154 | 0.535 | 0.570 | 0.060 | 0.552 | 0.709 | 0.064 |
| 3 | 2.358 | -1.508 | 1.791 | 0.409 | -0.744 | 1.102 | 0.100 | -1.307 | 3.980 | 0.307 |
| 4 | 1.777 | -0.360 | 0.102 | 0.041 | -1.246 | 3.090 | 0.492 | -0.979 | 2.235 | 0.304 |
| 5 | 1.498 | -0.239 | 0.045 | 0.026 | -0.289 | 0.166 | 0.037 | -1.361 | 4.315 | 0.825 |
| 6 | 2.461 | 0.218 | 0.037 | 0.008 | -0.950 | 1.797 | 0.149 | -1.056 | 2.596 | 0.184 |
| 7 | 4.188 | 1.099 | 0.952 | 0.069 | 2.527 | 12.706 | 0.364 | -1.974 | 9.078 | 0.222 |
| 8 | 2.706 | -1.536 | 1.859 | 0.322 | 0.461 | 0.422 | 0.029 | -2.012 | 9.431 | 0.553 |
| 9 | 2.271 | -0.609 | 0.293 | 0.072 | -0.656 | 0.856 | 0.083 | -1.444 | 4.860 | 0.404 |
| 10 | 2.415 | 0.000 | 0.000 | 0.000 | 1.079 | 2.315 | 0.199 | -1.941 | 8.779 | 0.646 |

Variables

| | Dim.1 | ctr | cos2 | Dim.2 | ctr | cos2 | Dim.3 | ctr | cos2 |
|---|---|---|---|---|---|---|---|---|---|
| i129_atoms | 0.853 | 21.222 | 0.728 | -0.209 | 3.219 | 0.044 | 0.090 | 0.698 | 0.008 |
| do18 | 0.931 | 25.243 | 0.866 | 0.015 | 0.018 | 0.000 | 0.243 | 5.110 | 0.059 |
| dh2 | 0.937 | 25.565 | 0.877 | 0.151 | 1.669 | 0.023 | 0.192 | 3.164 | 0.037 |
| deuterium_excess | 0.228 | 1.515 | 0.052 | 0.801 | 47.218 | 0.641 | -0.256 | 5.645 | 0.065 |
| temperature | 0.719 | 15.054 | 0.516 | -0.283 | 5.881 | 0.080 | 0.043 | 0.157 | 0.002 |
| ec | 0.354 | 3.662 | 0.126 | 0.434 | 13.878 | 0.189 | -0.608 | 31.911 | 0.370 |
| inclination | -0.510 | 7.569 | 0.260 | 0.126 | 1.161 | 0.016 | 0.365 | 11.490 | 0.133 |
| gps_ele | -0.077 | 0.171 | 0.006 | 0.605 | 26.957 | 0.366 | 0.697 | 41.826 | 0.485 |

# Abstract

With global warming proceeding, water stored beneath the earth's surface in form of permafrost will become increasingly important as a water resource in the future. Therefore, calls for further research about ice-bound water – especially in form of permafrost, which is expected to thaw delayed compared to glacier ice with a global increase in temperature – were made repeatedly in the past.

In mountainous regions, permafrost occurs often in form of rock glaciers. This thesis aims at closing some of the existing research gaps about alpine permafrost with a focus on rock glacier runoff. Analyses of springs in a small high alpine catchment located in the Tyrolean Alps were done. In this so-called Kaiserbergtal Valley the question whether and how glacier ice, rainwater and spring waters differ from each other in a geochemical perspective was addressed. For this purpose, conventional water parameters, such as stable isotopes, were combined with the not that commonly used radiogenic tracer iodine-129 ($^{129}I$). The footprint of the stable isotopes $^{18}O$ and $^{2}H$ was used to find springs with ice origin. Findings show that all spring waters are heavily influenced by isotopic fractionation, which points towards freezing-thawing-processes. Concentrations of the anthropogenic isotope $^{129}I$ were used to retrieve information about the age of waters. This relative age determination shows that spring water in the catchment is fed by 74.4 % to 96.1 % of old water. All in all, the utmost part of spring waters in mid and late summer is fed by thawed permafrost passive layer. This rate is particularly high in springs located near the thalweg, rather than in more exposed and elevated locations. The best investigated rock glacier in the centre of the research area loses about 19 l/s water coming from old ice on a September afternoon.

Although the study was conducted in the Austrian Alps, its findings let one draw conclusions on permafrost around the globe. Especially the rarely used tracer $^{129}I$ shows potential for overcoming problems regarding tritium's short half-life (12.3 a) and could replace it as tracer for age-measurements.

# Kurzfassung

Mit der fortschreitenden Erderwärmung wird Wasser, das unter der Erdoberfläche in Form von Permafrost gespeichert ist, in Zukunft immer größere Relevanz als Wasserressource erlangen. In näherer Vergangenheit wurden immer wieder Forderungen nach einer besseren Erforschung von eisgebundenem Wasser – insbesondere in Form von Permafrost, welcher bei einem globalen Temperaturanstieg im Vergleich zu Gletschereis verzögert auftaut – laut.

In Gebirgsregionen tritt Permafrost oft in Form von Blockgletschern auf. Die vorliegende Arbeit hat zum Ziel, einige der Forschungslücken über alpinen Permafrost zu schließen, wobei der Fokus auf dem Abfluss von Blockgletschern liegt. Anhand der Quellwasseranalysen aus dem Kaiserbergtal, einem kleinen hochalpinen Tal in den Ötztaler Alpen, wurde der Frage nachgegangen, ob bzw. inwiefern sich Gletschereis, Regenwasser und Quellwasser in geochemischen Gesichtspunkten voneinander unterscheiden. Zu diesem Zweck wurden Informationen von konventionellen Wasserparametern, unter anderem von stabilen Isotopen, mit dem nicht so häufig verwendeten radiogenen Tracer Iod-129 ($^{129}$I) kombiniert. Die stabilen Isotope $^{18}$O und $^{2}$H wurde verwendet, um Quellen mit Eisursprung zu finden. Mit der Konzentration des anthropogenen Isotops $^{129}$I lässt sich das Alter der Wässer relativ bestimmen. Die Ergebnisse zeigen, dass alle Quellen stark von Isotopenfraktionierung beeinflusst sind, was darauf hindeutet, dass das Wasser Gefrier-Tau-Prozesse durchlaufen hat. Die relative Altersbestimmung mit $^{129}$I zeigt, dass Quellen im Einzugsgebiet zu 74,4 % bis 96,1 % aus altem Wasser gespeist werden. Gemeinsam zeigen diese beiden Informationen, dass der größte Anteil des Quellwassers im Hoch- und Spätsommer aus auftauendem passive layer des Blockgletschers gespeist wird. Dieser Anteil ist bei Quellen in der Nähe des Talweges besonders hoch, in exponierten und höher gelegenen Gebieten etwas geringer. Der am besten untersuchte Blockgletscher im Zentrum des Forschungsgebiets verliert an einem Septembernachmittag rund 19 Liter Wasser, welches von Permafrost stammt, pro Sekunde.

Diese in den österreichischen Alpen durchgeführte Studie lässt Schlüsse auf das Verhalten von Permafrost weltweit zu. Insbesondere das noch wenig genutzte anthropogene Iod-Isotop $^{129}$I zeigt das Potenzial, Probleme durch die kurze Halbwertszeit von Tritium (12,3 Jahre) zu überwinden und dieses als Tracer für Altersbestimmung zu ersetzen.